



Review

State-of-the-art progress in the rational design of layered double hydroxide based photocatalysts for photocatalytic and photoelectrochemical H₂/O₂ production



Zhong-zhu Yang ^{a,b}, Chang Zhang ^{a,b,*}, Guang-ming Zeng ^{a,b,*}, Xiao-fei Tan ^{a,b}, Dan-lian Huang ^{a,b}, Jun-wu Zhou ^{a,b}, Qian-zhen Fang ^{a,b}, Kai-hua Yang ^{a,b}, Hou Wang ^{a,b}, Jie Wei ^c, Kai Nie ^d

^a College of Environmental Science and Engineering, Hunan University, Changsha 410082, China

^b Key Laboratory of Environmental Biology and Pollution Control (Hunan University), Ministry of Education, Changsha 410082, China

^c Power China Zhongnan Engineering Corporation Limited, Changsha, China

^d Department of Gastroenterology, The Third Xiangya Hospital of Central South University, Tongzipo Road, Changsha 410000, China

ARTICLE INFO

Article history:

Received 28 February 2021

Accepted 14 June 2021

Available online 13 July 2021

Keywords:

Layered double hydroxide
Photocatalytic H₂/O₂ production
Photoelectrochemical water splitting
Reactive sites

ABSTRACT

Photocatalytic (PC) and Photoelectrochemical (PEC) water splitting have been regarded as an attainable and sustainable strategy to obtain hydrogen and oxygen. Developing earth-abundant H₂/O₂-production catalysts with high catalytic activity and robust stability has attracted much attention. Due to the flexible multiple metal cations in the host layers, intercalated anions with interlayer spaces, and good chemical-/physical stability, Layered double hydroxides (LDHs) have been proved as versatile and robust catalysts/co-catalysts in PC/PEC water splitting. In this article, recent progress in the rational design of LDH-based catalysts toward PC/PEC are well reviewed. Firstly, the characteristic of LDH is briefly introduced. Then, we specifically addressed the recent research efforts toward the application of pristine LDHs and semiconductor/LDH materials as photocatalytic catalysts in photocatalytic H₂-generation, O₂-evolution and photoelectrochemical water splitting. Finally, the remaining challenges to investigate and optimize the catalyzing ability of LDH based catalysts are stated to promote possible future development of LDH.

© 2021 Elsevier B.V. All rights reserved.

Contents

1. Introduction	2
2. Strategies to prepare LDHs	4
2.1. Electrodeposition	5
2.2. Other synthesis strategy	5
3. Basics of photocatalytic and photoelectrochemical water splitting	6
4. Various LDH based materials towards light-driven water splitting	9
4.1. Bi/ter-nary LDH	10
4.2. Metal oxides/LDH	11
4.2.1. α -Fe ₂ O ₃ /LDH	11
4.2.2. BiVO ₄ /LDH	13
4.2.3. TiO ₂ /LDH	14
4.2.4. WO ₃ /Ldh	16
4.3. Metal sulfide/LDH	17
4.3.1. CdS/LDH	17
4.3.2. MoS _x /LDH	17
4.4. Carbon materials/LDH	18
4.4.1. C ₃ N ₄ /Ldh	18
4.4.2. GO/Ldh	20

* Corresponding authors at: College of Environmental Science and Engineering, Hunan University, Changsha 410082, China.

E-mail address: zhangchang@hnu.edu.cn (C. Zhang).

5. Summary and outlook	20
Declaration of Competing Interest	21
Acknowledgements	21
References	21

1. Introduction

The increasing energy crisis and growing environmental pollution issues have promoted scientists to develop clean and sustainable energy solutions [1–12]. Water splitting, based on photocatalytic (PC) or photoelectrochemical (PEC) technology, have been regarded as a capable and effective way for the future environmental remediation and energy conversion as the used semiconductors can directly harvest and convert renewable solar light into high-energy-density chemical energy [13–20]. The entire photo(electro)chemical process is progressed under ambient temperatures and atmospheric pressures with relatively stable photocatalytic semiconductors to dissociate two H₂O molecules into two H₂ molecules one O₂ molecule. Generally, photocatalytic H₂/O₂ production can be achieved by two routes: suspension photocatalyst systems and photoelectrode (i.e., photocatalyst immobilized on a conducting substrate) [16,21–23]. Hydrogen evolution reaction (HER) and oxygen evolution reaction (OER) are two important half reactions of water splitting (Fig. 1). The exploration and development of H₂-evolving and O₂-evolving photocatalysts with high photocatalytic activity and stability are extremely needed and important for boosting the water-splitting efficiency. Recently, various semiconductor photocatalysts, such as oxides [24,25], sulfides [26,27], and oxynitrides [28] have been widely developed and extensively studied based on photocatalytic principles. Currently, with the rapid growth of nanotechnology and various advanced characterization methods, 2D lamellar nanomaterials have aroused

considerable attention, which is resulted from their unique lamellar structures, electronic properties and intrinsic activity of active sites [29–31].

Layered double hydroxides (LDHs), also known as hydrotalcite-like materials, are composed of positively charged brucite-like host layers containing edge-sharing M(OH)₆ octahedra, with intercalated anions confined in the interlayer hydrated galleries (Fig. 2). Briefly, the general molecular formula can be described as [M_{1-x}M³⁺(OH)₂(Aⁿ⁻)_{x/n}]^{x+}·mH₂O, where M²⁺ and M³⁺ are bivalent metal cation (e.g., Mg²⁺, Ni²⁺, Zn²⁺, Cu²⁺, Co²⁺) and trivalent metal cation (e.g., Al³⁺, Fe³⁺, Ga³⁺, Mn³⁺) respectively, and Aⁿ⁻ are the counter ion (e.g., CO₃²⁻, Cl⁻, NO₃⁻, SO₄²⁻, PO₄³⁻) [32–34]. The metal octahedra in LDHs are bonded to each other through a metal-oxygen-metal oxo bridging linkage [35,36]. The presence of oxo-bridges are beneficial for the metal-to-metal charge migration which in turn act as a vital role for visible light redox reactions by mitigating undesirable electron-hole recombination [31,37,38]. In addition, the generated O-H bond perpendicular to the brucite layers in the coordination octahedron can react with holes of valence bands to produce ·OH, which is an important intermediate in photocatalysis oxidation reaction [39]. Moreover, the well dispersed positive charge of the octahedron is blocked within the brucite layers, which makes it an ideal host to implement electrostatic interactions with the intercalating anions. Those anions have been proved as the positive influence for enlarging specific surface area and different spaces among layers of LDHs and ultimately improve the photocatalytic performance by

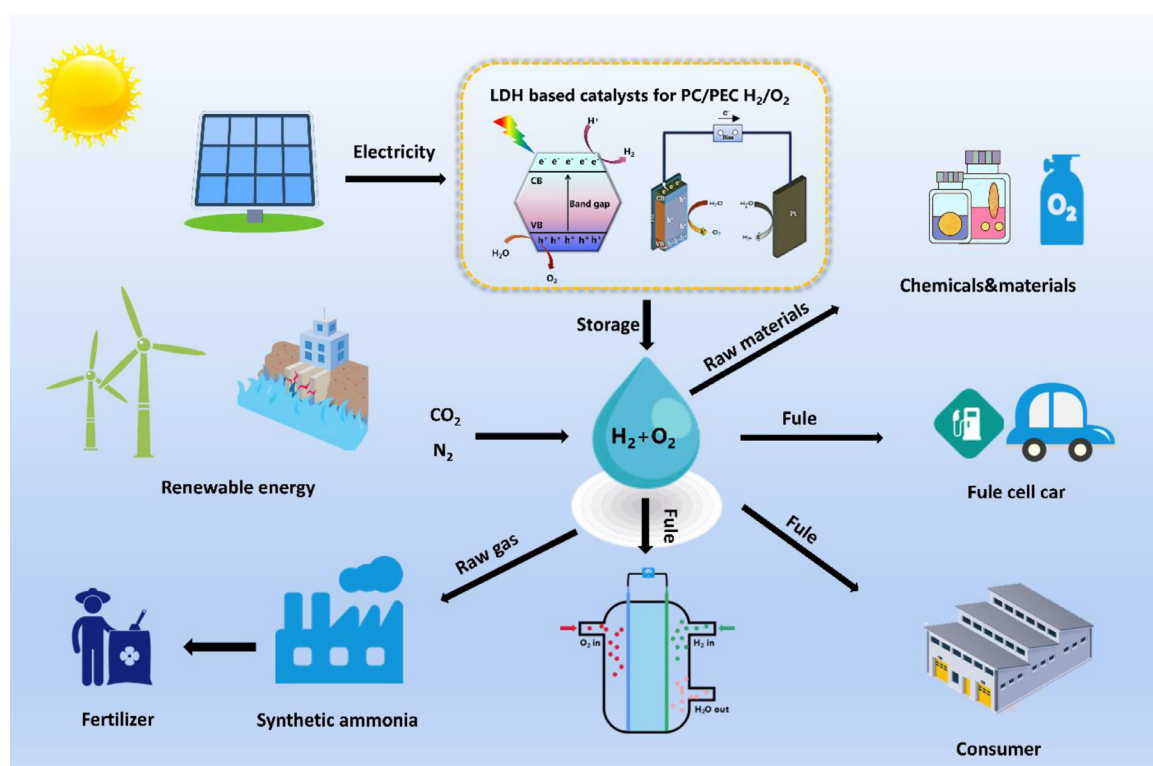


Fig. 1. A sustainable energy system based on an integrated PC/PEC water splitting system for renewable fuel generation.

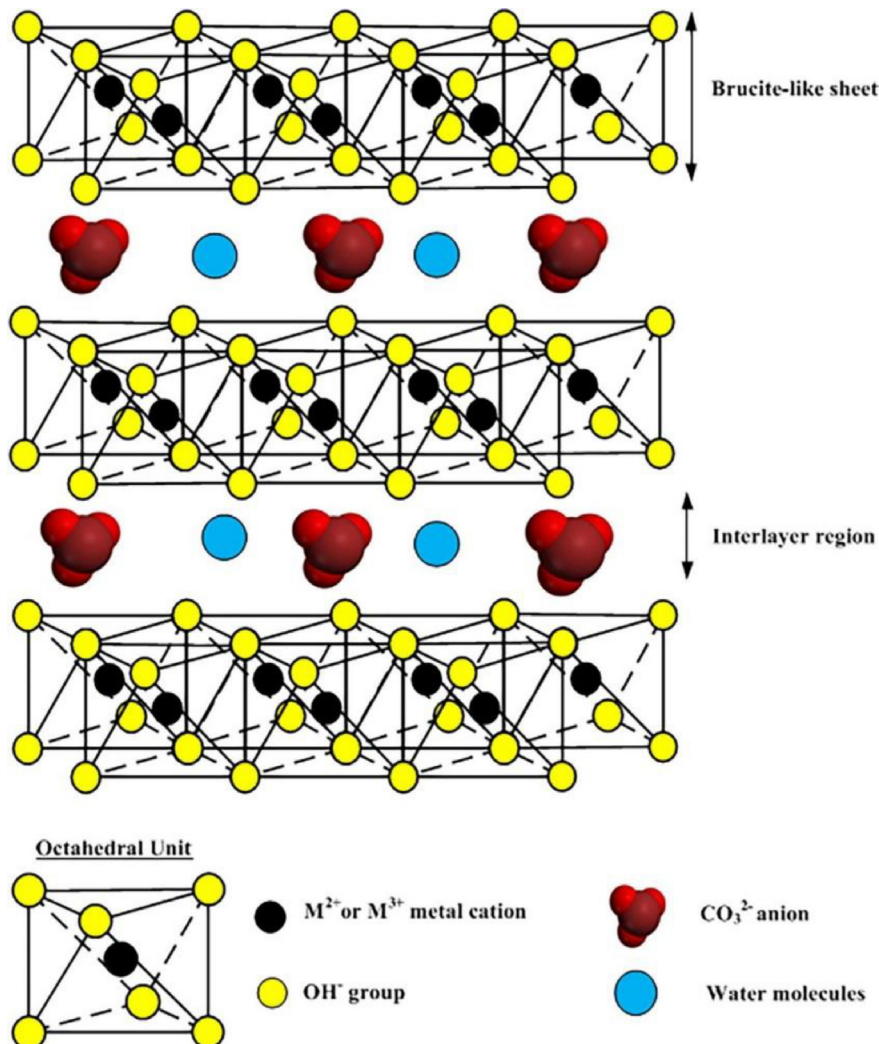


Fig. 2. The structure of a layered double hydroxide with interlayer CO_3^{2-} anions.

facilitating the essential reaction between the reactants and the photoinduced charge carriers [40,41]. Hence, LDH has been regarded as one of the most promising photocatalyst materials. In addition, other semiconductors (e.g. TiO_2 , BiVO_4) coated with high redox activity LDH photo(electro)catalysts layers are crucial components for boosting the water oxidation/reduction performance of semiconductor-based photocatalysts and photoelectrocatalysts [42,43]. The transitional metal elements (such as Fe, Co, and Ni) in LDH layers serve as the surface catalytic sites for oxygen generation process. The engineering of LDH-cocatalysts can give rise to the reduced photocurrent onset potential, enriched active sites, accelerated reaction kinetics, and suppressed corrosion [44].

The rapid development on LDH-based catalysts could be regarded as a “breakthrough” for renewable energy production and storage. Some excellent reviews related to the application of LDH-based advanced materials for water spilling, CO_2 reduction, supercapacitor, and battery have been published. However, early reviews have mainly focused on the electrocatalytic water spilling using LDH materials [32,45–55]. Researches on indexed journals concerning the keywords “layered double hydroxide” and “water splitting” are in a great amount and increasing rapidly year by year between 2010 and 2020 (Fig. 3). In 2016, Zhao et al [56] published the extensive “Layered Double Hydroxide Nanostructured Photocatalysts for Renewable Energy Production” review covering 96 references, which comprehensively summarized the utilization of

LDH derived materials for water splitting, CO_2 reduction and alcohol photo reforming. Recently, the use of LDH-based materials for photo(electro-) catalytic applications has been reviewed by Jiao et al [57]. But the content of PC/PEC water splitting is thin and concise. Seen from Fig. 3, the ever-growing researches on the use of LDH catalysts in water splitting require the timely updates of recent research, especially in the direction of photo-catalytical water splitting. Hence, it is of great importance for us to summarize the advanced progress about using LDHs based catalyst for photo/photoelectro-catalytic water splitting in a more accessible and detailed way. Herein, this review contains the fundamental aspects of PC and PEC water splitting under UV-Vis and special focus is given to LDH-based efficient and affordable catalysts. The quite disperse literatures regarding LDH photocatalysts or photoelectrocatalysts have been classified as Bi/ter-nary LDH, $\alpha\text{-Fe}_2\text{O}_3$ /LDH, BiVO_4 /LDH, TiO_2 /LDH, WO_3 /LDH, CdS /LDH, MoS_x /LDH, C_3N_4 /LDH, and GO/LDH (Fig. 4, and Tables 2 and 3). We will focus on the advantages as well as limitations of the most frequently used LDH based water-splitting photocatalysts and photoelectrocatalysts, major strategies applied to overcome these shortcomings. Special attention is placed on the most important design issues, the correlation among nanostructuring, composition engineering, physical/chemical properties, approaches, computational breakthroughs and functional mechanism that enable outstanding PC/PEC catalytic behaviors through rational engineering of nanoscale

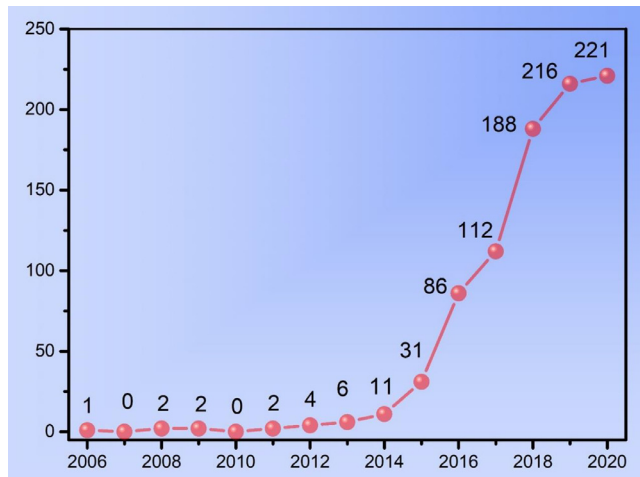


Fig. 3. Number of papers published on photocatalytic and photoelectrochemical water splitting by LDH based materials from 2006 to 2020 (Data was found from web of science database on November 1st, 2020 using water splitting and Layered double hydroxides as key words).

LDH photo-active materials. Finally, by integrating our systematic overview and analyses of all the representative related studies surveyed from 2015 to 2020, we will provide our insights for constructing robust LDH-based photocatalysts. The understanding and discussion presented in this review are believed not only beneficial for the rational design of efficient LDH based catalysts for PC/PEC water splitting system but also meaningful for other types of PC/PEC system used for solar energy conversion (e.g. CO₂ reduction, N₂ fixation) and water remediation (e.g. photocatalytic degradation, photoelectrochemical oxidation).

2. Strategies to prepare LDHs

In order to give the reader a comparative overview on the synthetic methods of LDH based semiconductors, the most-recent LDH catalysts that are applied as water splitting photocatalysts and photoelectrocatalysts are well summarized in [Tables 2 and 3](#). By summarizing the methods provided in these literatures, the most frequently used methods are mainly Co-precipitation, hydrothermal method, sol-gel method, solvothermal method, and

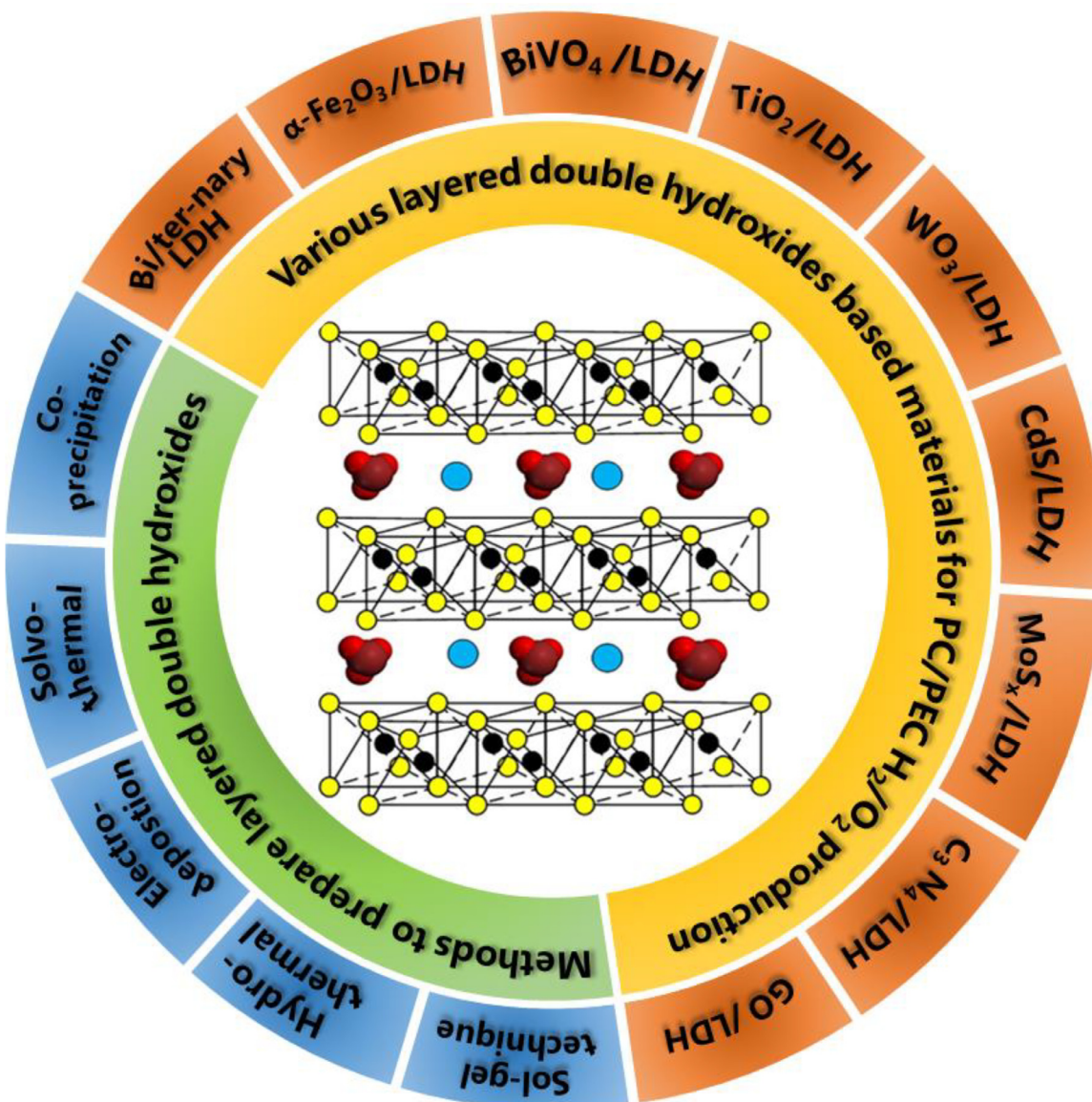


Fig. 4. Schematic representation of typical synthetic methods and typical LDH based photocatalysts for PC/PEC H₂/O₂ production.

Table 1

Comparison of available approaches for LDH based photocatalysts preparation.

Fabrication strategy	Advantages and Disadvantages
Co-precipitation method	<ol style="list-style-type: none"> It can directly obtain nano LDHs powder nanomaterials with uniform chemical composition [11,57]. Easily fabricate nano LDHs powder nanomaterials with small particle size and uniform distribution [57,62]. The morphological control of the synthetic LDH material would be very unstable [52].
Hydro/solvothermal method	<ol style="list-style-type: none"> The structure and morphology tuning of LDH to be fabricated is much easier [38,52]. High particle purity, good distribution, ideal crystal form and controllability [57]. Various different morphologies and dimensions LDHs can be fabricated via controlling the reaction time, aging temperature as well as adding some structural guide reagents [57]. Solvothermal method avoids the shortcoming that hydrothermal method is not appropriate for preparing water-sensitive catalysts [63]. Critical reaction conditions: High pressure and high temperature [58]. Low yield in the case of the urea method [60].
Sol-gel technique	<ol style="list-style-type: none"> High purity and homogeneity [59,64]. This method exhibits prospective manage over the textural and surface characteristics of the composites [59]. The uniformity and structural performance of the resulting solid can be controlled at the preparations level via changing the precursors, synthesis temperature, reaction time as well as reactant species [57].
Electrodeposition	<ol style="list-style-type: none"> No additional reagents beyond the metal precursors are needed to induce the generation of hydroxide species, resulting the binder-free nanostructure [65–67]. The LDH films can be deposited on various active substrates with strong interfacial adhesion in situ at room temperature, which is beneficial for subsequent treatment [68,69]. The nucleation density, thickness, orientation, and morphology of deposition products can be easily controlled by the applied potential/current, and additives of the deposition solution [70]. Electrodeposition is time-saving, flexible, controllable and environmental friendliness, showing great potential in large-scale material production [71]. It is difficult to prepare the designed nanostructure and composition only by the electrodeposition, thus applying assistive process or novel templates is still an effective strategy [72].

electrodeposition method (Table 1). The former methods (Co-precipitation, hydrothermal method, sol-gel method, solvothermal method) to prepare photocatalytic or photoelectrocatalytic LDHs-based materials have been described in other reviews [57–61]. So in this section, we emphasized the characteristics of electrodeposition synthesis strategy. The LDH materials tabulated here are within the last six years (2015–2020) and particularly synthesized for suspending photocatalyst and photoanode.

2.1. Electrodeposition

Seen from Table 3, cathodic electrodeposition was the most frequently used method to prepare LDH photo-electro-catalysts. Cathodic electrodeposition is performed under a negative applied potential in a three-electrode cell setup as shown in Fig. 5. Typically, the electrolyte solution was prepared by dissolving corresponding metallic nitrate in distilled water. The shifting current can initiate the NO_3^- reduction process at the cathodic surface dur-

ing electrodeposition, leading to the generation of OH^- ions. Ultimately, the pH level near the working electrodes increases, starting the precipitation of metal ions to generate LDHs films (Fig. 5). Recently, a series of high-purity LDHs materials prepared via electrodeposition method have been considered as an optional photo(electro-) catalysts. For example, Wang et al. [73] successfully synthesized two kinds of $\text{BiVO}_4/\text{Ni-Co}$ LDH heterostructure composites at -0.7 V vs. Ag/AgCl and -1.0 V vs. Ag/AgCl . It was obvious that the photocurrent of $\text{BiVO}_4/\text{Ni-Co}$ LDH (-1.0 V) photoanode was smaller than $\text{BiVO}_4/\text{Ni-Co}$ LDH (-0.7 V). This was due to the smaller LDH nanosheet formed on $\text{BiVO}_4/\text{Ni-Co}$ LDH (-0.7 V) surface, facilitating the hole transfer. Fan et al. [74] deposited the Ni-Co LDH on C_3N_4 surface under -1 V vs. SCE with different electric quantity of 5, 10, 15, 30 mC and denoted as g-CN/LDH-1, g-CN/LDH-2, g-CN/LDH-3 and g-CN/LDH-4, respectively. It was found that only small amount of LDH wrinkles generated in g-CN/LDH-1. As the LDH deposition electric quantity gradually increased to 10 mC, the LDH nanosheets were dispersed the entire g-CN film equably except for the top of the large g-CN spheres. The more deposited electric quantity led excess LDH nanoflakes to be anchored onto the whole g-CN framework, resulting in high recombination rate. Ultimately, the g-CN/LDH-2 displayed the superior photocatalytic O_2 evolution.

2.2. Other synthesis strategy

The researchers have also tried other methods, such as drop casting [75–77] and sonication technique [78,79]. Sinclair et al. [77] used a drop casting method to deposit Ni-Fe LDH nanosheets (ca. 12 nm diameter) on BiVO_4 photoanode. Typically, a certain amount of LDH or exfoliated LDH nanosheets solution was loaded on spin-cast $\alpha\text{-Fe}_2\text{O}_3$ or BiVO_4 film coated FTO substrate by drop casting using a pipette. After drying at suitable temperature, these photoanodes can be directly used for further PEC research content. Li et al. [78] synthesized a catalyst for the coupling of $\text{Zn}_{x}\text{Cd}_{1-x}\text{S}$ nanoparticles with Co-Al LDH used a simple ultrasonic treatment. An ethanol solution containing these 2 contents were stirred for 30 min and further sonicated for 90 min under room temperature. Then the as-prepared solution was immersed in a water bath under 80°C to evaporate the ethanol. The major advantage of this conventional method is short reaction time and positive effect on primary nucleation [80].

As demonstrated above, various reasonable methods have been used for fabricating the specific LDH photo(electro)catalysts. Although co-precipitation and sol-gel methods can construct functional LDHs in a large scale, it is not easy to prepare functional LDHs materials with the targeted micro-nano structure. In the cases of solvothermal and hydrothermal routes, the time-consuming of production and the requirement of using high temperature/pressure make both strategies costly, thus hindering their widespread application [66]. Alternatively, the electrodeposition method enables the fabrication process LDH-based photoelectrodes with a short time (hundreds of seconds) at room temperature. Due to the versatility and flexibility of substrates, a great number of core-shell nanostructures with the photoreactive or super conductivity substrate as core and high active LDH as shell can be well-designed. The large-scale photocatalyst synthesis accounts for the majority of studies on photocatalytic water splitting, the production of $< 100 \text{ nm}$ metal oxide, hydroxide, sulfide, and phosphate nanoparticles in the kg h^{-1} scale has been readily realized via the continuous hydrothermal flow synthesis method [81]. Combined with the high performance of LDH for PC/PEC hydrogen production, it is believed that more efforts shall be committed to translate the basic research findings to commercial applications.

Table 2Summary of LDH based materials in photocatalytic H₂/O₂ production.

Photocatalyst	Synthesis methods	Catalyst dosage/reaction time	Light intensity	Reaction solution	Activity		Ref
					H ₂ evolution	O ₂ evolution	
<i>Bi/ter-nary LDH</i>							
Mg-Al LDH	Co-precipitation	40 mg/2h	Vis/300 W Xe lamp	40 mL 20 vol% methanol	2.7 $\mu\text{mol h}^{-1}\text{g}^{-1}$		[98]
Ni-Fe LDH	Hydrothermal	50 mg/4h	Vis/300 W Xe lamp	100 mL 10 vol% TEOA	0.045 mmol h ⁻¹ g ⁻¹		[99]
Ni-Fe LDH	Liquid-phase	30 mg/1h	Vis/125 W Hg lamp	30 mL 10 vol% methanol	1.52 mmol h ⁻¹ g ⁻¹		[94]
Ni-Cr LDH	Co-precipitation	20 mg/2h	Solar light/300 W Xe lamp	100 mL 0.01 g AgNO ₃		1037 $\mu\text{mol h}^{-1}\text{g}^{-1}$	[85]
Ni-Ti LDH	Reverse microemulsion	50 mg/30 min	Vis/300 W Xe lamp	50 mL 0.01 M AgNO ₃		2148 $\mu\text{mol h}^{-1}\text{g}^{-1}$	[100]
Zn-Cr LDH	Co-precipitation	40 mg/3h	Vis/300 W Xe lamp	40 mL 0.01 M AgNO ₃		1 $\mu\text{mol h}^{-1}\text{g}^{-1}$	[101]
Tb-Zn-Cr LDH	Co-precipitation	45 mg/1h	Vis/150 W Xe arc lamp	AgNO ₃ (0.01 M)		1022 $\mu\text{mol h}^{-1}\text{g}^{-1}$	[102]
Mn-Zn-Al LDH	Co-precipitation	10 mg/1h	Vis/300 W Xe arc lamp	30 mL 0.01 M AgNO ₃		5.31 $\mu\text{mol h}^{-1}\text{g}^{-1}$	[103]
<i>Metal oxides/LDH</i>							
TiO ₂ /LDH							
TiO ₂ /Zn-Al MMO	Co-precipitation	20 mg/150 min	Vis/400 W metal halide	100 mL 0.001 mol/L AgNO ₃		371 $\mu\text{mol h}^{-1}\text{g}^{-1}$	[104]
TiO ₂ /Zn-Al LDH	Co-precipitation	20 mg/150 min	Vis/400 W metal halide	100 mL 0.001 mol/L AgNO ₃		255 $\mu\text{mol h}^{-1}\text{g}^{-1}$	[104]
TiO ₂ /Co-Al LDH	Hydrothermal	-/2h	Vis/300 W Xe lamp	100 mL 0.01 g AgNO ₃		2.24 mmol h ⁻¹ g ⁻¹	[105]
<i>Metal sulfide/LDH</i>							
CdS/LDH							
CdS/Ni-Fe LDH	Co-precipitation	50 mg/3h	Solar light/300 W Xe lamp	50 mL 10 vol% methanol	469 $\mu\text{mol h}^{-1}\text{g}^{-1}$		[106]
CdS/Ni-Fe LDH	Hydrothermal	1 mg/5h	Solar light/150 W Xe lamp	15 mL 20 vol% Lactic acid	72 mmol h ⁻¹ g ⁻¹		[107]
CdS/BiVO ₄ /Mg-Al LDH	Sonication	20 mg/1h	Solar light/125 W Hg lamp	20 mL 0.05 M AgNO ₃	33 mmol h ⁻¹ g ⁻¹	17.3 mmol h ⁻¹ g ⁻¹	[79]
ZnS/Mn-Zn-Al LDH	Co-precipitation	15 mg/1h	Vis/300 W Xe arc lamp	30 mL 0.01 M AgNO ₃		12.46 $\mu\text{mol h}^{-1}\text{g}^{-1}$	[103]
CdTe/CdS/Ni-Fe LDH	Co-precipitation	20 mg/10 h	Vis/300 W Xe lamp	30 mL 20 mg/L H ₂ A	0.06 $\mu\text{mol h}^{-1}\text{g}^{-1}$		[108]
FeNiS-CdTe/CdS Zn _x Cd _{1-x} S/Co-Al LDH	Sulfur treatment	20 mg/10 h	Vis/300 W Xe lamp	30 mL 20 mg/L H ₂ A	26.5 $\mu\text{mol h}^{-1}\text{g}^{-1}$		[108]
	Sonication	10 mg/5h	5 W LED white light	30 mL 10 vol% lactic acid	30.32 mmol h ⁻¹ g ⁻¹		[78]
NiS/Mg-Al LDH	Co-precipitation	40 mg/3h	Vis/300 W Xe lamp	40 mL 20 vol% methanol	35.8 $\mu\text{mol h}^{-1}\text{g}^{-1}$		[98]
P-CdS/Ni-Co LDH	Hydrothermal	-/4h	Vis/300 W Xe lamp	100 mL 10 vol% lactic acid	8.665 mmol h ⁻¹ g ⁻¹		[109]
<i>MoS_n/LDH</i>							
MoS ₂ /Ni-Fe LDH	Hydrothermal	20 mg/2h	Vis/125 W Hg lamp	30 mL 10 vol% methanol	13.75 mmol h ⁻¹ g ⁻¹		[94]
MoS _x /Co-Al LDH	Photoreduction	-/320 min	Vis/300 W Xe lamp	100 mL of 15 vol% TEOA	90 mmol h ⁻¹ g ⁻¹		[110]
<i>Carbon materials/LDH</i>							
g-C ₃ N ₄ /Ni-Co LDH	Weight impregnation	50 mg/8h	Vis/300 W Xe lamp	100 mL 0.17 g AgNO ₃		100 $\mu\text{mol h}^{-1}\text{g}^{-1}$	[111]
g-C ₃ N ₄ /Mg-Fe MMO	Thermal decomposition	30 mg/4h	Vis/150 W Xe lamp	100 mL 10% trichloroamine	1.26 mmol h ⁻¹ g ⁻¹		[112]
g-C ₃ N ₄ /Ni-Fe-S	Hydrothermal	50 mg/2h	Vis/300 W Xe lamp	100 mL 10 vol% TEOA	1.152 mmol h ⁻¹ g ⁻¹		[99]
g-C ₃ N ₄ /Ni-Fe LDH	Hydrothermal	50 mg/2h	Vis/300 W Xe lamp	100 mL 10 vol% TEOA	0.337 mmol h ⁻¹ g ⁻¹		[99]
N-rGo/g-C ₃ N ₄ /Ni-Fe LDH	Hydrothermal	20 mg/2h	Vis/125 W Hg lamp	30 mL 10 vol% of methanol	1254 $\mu\text{mol h}^{-1}\text{g}^{-1}$	640 $\mu\text{mol h}^{-1}\text{g}^{-1}$	[113]

3. Basics of photocatalytic and photoelectrochemical water splitting

Hydrogen evolution reaction (HER) and oxygen evolution reaction (OER) are two important half reactions of water splitting. For the HER and the OER reaction, the energy CB energy level has to be more negative than the hydrogen evolution potential (0 V vs. NHE) and the VB energy level needs to be more positive than the water

oxidation potential (1.23 V vs. NHE), respectively. Photocatalytic water splitting mechanism can be elaborated as following steps (Fig. 6)[82]: First, the electrons of LDHs can be excited and transferred from valence band (VB) to conduction band (CB) after activated by incident light. Meanwhile, the holes of LDHs are left in the VB, therefore generating electron-hole pairs (stage a and b). The photoinduced electrons and holes subsequently travel to the photocatalyst surface (stage c and d), while some of them recom-

Table 3

Summary of LDH based materials in photoelectrocatalytic water splitting.

Photo-electrode	Synthesis methods	Electrolyte	Photocurrent (mA cm^{-2})	IPCE	Ref
<i>Binary LDH</i>					
Ni-Al LDH	Nitrogen plasma	1 M KOH	1.52 mA cm^{-2} at 1.23 V vs. RHE	8.23%	[114]
Co-Fe LDH	Co-precipitation	1 M KOH	1.38 mA cm^{-2} at 1 V Vs Ag/AgCl	-	[115]
DAS-DNS/Zn-Al LDH	Co-precipitation	0.5 M Na_2SO_4	4.67 mA cm^{-2} at 0.8 V vs. SCE	1.31% at 365 nm	[116]
<i>Metal oxides/LDH</i>					
α - Fe_2O_3 /LDH					
Sn^{4+} - α - Fe_2O_3 /Zn-Co LDH	Dip coating	1 M KOH	2.00 mA cm^{-2} at 1.50 V vs. RHE	28.71% at 380 nm	[117]
α - Fe_2O_3 /Ni-Mn LDH	Drop casting	1 M NaOH	1.98 mA cm^{-2} at 1.23 V vs. RHE	-	[76]
α - Fe_2O_3 /Ni-Fe LDH	Electrodeposition	0.5 M Na_2SO_4	141 $\mu\text{A cm}^{-2}$ at 1.23 V vs. RHE	-	[118]
α - Fe_2O_3 /Ni-Fe LDH	Drop casting	1 M NaOH	0.38 mA cm^{-2} at 1.0 V vs RHE	-	[75]
α - Fe_2O_3 /Co-Al LDH	Hydrothermal	1 M NaOH	2 mA cm^{-2} at 1.23 V vs. RHE	-	[119]
α - Fe_2O_3 /Co-Al LDH	Co-precipitation	1 M KOH	4.30 mA cm^{-2} at 1.23 V vs. RHE	-	[120]
F- Fe_2O_3 /Co-Al LDH	CBD	1 M KOH	2.46 mA cm^{-2} at 1.23 V vs. RHE	47.66% at 300 nm	[121]
α - Fe_2O_3 /Ni-Co-Al LDH	Hydrothermal	0.5 M K_2HPO_4	2.56 mA cm^{-2} at 1.23 V vs. RHE	-	[122]
Ti- α - Fe_2O_3 /Zn-Co LDH	Electrodeposition	1 M KOH	1.73 mA cm^{-2} at 1.23 V vs. RHE	-	[123]
Mn- α - Fe_2O_3 /Ni-Fe LDH	Hydrothermal	1 M NaOH	2 mA cm^{-2} at 1.23 V vs. RHE.	35% at 350 nm	[124]
BiVO_4 /LDH					
CdTe@LDH@ BiVO_4	Hydrothermal	0.1 M PBS	2.23 mA cm^{-2} at 1.23 V vs RHE	43% at 400 nm	[125]
G@LDH@ BiVO_4	Hydrothermal	0.1 M PBS	2.13 mA cm^{-2} at 1.23 V vs RHE	52% at 400 nm	[126]
BiVO_4 /CD/Ni-Fe LDH	Electrodeposition	0.5 M PBS	2.84 mA cm^{-2} at 1.23 V vs RHE	40.94% at 380 nm	[127]
LDH/Au@ SiO_2 / BiVO_4	Hydrothermal	0.1 M PBS	1.92 mA cm^{-2} at 1.23 V vs RHE	-	[128]
Au@ SiO_2 /LDH/ BiVO_4	Hydrothermal	0.1 M PBS	1.25 mA cm^{-2} at 1.23 V vs RHE	-	[128]
Mo-BiVO ₄ /Ni-Fe LDH	Electrodeposition	0.1 M Na_2SO_4	1.58 mA cm^{-2} at 1.23 V vs RHE	64% (420 nm)	[129]
BiVO_4 /rGO/NiFe-LDH	Electrodeposition	0.1 M PBS	1.13 mA cm^{-2} at 1.23 V vs. RHE	51.08% at 420 nm	[130]
BiVO_4 /Co-Fe-LDH	Electrodeposition	1 M KOH	2.48 mA cm^{-2} at 1.23 V vs RHE	-	[131]
BiVO_4 /NiCo-LDH	Electrodeposition	0.5 M Na_2SO_4	3.4 mA cm^{-2} at 1.23 V vs RHE	59% at 380 nm	[73]
TiO_2 /LDH					
TiO_2 /Co-Ni LDH	Electrodeposition	0.1 M Na_2SO_4	4.4 mA cm^{-2} at 1.23 V vs. RHE	1.55% at 350 nm	[132]
TiO_2 /Co-Cr LDH	Electrodeposition	1 M KOH	0.93 mA cm^{-2} at 1.23 V vs. RHE	81% at 360 nm	[133]
TiO_2 /Zn-Fe LDH	PED	0.5 M Na_2SO_4	1.51 mA cm^{-2} at 1.23 V vs. RHE	4.86% at 400 nm	[134]
TiO_2 /Co-Fe LDH	Co-precipitation	1 M KOH	6.3 mA cm^{-2} at 1.23 V vs. RHE	-	[115]
TiO_2 /graphene/Ni-Fe LDH	Electrodeposition	0.5 M Na_2SO_4	1.74 mA cm^{-2} at 0.6 V vs. RHE	5.12% at 400 nm	[135]
Cu_7S_4 / TiO_2 /Co-Cr LDH	Hydrothermal	0.5 M Na_2SO_4	2.04 mA cm^{-2} at 1.23 V vs. RHE	17% at 360 nm	[136]
TiO_2 @Ni-Co LDH	Hydrothermal	0.5 M PBS	0.33 mA cm^{-2} at 1.23 V vs RHE	-	[137]
WO_3 /LDH					
WO_3 /Ag/Zn-Fe LDH	Electrodeposition	0.1 M PBS	1.15 mA cm^{-2} at 1.23 V vs. RHE	82% at 360 nm	[138]
CD/ WO_3 /Ni-Fe LDH	Deposition	0.2 M Na_2SO_4	1.43 mA cm^{-2} at 1.23 V vs. RHE	38.6% at 405 nm	[139]
WO_3 /Ni-Fe LDH	Hydrothermal	0.2 M Na_2SO_4	1.10 mA cm^{-2} at 1.20 V vs. SCE	-	[140]
WO_3 / Fe_2O_3 /Ni-Fe LDH	Hydrothermal	1 M NaOH	3.0 mA cm^{-2} at 1.8 V vs RHE	-	[141]
<i>Carbon materials/LDH</i>					
g - C_3N_4 /LDH					
g - C_3N_4 /Zn-Cr LDH	Co-precipitation	0.1 M Na_2SO_4	26 $\mu\text{A cm}^{-2}$ at 1.23 V vs RHE		[39]
g - C_3N_4 /N-GO/Ni-Fe LDH	Hydrothermal	0.01 M Na_2SO_4	162.3 $\mu\text{A cm}^{-2}$ at 1.4 V vs RHE	2.5% at 350 nm	[142]
g - C_3N_4 /Co-Mn LDH	Co-precipitation	1 M KOH	40 mA cm^{-2} at an overpotential of 350 mV		[143]
Co-Fe-LDH- g - C_3N_4	Hydrothermal	1 M KOH	0.196 mA cm^{-2}		[144]
g - C_3N_4 /Ni-Co LDH	Electrodeposition	0.2 M Na_2SO_4	11.8 $\mu\text{A cm}^{-2}$ at 0.6 V vs. SCE		[74]

BBS: Borate buffer solution

CBD: Chemical bath deposition

IPCE: Incident photon-to-current efficiency

PBS: Phosphate buffer solution

PED: Photo-assisted electrodeposition

bined in this step. Finally, water molecules are oxidized by holes (stage e) or reduced by electrons (stage f) at the surface of LDHs catalysts. These steps affect the overall efficiency of water splitting based on a semiconductor-based photocatalyst. However, the major challenge in these steps is the charges (e^-/h^+) recombination and then the efficiency of HER/OER is restrained. Consequently, photocatalytic H_2/O_2 production is usually studied in the presence of sacrificial reagent to consume electrons or holes. Strategies such as metal codoping, constructing heterojunction, shrinking particle size have also been applied for suppressing recombination of charges carriers [83]. The use of molecular photosensitizers in PEC system is another way to facilitate light-driven charge separation and has been extensively applied in TiO_2 PEC system [84]. However, this strategy in LDH PEC device is far less developed.

In a series of insightful fundamental studies by Xu et al., the reaction mechanism of LDHs for photocatalytic OER was investigated. H_2O molecules can be easily adsorbed on the LDH sheets

via the help of surface hydrophilic hydroxyl group. Then the adsorbed H_2O molecules are deprotonized to generate hydroxyl radicals. The resulting hydroxyl radical is subsequently oxidized to yield $\cdot\text{O}$, which then reacts with another H_2O molecule for the generation of $\cdot\text{OOH}$. At last, O_2 is released from $\cdot\text{OOH}$ (Fig. 7). The free energy difference of all adsorbed intermediates (OH^* , O^* , and OOH^*) on the (003) surface of LDH was investigated by using the density functional theory plus U (DFT + U) method. As illustrated in Fig. 7, the combination of $\cdot\text{O}$ and H_2O molecules to generate $\cdot\text{OOH}$ was the most difficult step to proceed for $\text{Zn}_2\text{Ti-Cl-LDH}$, $\text{Cu}_2\text{Ti-Cl-LDH}$, $\text{Cu}_2\text{Cr-Cl-LDH}$ and $\text{Co}_2\text{Fe-Cl-LDH}$ as ΔG_c was the largest among the four steps. In other words, the rate-determining step was determined to be the generation of OOH^* from O^* for these four LDHs. In the meantime, the formation of $\cdot\text{O}$ was the most difficult step to occur for the other eight LDHs. By the DFT + U method, Xu et al. subsequently calculated the OER driving force of $\text{Ni}_2\text{Cr-Cl LDH}$ (0.594 eV), $\text{Zn}_2\text{Cr-Cl LDH}$

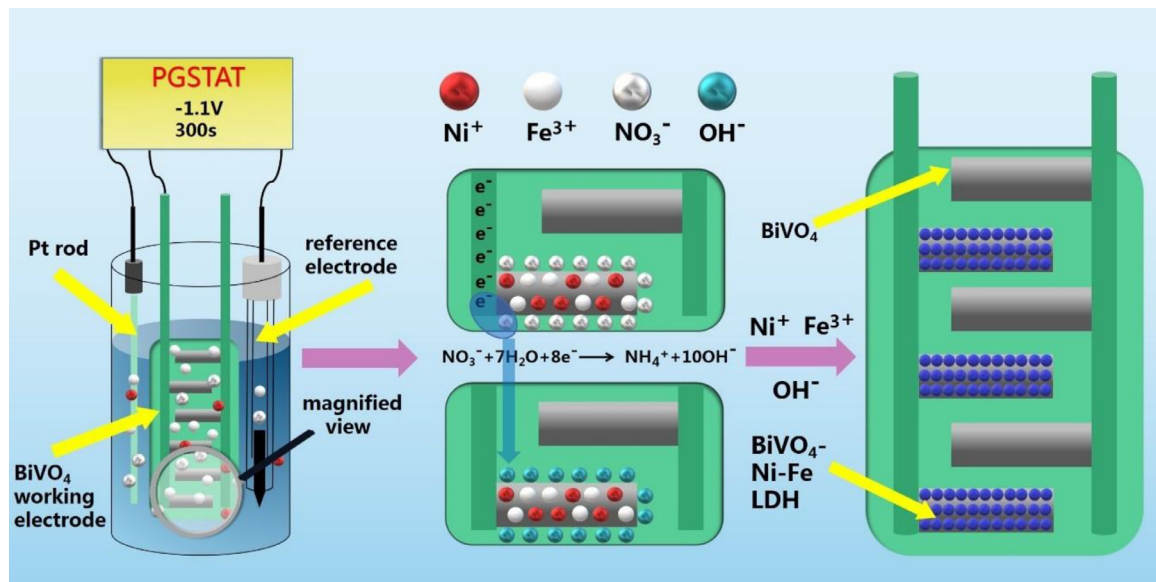


Fig. 5. Fabrication of the BiVO_4/LDH photoanode using cathodic electrodeposition method.

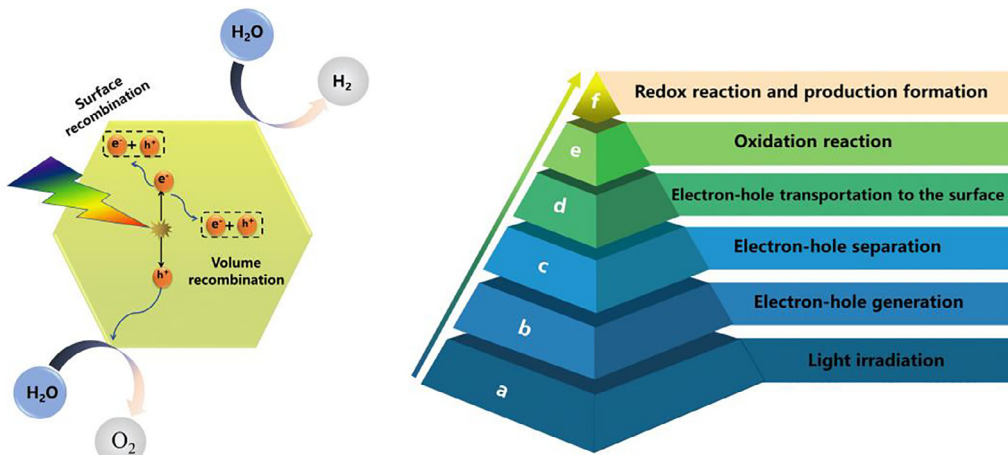


Fig. 6. Main processes in photocatalytic water splitting.

(1.051 eV) and $\text{Mg}_2\text{Cr}-\text{Cl}$ LDH (0.914 eV). The OER overpotential over models $\text{Ni}_2\text{Cr}-\text{Cl}$ LDH, $\text{Zn}_2\text{Cr}-\text{Cl}$ and $\text{Mg}_2\text{Cr}-\text{Cl}$ were determined to be 0.581 V, 0.910 V and 1.351 V, respectively. Therefore, $\text{Mg}_2\text{Cr}-\text{Cl}$ LDH owned a less driving force than its overpotential. Experimental observations further indicated the $\text{Mg}_2\text{Cr}-\text{Cl}$ LDH with no OER activity, which is consistent with the theoretical prediction. Meanwhile, $\text{Ni}_2\text{Cr}-\text{Cl}$ LDH exhibited the highest photocatalytic active oxygen generation performance, reaching up to O_2 generation rate $1037 \mu\text{mol h}^{-1}\text{g}^{-1}$ [85].

An alternative route for H_2O splitting is the photoelectrocatalysis, which integrates photocatalysis and electrocatalysis [58,86]. Since the photoelectrocatalytic water splitting for hydrogen production was first proved by Fujishima and Honda in 1972 [87], PEC water splitting has aroused increasing attention in recent years. The water splitting mechanism over PC and PEC systems are in accordance with each other [88]. Compared to photocatalysis, the photoinduced electrons can jump from the VB of LDHs to the CB, and then be transported to the counter electrode (e.g., Pt) through the external circuit in PEC system. The holes reach the surface of the photoanode to oxidize water to produce O_2 on the semi-

conductor surface, whereas the electrons at the counter electrode to reduce water molecules into hydrogen, as illustrated in Fig. 8a. Therefore, the external bias potential can significantly facilitate the separation of the photoexcited electron-hole pairs, thus improving the photoelectrocatalytic hydrogen production efficiency. However, only a small quantity of photogenerated holes join in water oxidation because the holes suffer decrease processes for charge recombination both in bulk and on surface, which finally reduces the solar-to-hydrogen (STH) transition efficiency of the PEC cell. As shown in Fig. 8b, the efficiency of the different procedures included in water oxidation on a photoanode availing the yielded photocurrent; sunlight absorption (η_{abs}), bulk charge separation (η_{tr}), charge transfer to the solid-electrolyte interface (η_{ct}), and reaction efficiency i.e., Faradaic efficiency (η_{F}). Incident photonflux (Φ) and above various efficiencies are directly proportional to photocurrent (J) as: $J = q \cdot \Phi \cdot \eta_{\text{abs}} \cdot \eta_{\text{tr}} \cdot \eta_{\text{ct}} \cdot \eta_{\text{F}}$, where, q is the elementary charge [89]. The incident photon-to-current efficiency (IPCE) also is the another crucial element to estimate photoactive behavior, meaning the photocurrent gathered each incident photon flux as a function of incident-light wavelength. The IPCE could

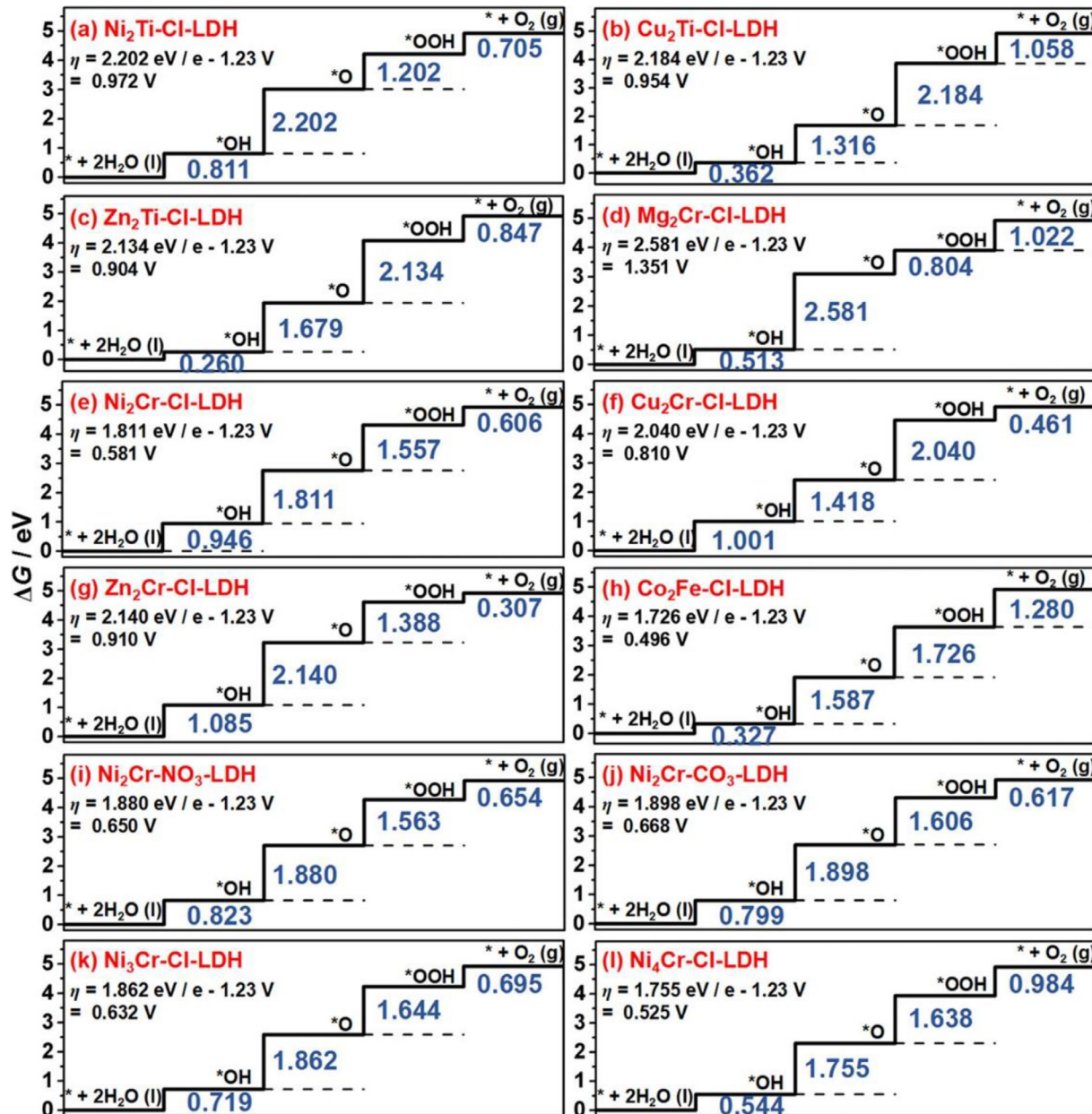


Fig. 7. Standard free energy diagrams for the OER on M^{II}M^{III}/IV-A-LDHs (M^{II} = Mg, Co, Ni, Cu, Zn; M^{III} = Cr, Fe; M^{IV} = Ti; n = 2, 3, 4; A = Cl, NO₃, CO₃). Blue numbers (in eV) represent the Gibbs free energy changes of the corresponding OER elementary steps (adapted with permission from Ref. [85] @Copyright 2016 American Chemical Society).

be computed at a prospective bias voltage as: IPCE = 1240 J/(λ·I) · 100%, where, λ corresponds to the wavelength of incident light and I is the incident light intensity [90].

As opposed to the PC system, the PEC cell generates H₂ and O₂ on the counter electrode (cathode) and the working electrode (anode), respectively (Fig. 8a). Thus this kind of spatial separation of H₂ and O₂ evolutions endow the PEC system with more practical, efficient, and safer properties than PC production systems. From Fig. 9, it can be seen the favorable band alignment between LDH and other typical semiconductors. Integrating two or more semiconductors with well-matched band edge positions is a very efficient strategy to achieve efficient light absorption, electron transport, and photogenerated charge separation in case of semiconductors/LDH hybrids. Hence, in most cases, the LDH materials typically adopted for H₂O photocatalytic H₂/O₂ generation have also been exploited for H₂O photoelectrocatalysis.

4. Various LDH based materials towards light-driven water splitting

We have searched all the PC/PEC water splitting studies conducted mainly between 2015 and 2020 on the application of various types of LDH photocatalysts with controllable composition. Considering the similar basic reaction steps and the pivotal role of catalysts in PC/PEC water splitting process, we clustered our discussion about these novel LDH based materials into four basic categories: Bi/ter-nary LDH, Metal oxides/LDH (α -Fe₂O₃/LDH, BiVO₄/LDH, TiO₂/LDH, WO₃/LDH), Metal sulfide/LDH (CdS/LDH, MoS_x/LDH) and Carbon materials/LDH (C₃N₄/LDH, GO/LDH). In addition, according to our recent review [62], Bi/ter-nary LDH, C₃N₄/LDH, TiO₂/LDH, and Metal sulfide/LDH are also frequently used in heterogeneous photocatalysis for water depollution. Nowadays, the most commonly used LDH co-catalysts are Ni-Fe LDH (seen

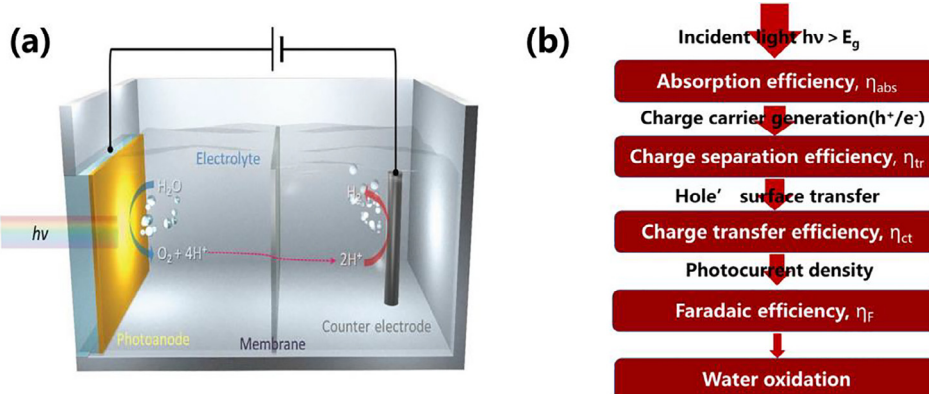


Fig. 8. (a) Schematic of photoelectrochemical cell for solar water splitting. (adapted with permission from Ref. [91] @Copyright 2019 Wiley). (b) Block diagram for different steps involved in water oxidation on photoanode. (adapted with permission from Ref. [89] @Copyright 2019 Wiley).

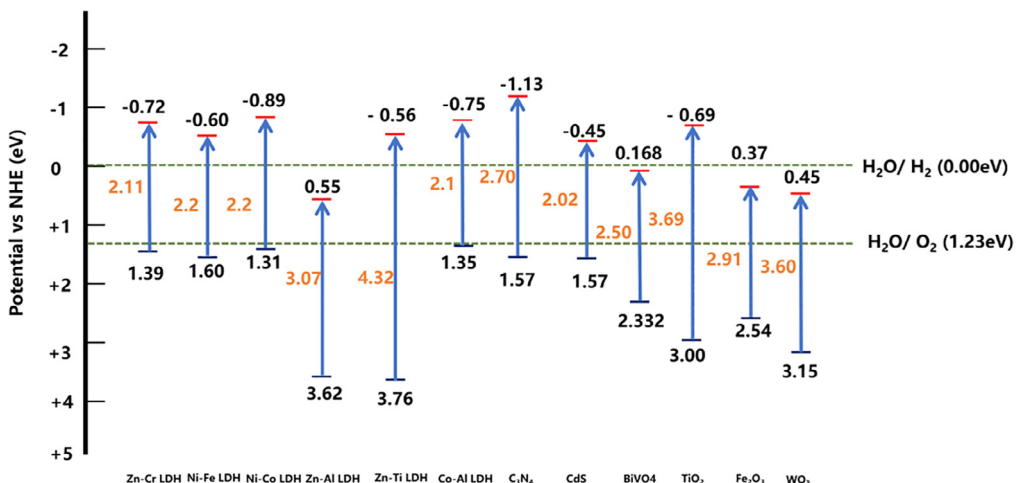


Fig. 9. Band gap structures of several typical LDH photocatalysts.

from table 3). To some extent, this is the direct result of four unique characteristics: (i) the earth-abundant of Ni and Fe [42,92,93], (ii) a reasonable narrow band gap energy [94], (iii) its transparency towards visible light irradiation [95,96] and (iv) excellent electrocatalytic activity and durability for OER catalysis [46,97].

4.1. Bi/ter-nary LDH

Mostafa et al. [145] reported that the Co-Ti LDH nanorods is a promising photocatalyst to efficiently generate O₂ under UV-vis and Infrared (IR) light without adding scavenger.

The multilayered structure of Cobalt titanate nanorods LDH, surface, and interlayer water and interlayer carbonate molecules greatly improved the IR absorbance/transferring through the photocatalyst particles for maximum water splitting. Consequently, these nanorods were fairly active for IR irradiation and induced O₂ production with a rate of 5300 μmol g⁻¹ h⁻¹ at 55 °C for 3 h. Fu and coworkers prepared a series of active ternary Tb-Zn-Cr-LDHs with (Tb + Zn)/Cr ratio 2.0, while varying the Tb³⁺/(Tb³⁺+Cr³⁺) atomic ratio to 0%, 0.1%, 0.5%, 1%, and 5%, and tested them for oxygen evolution through photocatalytic water splitting under visible-light illumination. The most active material was found to be Tb-Zn-Cr-LDHs with Tb³⁺/(Tb³⁺+Cr³⁺) ratio of 0.5% that exhibited two absorption bands in the visible region at λ_{max} of 410 and 570 nm. Terbium had a great role in photoluminescence intensity, as the

optimum amount of Tb dopant suppressed the recombination of electron-hole pairs, but become the electron-hole recombination centers with an excess amount. The ESR spectra confirmed that the peaks of DMPO-OH of Tb³⁺-doped Zn-Cr LDH materials is much stronger than the undoped Zn-Cr LDH. The increased .OH generation was attributed to the fact that Tb in the LDH matrix played as hole acceptors to facilitate such charge injection and hence accelerated the surface oxidation process. Consequently, the introduction of Tb gave rise to an enhanced oxygen productivity from 543 mmol h⁻¹ g⁻¹ to 1022 mmol h⁻¹ g⁻¹ with the increase of Tb³⁺ doping from 0% to 0.5% at 40 °C for 60 min [102]. After the calcination between 400 ~ 700 °C, the pristine Zn-Al LDH was transformed into a two-phase composite (ZnO/ZnAl₂O₄ or ZnO/Zn₆Al₂O₉) and the crystal size of ZnAl₂O₄ and ZnO slowly increased with the increase of calcination temperature. Although the higher calcination temperature resulted in a higher crystallinity of the material, the yield of H₂ obtained over this photocatalyst was lower than that obtained with the material calcined at 600 °C. The major reason of better photocatalytic H₂-production activity in the case of the Zn-Al MMO catalyst prepared at lower calcination temperature was the higher recombination rate of the ZnO/ZnAl₂O₄ heterojunction in comparison with that of ZnO/Zn₆Al₂O₉ [146]. Furthermore, the effects of compensating anions (CO₃²⁻, Cl⁻, SO₄²⁻ and NO₃⁻) on the performance of Zn-Cr LDH for photocatalytic O₂ evolution from water with AgNO₃ as a sacrificial agent were comparatively investigated. Among various interlayer anions, Cl⁻

intercalated and SO_4^{2-} -intercalated LDH exhibited the highest and the lowest photocatalytic O_2 -production rate, respectively. After photocatalytic reactions, both Ag and AgCl particles were observed in Zn-Cr-Cl LDH, and the new formed Ag/AgCl/LDH composites were proved to be visible light active catalysts. The Zn-Cr- CO_3^{2-} LDH owned twice the surface area of Zn-Cr- NO_3^- LDH, but NO_3^- -intercalated LDH possessed the more robust photocatalytic O_2 evolution activity than that of CO_3^{2-} -intercalated LDH [101].

The attempted use of organic molecules intercalated-LDHs for photoelectrochemical water splitting was reported by Zheng and co-workers in 2015. In their study, the interlayer of Zn-Al LDH was co-intercalated with inexpensive 4,4-diaminostilbene-2,2-disulfonic acid (DAS) (donor) and 4,4-dinitro-stilbene-2,2-disulfonic acid (DNS) (acceptor) anions, resulting in electron donor-acceptor (D-A) system after mixing. Because of the organic $\pi^*-\pi$ electron transition of guest anion, the resulting DAS-DNS/Zn-Al LDH organic-inorganic hybrid materials possessed the broad and strong optical absorption in the absorption of solar light. This kind of combination endowed the resulting photoanode with a 1.31% incident photon-to-current efficiency (IPCE) at 365 nm and enhanced photo-generated current (4.67 mA/cm^2 at 0.8 V vs. SCE) for water splitting. The researchers ascribed the outstanding PEC behavior to the 2D photo-induced electron transfer (PET) under UV-visible-light illumination between the co-intercalated DAS and DNS. In this host-guest configuration, the photo-generated electrons and holes were created by the PET process between DAS and DNS anions under illumination. Subsequently, photo-generated electron transferred from DAS to DNS anions due to the well matched energy level alignment, which is beneficial for the charge separation in the photoanode. Moreover, the positive-charged host layers and oxo-bridges in the LDH further facilitated the separation of electron-hole pairs during the PET process [116].

The attempted use of organic molecules intercalated LDHs for PC/PEC water splitting should be encouraged. In contrast with inorganic-intercalated LDH photocatalysts, the organic molecules intercalated-LDHs could improve the thermo/photostability of photocatalysts due to the UV-shield effect of host layers [147]. In this context, further exploration can be focused on the increased interlayer distance, the improved crystallinity and establishment of the intercalation structure [148]. Notably, the introduction of various defects (oxygen vacancy and cation vacancy) to catalysts surface would have a great effect on electronic properties. Oxygen vacancies can reduce photoelectron-hole recombination [149] and electrochemical impedance [150] and narrow the bandgap [151], which lead to the higher charge transfer efficiency during photocatalysis. Further to oxygen vacancies, metal cation vacancies also would be a significant influence on the photocatalytic activity, owing to their boosted H_2O adsorption [152], various electron and orbital distribution [153]. Therefore, considering the effect of defects on the LDHs, it is expected that effects of the LDHs materials can enhance their PC or PEC water splitting performance.

4.2. Metal oxides/LDH

4.2.1. $\alpha\text{-Fe}_2\text{O}_3$ /LDH

Earth-abundant hematite ($\alpha\text{-Fe}_2\text{O}_3$) was extensively studied and has shown attractive OER performance, which is resulted from the favorable optical bandgap (2.1–2.2 eV) and suitable valence band level. However, the $\alpha\text{-Fe}_2\text{O}_3$ photoanode still suffers from inferior PEC performance, mainly due to inferior charge transfer, short hole migration lengths and slow water oxidation kinetics. In response, surface modification of $\alpha\text{-Fe}_2\text{O}_3$ with oxygen evolution co-catalyst (OEC) is a practical solution for accelerating the occurrence of surface reaction [97]. Except the most investigated expensive noble metals co-catalysts, the LDH materials have also been identified as the high-performance and cost-effective cocatalysts

in photocatalytic H_2/O_2 production. Several means have been applied for the growth of oxy-hydroxide and LDH layers onto hematite nanocomposite, the most common being e.g. hydrothermal method [85,100,154], electrodeposition [123] or drop casting [104] and chemical bath deposition [121].

Notably, the p-type Co-Al LDH integrated with the $\alpha\text{-Fe}_2\text{O}_3$ photoanode not only facilitated electron-hole separation via forming a p-n junction but also capably photoelectrochemically catalyzed the water oxidation reaction, resulting in reduced overpotential and enhanced PEC behavior [120–122]. Upon irradiance, the energy level matching between Co-Al LDH and $\alpha\text{-Fe}_2\text{O}_3$ facilitated the transport of photo-generated holes from the VB of $\alpha\text{-Fe}_2\text{O}_3$ to the VB of Co-Al LDH. These photogenerated holes were trapped by the low valence of Co^{2+} of Co-Al LDH to generate high valence of Co^{3+} or/and Co^{4+} . As a consequence, Co^{3+} and/or Co^{4+} attended the oxidation reaction of the adsorbed $\text{H}_2\text{O}/\text{OH}^-$ at the surface of LDH to produce O_2 and regenerate Co^{2+} . Simultaneously, the photoinduced electrons (e^-) in CB of Co-Al LDH travelled to that of $\alpha\text{-Fe}_2\text{O}_3$. The electrons further travelled to the Pt counter electrode surface through the external circuit, thereby resulting in hydrogen evolution [120,121]. To reveal the place where the water oxidation reaction occurs in $\alpha\text{-Fe}_2\text{O}_3/\text{Co-Al LDH}$, 1D Co-Pi water oxidation cocatalyst was further deposited on $\alpha\text{-Fe}_2\text{O}_3/\text{Co-Al LDH}$, and thus the interspaces between the Co-Al LDH nanosheets were covered with Co-Pi nanoparticles. The photocurrent of the resulting components significantly decreased, compared to those of $\alpha\text{-Fe}_2\text{O}_3/\text{Co-Al LDH}$, primarily due to less immigration of photoinduced holes from Co-Al LDH to Co-Pi. Hence, the relatively layered and open nanostructures of LDH is prerequisite for $\alpha\text{-Fe}_2\text{O}_3/\text{LDH}$ as the PEC water oxidation process on $\alpha\text{-Fe}_2\text{O}_3/\text{Co-Al LDH}$ was proved to occur in the inner interlayers instead of on the Co-Al LDH surface. Interestingly, Co and Al played different roles in the PEC process. Co was believed to act as active reaction sites for PEC water oxidation and Al provided support for the double layered skeleton [119]. By coupling Co-Al LDH with a Fluorine anion doped Fe_2O_3 photoanode, a pronounced cathodic shift of up to 190 mV in the current onset potential relative to $\text{F-Fe}_2\text{O}_3$ was yielded, increasing their photocurrent density to as much as 2.46 mA cm^{-2} at 1.23 V vs. RHE. The doped fluorine anion can effectively remove the surface trapping states partially. Moreover, the surface defects of $\text{F-Fe}_2\text{O}_3$ can be passivated by the Co-Al LDH overlayer, hence leading to the Fermi-level pinning effect, which is beneficial for reducing the onset potential [121]. As further investigation, the PEC water splitting of hematite/Co-Al LDH photoanode was reported to be a function of the high charged and spatial anions of the interlayer guest. Chong and co-workers examined a general relationship between the PEC activities of LDHs/photoanode with the photocurrents of 4 different interlayer anions ($\text{PO}_4^{3-}, \text{SO}_4^{2-}, \text{NO}_3^-, \text{CO}_3^{2-}$). There is a slightly negative shift of the binding energy for CO^{2+} in $\text{PO}_4^{3-}\text{-Co-Al-LDH}/\alpha\text{-Fe}_2\text{O}_3$, indicating the presence of electron-rich Co sites in this configuration. Among these 4 photoanodes, $\text{PO}_4^{3-}\text{-Co-Al-LDH}/\alpha\text{-Fe}_2\text{O}_3$ presented the smallest diameter of the semicircular arc in EIS, indicating the fastest charge transformation. The $\text{PO}_4^{3-}\text{-Co-Al-LDH}/\alpha\text{-Fe}_2\text{O}_3$ photoanode also showed the largest charge separation efficiency, as the anion with higher charges between Co-Al LDH and $\alpha\text{-Fe}_2\text{O}_3$ would cause much more enhancement on the internal static electric field. As a result, intercalation of the Co-Al-LDH/ $\alpha\text{-Fe}_2\text{O}_3$ with PO_4^{3-} catalyst could not only achieve a photocurrent of 4.30 mA cm^{-2} at 1.23 V vs. RHE, but also present the excellent PEC stability under 2 h irradiation in alkaline solution [120]. As compared with $\alpha\text{-Fe}_2\text{O}_3/\text{Co-Al LDH}$ and $\alpha\text{-Fe}_2\text{O}_3/\text{Ni-Al LDH}$, the as-prepared $\alpha\text{-Fe}_2\text{O}_3/\text{Ni-Co-Al LDH}$ showed the smallest charge transfer resistance due to the local structure distortion of MO_6 ($M = \text{Ni}$ or Co) caused by the synergistic effect of Ni and Co. $\alpha\text{-Fe}_2\text{O}_3/\text{Ni-Co-Al LDH}$ showed a lower onset potential than either $\alpha\text{-Fe}_2\text{O}_3/\text{Ni-Al LDH}$ or $\alpha\text{-Fe}_2\text{O}_3/\text{Co-Al LDH}$, which was resulted

from the slightly lower formation energy barrier of M^{3+} ($M = \text{Ni or Co}$, $0 < g < 1$) species than M^{4+} species [122]. The Al^{3+} ions in Ni-Co-Al LDH were inactive and only provided structural support, which is consistency with that of Co-Al LDH [119]. However, the excess loading amount of LDH forms a too thick layer that may hinder the light absorption of $\alpha\text{-Fe}_2\text{O}_3$ and lead to bad charge transfer ability. The overlayer blocks the majority of holes, which leads to the formation of more recombination centers [123,124,155].

Particularly noteworthy was that $\alpha\text{-Fe}_2\text{O}_3$ photoanode loaded with exfoliated Ni-Fe LDH monolayer cocatalyst presented 241 times higher electro chemical surface area than bulk LDH/ $\alpha\text{-Fe}_2\text{O}_3$, which is ascribed to the more uniform loading compared to unexfoliated LDH stacks. Exfoliation or delamination not only provides a larger number of exposed active sites, but also fabricates more edge and corner sites. As a result, exfoliation of LDH increased photocurrent density by 50%, along with a negative shift of the onset potential by 140 mA compared to stacked LDH [75]. Specifically, it deserves to be mentioned that the electronic band structure can be modified through delamination treatment as well [48]. Kim and co-workers applied a facile dry exfoliation using nitrogen plasma exfoliation of bulk Ni-Al LDHs method to fabricate ultrathin Ni-Al nanosheets of mono and dual layers with rich oxygen vacancies and doped nitrogen sites (Fig. 10A). As shown in Fig. 10B, the nitrogen plasma etched Ni-Al LDH exhibited a thickness ranging from 1.37 nm to 1.91 nm, which is much smaller than that of the pristine bulk Ni-Al LDHs (3.90 nm to 6.01 nm). Two new peaks at 398.16 eV and 399.74 eV appeared in the XPS pattern of N-doped Ni-Al nanosheets, which can be referred to the metal-N

(M-N) species ascribing to the substitutional N doping of the lattice O site and the N-O species from interstitial N doping (Fig. 10D). The peaks at approximately 531.4 eV were associated with oxygen vacancy (V_0) in N doped LDH nanosheets (Fig. 10E). The presence of V_0 acted as additional catalytic active sites to improve the adsorption for water oxidation oxygen intermediates such as $-\text{OH}$ and $-\text{OOH}$ onto the nearby low-coordinated Ni ions having weaker metal–oxygen bonds. Besides, the doped nitrogen is beneficial for the adsorption of water oxidation intermediates on V_0 as the doped nitrogen will pull their electrons (Fig. 10F). On the one hand, oxygen vacancies and doped nitrogen can effectively increase charge carrier density at the interface. On the other hand, resistance at the interface for charge transfer was further decreased. As expected, the authors observed that the N-doped Ni-Al nanosheets/hematite photoelectrodes led to the impressive enhancement (about 40%) in photocurrent relative to that of the V_0 -rich Ni-Al LDH nanosheets/hematite (at 1.23 V vs RHE) [114].

Seen from Table 3, most of the $\alpha\text{-Fe}_2\text{O}_3/\text{Ni-Fe LDH}$ hybrid were prepared by electrodeposition and hydrothermal methods. However, due to the quite different redox potentials of Ni and Fe ions, the Ni/Fe ratio during electrodeposition is uncontrollable [156]. As for hydrothermal method, it is hard to control the thickness of LDH [157]. Hence, it is a major challenge to optimize highly-matched $\alpha\text{-Fe}_2\text{O}_3/\text{Ni-Fe}$ interface and this optimized “adaptive-interface” undoubtedly lead to the enhanced PEC properties. In addition, coupling $\alpha\text{-Fe}_2\text{O}_3/\text{LDH}$ photoelectrodes with noble metal (e.g., Au and Ag) can been regarded as an alternative method for enhancing the solar-to-hydrogen conversion efficiency, due to both the

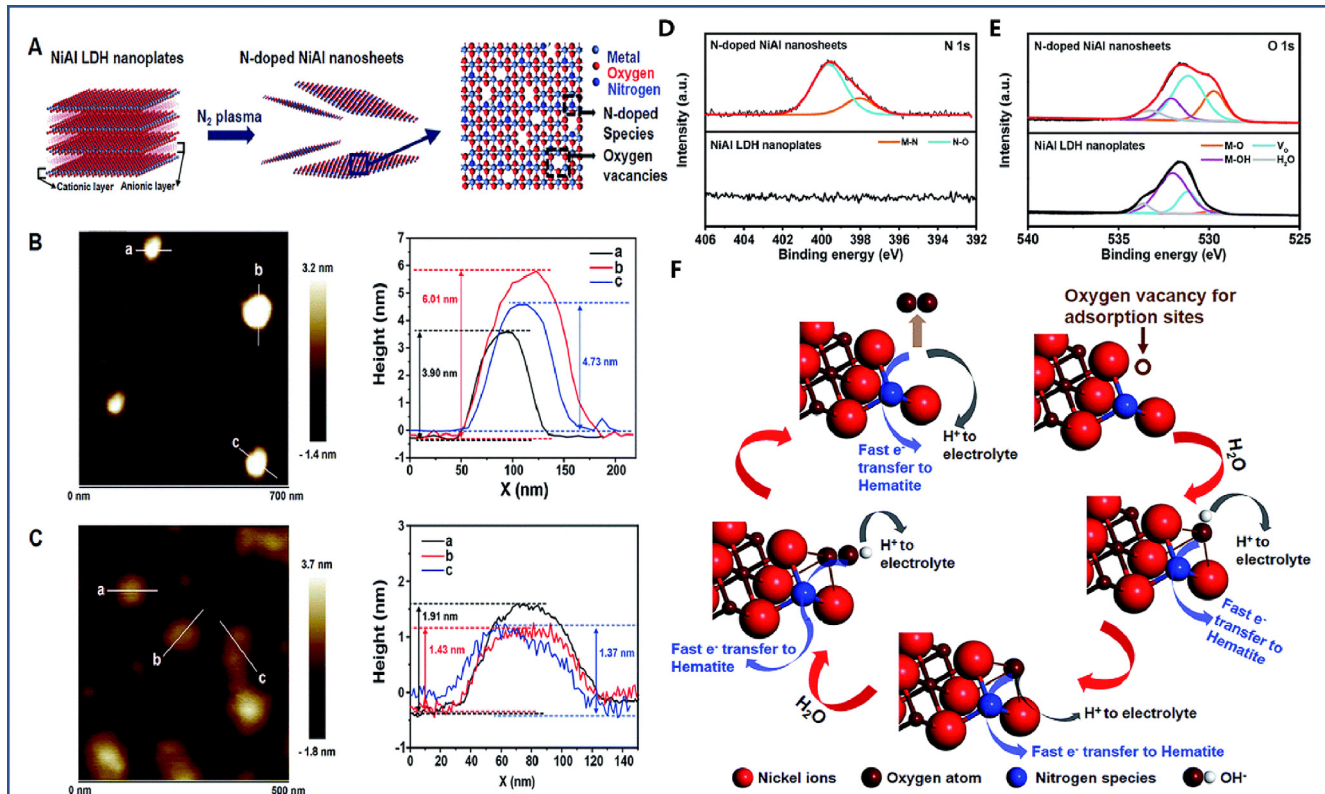


Fig. 10. (A) The schematic illustration of the processes to fabricate Ni-Al LDH nanoplates into ultrathin N-doped nanosheets by a dry exfoliation method using nitrogen plasma. Also, it describes the atomic configurations of an exfoliated ultrathin Ni-Al nanosheet with rich oxygen vacancies (V_0) and doped nitrogen, where metals share octahedral edges with lattice O atoms. (B) The atomic force microscopy (AFM) images of LDH nanoplates. (C) The atomic force microscopy (AFM) images of N-doped nanosheets with corresponding height curves. (D) The XPS spectra for N 1s orbitals of Ni-Al LDH nanoplates and N-doped Ni-Al nanosheets. (E) The XPS spectra for O 1s orbitals of Ni-Al LDH nanoplates and N-doped Ni-Al nanosheets. (F) A schematic picture describing the mechanism of the water oxidation reaction with oxygen vacancies and nitrogen doping sites on N-doped Ni-Al nanosheets (adapted with permission from Ref. [114] @Copyright 2018 The Royal Society of Chemistry).

formation of Schottky junctions and the surface plasmon resonance effects [158]. However, the performance of this ternary nanostructured photoanode has not been reported so far.

4.2.2. BiVO_4/LDH

Similar to the case of Fe_2O_3 , BiVO_4 is a capable photoanode candidate but BiVO_4 also suffer from the sluggish electron mobility [159,160]. The large surface areas of BiVO_4 nanofibers are beneficial for the uniform dispersion of LDH. LDH can be used as a stepping stone to extract holes formed from BiVO_4 to the electrode/electrolyte interface, thereby effectively facilitate holes-electrons separation and lead to enhanced performance for O_2 evolution by water oxidation, which is also proved in the PL intensity of BiVO_4 and $\text{BiVO}_4/\text{Ni-Co}$ LDHs. Obviously, the relative electrochemical surface area of BiVO_4 was increased dramatically after the deposition of Ni-Co LDH. After the LDH was successfully deposited onto the surface of BiVO_4 , the resulting composites showed the highest O_2 generation activity of $443 \mu\text{mol}\cdot\text{h}^{-1}\cdot\text{g}^{-1}$, about 18-times larger than that of pristine Ni-Co LDHs [161]. Remarkably, doping BiVO_4 photoanodes with Mo^{6+} could not only increased the photocurrent density ($1.26 \text{ mA}/\text{cm}^2$ at 1.23 V vs. RHE) for the 3% Mo-doped photoanode by 2.5-fold higher relative to bare BiVO_4 .

photoanode ($0.50 \text{ mA}/\text{cm}^2$), but most interestingly a significant negative shift in the onset potential for the OER was measured with respect to pure BiVO_4 . To further minimize the aggregation of LDH on BiVO_4 photoanodes surfaces, surfactants (SDS, sodium benzoate, citrate) were added into aqueous suspensions of Ni-Fe LDH nanocatalysts. The SEM/EDS images indicated that drop-casting aqueous Ni-Fe LDH nanosheet suspensions with surfactant reduced the aggregation on BiVO_4 surfaces. Among systematically explored surfactants, the addition of citrate led the LDH catalysts to be more deposited evenly on BiVO_4 surfaces, thereby improved photocurrent production more than that of SDS or benzoate surfactants. Due to the dipositive transition metal ions in LDH layers, citrate preferentially forms stable complexes with them. As a result, use of citrate surfactant in the preparation of $\text{BiVO}_4/\text{Ni-Fe}$ LDH photoanode ensured that authors used only a third of the mass loading relative to constructions without surfactants for a much enhanced photocurrent density [77]. In a more recent study, Y atoms were introduced into the nanosheets of Ni-Fe LDH (Fig. 11a), the resulting ternary Ni-Fe-Y LDH was then deposited on a porous BiVO_4 photoanode aiming for a better PEC activity and stability. For comparation, the materials scientists systematically deposited a series of NiOOH , Y-NiOOH , Ni-Fe LDH, and

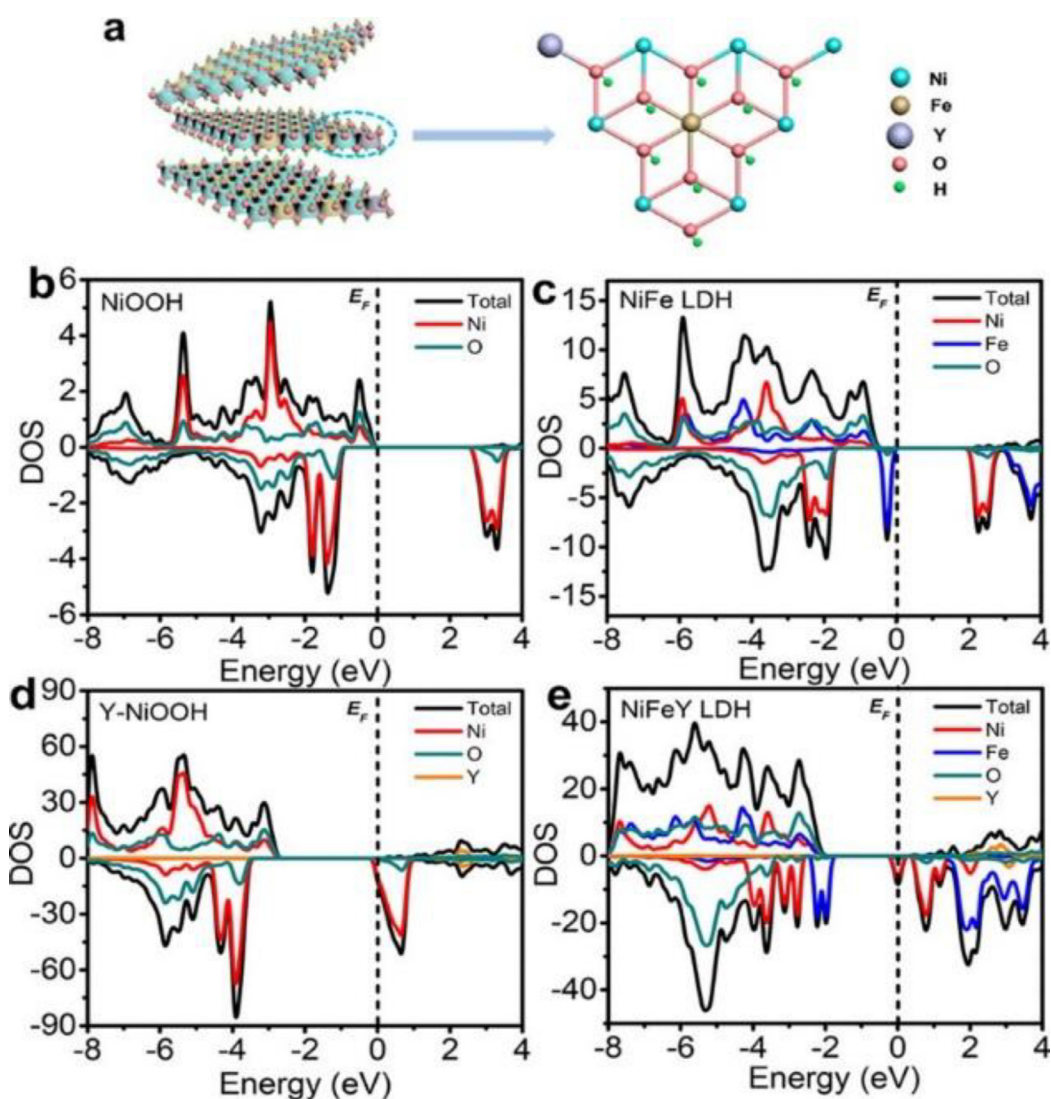


Fig. 11. (a) Structure model of Ni-Fe-Y LDH; (b-e) DFT-based DOS spectra of (b) NiOOH , (c) NiFe LDH, (d) Y-NiOOH , and (e) Ni-Fe-Y LDH. (adapted with permission from Ref. [162] @Copyright 2020 American Chemical Society).

Y-Ni-Fe LDH onto BiVO₄ surface. Firstly, the band-gap energy of NiOOH was decreased from 2.52 eV to 1.83 eV with the introduction of Y element (Fig. 11b,c), originating from a more conductive electronic structure of Ni-Fe LDH. Notably, with the further incorporation of Y atoms, both NiOOH and Ni-Fe LDH showed an evolution to a metallic state, which was indicated by the finite density of states of the Fermi level (Fig. 11d,e). Secondly, the morphology of Ni-Fe LDH or NiOOH changed from nanoparticles to nanosheets layer with the combination of Y elements. Thirdly, Ni 2p XPS spectra exhibited a negative shift as Y was introduced, which indicated that an electron transformation from Y³⁺ to Ni^{2+/Ni³⁺ site. All the aforementioned factors endowed Ni-Fe-Y LDH/BiVO₄ with a photocurrent density of 5.2 mA cm⁻² at 1.23 V_{RHE} and a maximum IPCE of about 80% at 450 nm. Importantly, the well-designed electrode achieved a photostability for more than 25 h in borate buffer, which can be deduced from a fast charge migration caused by the Y incorporation [162]. The beauty of this work is not only achieve the better PEC performance of the LDH/BiVO₄ composites, but also put forward a general and facile strategy to tune the electronic property of LDH/BiVO₄ catalyst. When the CdTe QD@ Ni-Fe LDH nanostructure was under irradiation, the photo-generated in the CB of CdTe QD traveled to the CB of Ni-Fe LDH as more negative CB value of the CdTe QD, thus improving the stability of QDs. Hence, the triadic CdTe QD/Ni-Fe LDH/BiVO₄ photoanodes possessed two sets of consecutive Type-II band alignments, dramatically improving the separation of electron-hole pairs. It is worth noting that the loaded QDs enhanced the light harvesting rather than to increase the amount of catalytic sites as the photo-generated holes in QDs were extracted by LDH for the subsequent water oxidation at the LDH surface. In particular, the QD@LDH@BiVO₄ exhibited a 200% higher IPCE than that of dyadic LDH@BiVO₄ at 1.23 V vs RHE [125].}

During the water oxidation half-reaction, it is well known that some active reactive oxygen species (ROS) intermediates generate before oxygen generation. These photo-generated ROS can be capable of selective oxidation of various substrates. When the graphene@CoAl-LDH@BiVO₄ multi-composite was applied as photoanodes, O₂ was not produced in substantial amounts in the presence of benzyl alcohol. On the one hand, the holes accumulated on the surface of photoanodes can directly oxidize the benzyl alcohol into benzaldehyde (BAD) and then benzoic acid. On the other hand, the holes catalyzed water molecules into .OH radicals and also activated BA to carbon-centered radicals, the resulting two kinds of radicals subsequently reacted with BA for the generation of benzaldehyde, with the selectivity above 99%. The authors further stated that the .OH radicals adsorbed on the surface of catalyst rather than the free .OH radicals played a key role on the high selectivity for BAD, as the addition of H₂O₂ into the reaction system reduced the selectivity [163].

Until now, most of the BiVO₄/LDH nanomaterials present a type II heterojunction system, which have been confirmed to be outstanding to harvest visible light and efficient electron migration with less recombination. Only one study has focused on the BiVO₄/LDH based Z-scheme heterojunction for PC water splitting [79]. Therefore, integrating BiVO₄ and LDH with other semiconductors with Z-scheme construction will be more attractive in the future. It is also worth noting that very recently some comparative studies were carried out to demonstrate the high-performance of defect controlling [164–166] and facets exposing [167–169] in facilitating the charge separation efficiency, thereby enhancing the performance of BiVO₄ based photocatalysts. Both strategies are highly desired as no studies on modulating the electronic structure of BiVO₄/LDH to date have been explored for boosting photocatalytic performance.

4.2.3. TiO₂/LDH

TiO₂ nanocrystal can act as excellent acceptor for photogenerated electrons with the fabrication of TiO₂/LDH, which would provide the optional way to improve the photogenerated carriers separation and thus the photocatalytic efficiency. Moreover, the full utilization of sunlight will be obtained because of the coupling of visible-light- responsive LDHs with UV-light-active TiO₂ [105].

The TiO₂/Zn-Al LDH sample showed an increase in the rate of electron transfer from VB to CB, owing to the a narrower bandgap energy of TiO₂/Zn-Al LDH than that of TiO₂. The resulting TiO₂/Zn-Al LDH showed a O₂ generation rates of 254.5 μmol h⁻¹g⁻¹ upon visible light irradiation, which is much higher than that of unary TiO₂. After being calcined at 430 °C, TiO₂/Zn₂Al-LDH material was converted into a three-phase composite (ZnO, Al₂O₃ and TiO₂) and the ZnO nuclei were homogeneously dispersed in the amorphous Al₂O₃. This good dispersed metal mixed oxide (MMO) solid exhibited a much better photocatalytic water oxidation activity (371 μmol h⁻¹g⁻¹) than that of TiO₂/Zn-Al LDH precursor under visible-light illumination, which was ascribe to the large pore volume, high visible-light absorbance, high surface area, and decreased bandgap energy. The quantum efficiency of TiO₂/MMO and TiO₂/ZnAl-LDH was 84% and 66% at 400 nm, respectively [104].

Although, TiO₂ combined with narrow-bandgap LDH can lead to the decrease of bandgap withing heterostructure. The intimate interfacial contact area in hybrid photocatalysts is another critical factor for better charge transfer at the interface. In this context, Min Wei and co-workers elaborately prepared a core-shell hybrid photocatalyst in which TiO₂ hollow nanospheres serve as the core component and Co-Al LDH nanoplatelets serve as the shell component (Fig. 12A). This configuration of materials endowed the TiO₂-LDH samples with a larger surface area (285.5 m² g⁻¹) and a mesopore distribution in the range 2–5 nm, which are beneficial for the exposure of active sites. Due to the well-matched band structure and inner electrical field formed between LDH and TiO₂, the photoexcited electrons migrated from the CB of LDH to the CB of TiO₂; meanwhile, the photoinduced holes transferred from the VB of TiO₂ to the VB of LDH. Specially, the average distance between the terminal oxygen atom in TiO₂ surface and the hydrogen atom in LDH surface was only 2.04 Å. The target core@shell nanospheres showed an O₂ generation rate of 2.34 mmol h⁻¹g⁻¹, which was almost 9- and 2-times higher than those observed for TiO₂ nanospheres, and Co-Al LDH nanoplatelets, respectively. This was predominately ascribed to the efficient transfer and separation of the photoinduced charge carriers resulting from the intimate contact at the interfaces between LDH shell and TiO₂ hollow nanospheres [105]. It is notable to point out that the core–shell structure also showed remarkable CO₂ photo-reduction activity as well as high selectivity (against competitive H₂ production). Most recently, Tonda et al. prepared TiO₂/LDH core–shell hybrid via hydrothermal and calcination methods, which was similar to the treatments applied by Min Wei. The most difference between them was that the carbon spheres were first synthesized as the self-sacrificing template (Fig. 12B). The obtained TiO₂/LDH core–shell hybrid was far superior to a different structure of TiO₂/LDH hybrid catalyst systems in terms of CH₄ production [170]. The unique core–shell geometric structure could grant an intimate interfacial contact area and enlarge the interfacial contact area, thus providing a broader platform for efficient charge transfer. The major production of CH₄ rather than CO could be also ascribed to a substantial number of available electrons (required for CH₄ formation) existing in the CB of TiO₂ [171]. With the aforementioned advantages and outstanding performance of TiO₂@LDH hybrids in mind, future work within this core@shell architecture may be directed towards the fabrication of surface defects such as Ti³⁺ and oxygen vacancies, the layer film thickness of the catalyst and doping the core–shell TiO₂/LDH by various elements. In addition,

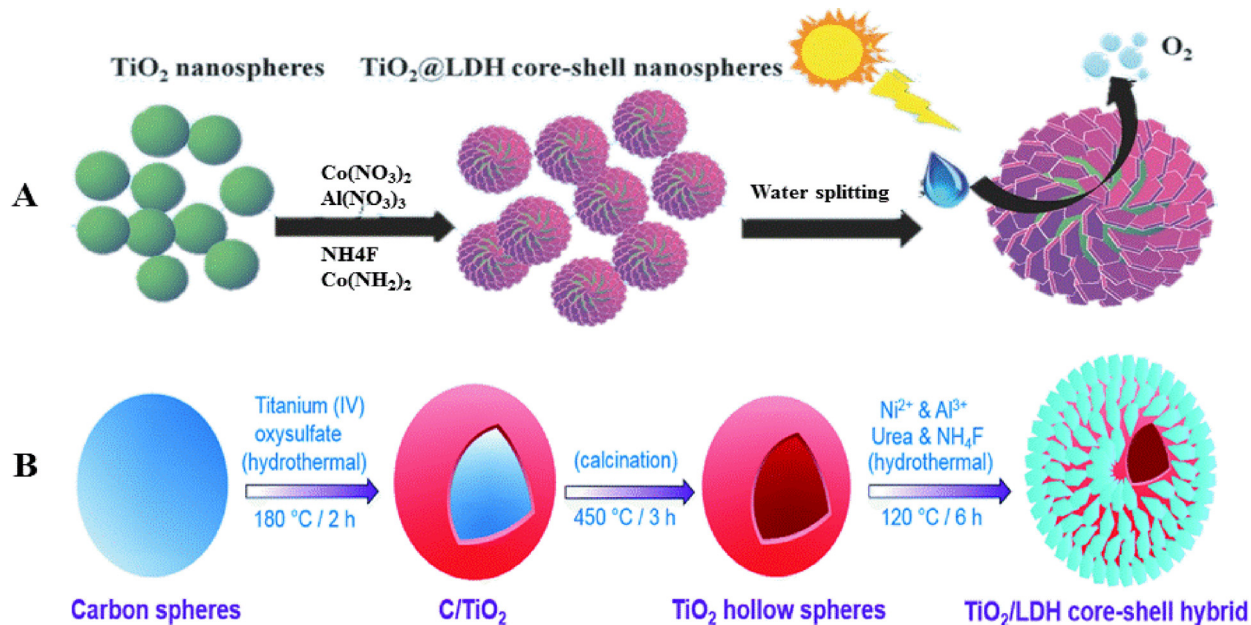


Fig. 12. Schematic representation of the synthesis of the TiO_2/LDH core–shell hybrid photocatalyst. A (adapted with permission from Ref. [105] @Copyright 2015 wiley). B (adapted with permission from Ref. [170] @Copyright 2020 Royal Society of Chemistry).

the formation of surface hydroxyl groups can be promoted owing to the acidification of the TiO_2 surface with H_2SO_4 , which seemed to be beneficial to the CO_2 reduction and the in-situ formation of LDH shell [172]. Therefore, we can reasonably speculate that the acidification of TiO_2 surface may affect the product formation of TiO_2/LDH core–shell hybrid in PC even PEC H_2/O_2 production.

It was reported that the pristine Co–Fe LDH photoanode, with a Co/Fe ratio of 2, yielded a relatively low photo current of $1.38 \text{ mA}/\text{cm}^2$ at 1 V Vs Ag/AgCl , which is mainly ascribed to the mutual shading between stacked LDH layers. After the LDH was physically mixed with titanate nanowires, the resulting sample presented a limited PEC activity with only $0.33 \text{ mA}/\text{cm}^2$. Subsequently, the LDH was decorated on to TiO_2 via coprecipitation method by added metal salts solution onto the TiO_2 suspension for boosting the PEC performance. No layered structure was observed at low LDH to TiO_2 weight ratios (<1), as Co and Fe ions were partial incorporated into the titanate structure during the hydrothermal process. The TiO_2/LDH with a ratio of 1:1 enabled the uniform distribution of the LDH layers on TiO_2 surface, leading to the enhancement of light absorption, decrement of the mutual shading between the layers, as well as the increased active surface area. As a result, the in-situ generation of LDH on TiO_2 nanowires surface resulted in a photocurrent density of $3 \text{ mA}/\text{cm}^2$ at 1 V Vs Ag/AgCl , in addition to a 220 mV cathodic shift in the onset potential for the oxygen evolution [115]. In a more recent study, the Ni–Fe LDH/ TiO_2 can be further converted into Ni–Fe MOF/ TiO_2 by in-situ etching under coordination environment with 1,4-benzenedicarboxylic acid. The new formed octahedral coordination mode within Ni–Fe MOF can expose a larger number of surface unsaturated active sites from Ni and Fe atoms, thus facilitating the water oxidation kinetics. The NiFe-MOF/ TiO_2 heterojunction photoanode produced a photocurrent density of $0.77 \text{ mA}/\text{cm}^2$, up to 3.35 times higher than that of bare TiO_2 . In addition, the prepared photoelectrode presented excellent photostability under 4 h of continuous illumination and an charge injection of 92.8% and charge separation efficiency of 37.4% [173].

Aiming at designing the well-formed metal–oxide interfaces, Shao et al. [134] utilized a nanoscale catalytic nanoarrays from a thin LDH layer on TiO_2 that forms a nanoscale TiO_2/LDH interface

to determine the influence of the adaptive-interface on PEC water splitting performance (Fig. 13A). The authors synthesized two configurations via conventional electrodeposition (denoted as $\text{TiO}_2/\text{Zn-Fe LDH-E}$) and photo-assisted electrodeposition (denoted as $\text{TiO}_2/\text{Zn-Fe-LDH-PE}$) processes, and then found that both $\text{TiO}_2/\text{Zn-Fe LDH}$ enabled the higher photochemical performance than unary TiO_2 . Photo-assisted electrodeposition strategy, however, was superior to construct photocatalyst with high catalytic activity compared to the commonly electrosynthesis method. The major reason of better photocatalytic H_2 -production activity for $\text{TiO}_2/\text{Zn-Fe-LDH-PE}$ photoelectrode was higher uniformity and the well-defined plate-like morphology of LDH on the surface of TiO_2 (Fig. 13B and C), which result in stronger interactions and thus, more efficient electron transfer. Photo-assisted electrodeposition treatment enhanced the photocurrent density of unary TiO_2 and $\text{TiO}_2/\text{ZnFe-LDH-E}$ photoelectrode by up to 1.91 and 1.20 times at 1.23 V vs. RHE , respectively. For $\text{TiO}_2/\text{ZnFe-LDH}$ system, a negative shift of the onset potential has also been observed (Fig. 13D). The increase of illumination power density from 0 to 100 mW cm^{-2} led to the increase of photocurrent density, indicating the crucial role of photo-assisted deposition in PEC performance (Fig. 13E). In particular, the LDH deposition time also played a significant role and a maximum photocurrent (1.51 mA cm^{-2} at 1.23 V vs.RHE) can be obtained for 100 s. Under the same LDH deposition time, the $\text{TiO}_2/\text{ZnFe-LDH-PE}$ assemblies showed a higher photocurrent density than that of $\text{TiO}_2/\text{ZnFe-LDH-E}$ configuration (Fig. 13F). To further illuminate the synergistic effect between TiO_2 and Zn–Fe LDH on the enhancement of the electrode PEC performance, the average distance between the terminal oxygen atom in TiO_2 surface was calculated and the hydrogen atom in Zn–Fe LDH surface was only 2.27 \AA (Fig. 13G). Furthermore, the binding energy between them was as low as -9.96 eV . Such low interaction energy combined with short distance indicates an intimate interfacial contact. When $\text{TiO}_2/\text{Zn-Fe LDH}$ was irradiated and excited by illumination, the charge carriers firstly photogenerated in TiO_2 and the induced holes on the VB of TiO_2 rapidly transferred to Zn–Fe LDH. The electrons of Zn–Fe LDH tended to travel to the current collector through TiO_2 owing to the electric potential difference (Fig. 13H). The incorporation of rGO into the TiO_2/LDH was also achieved

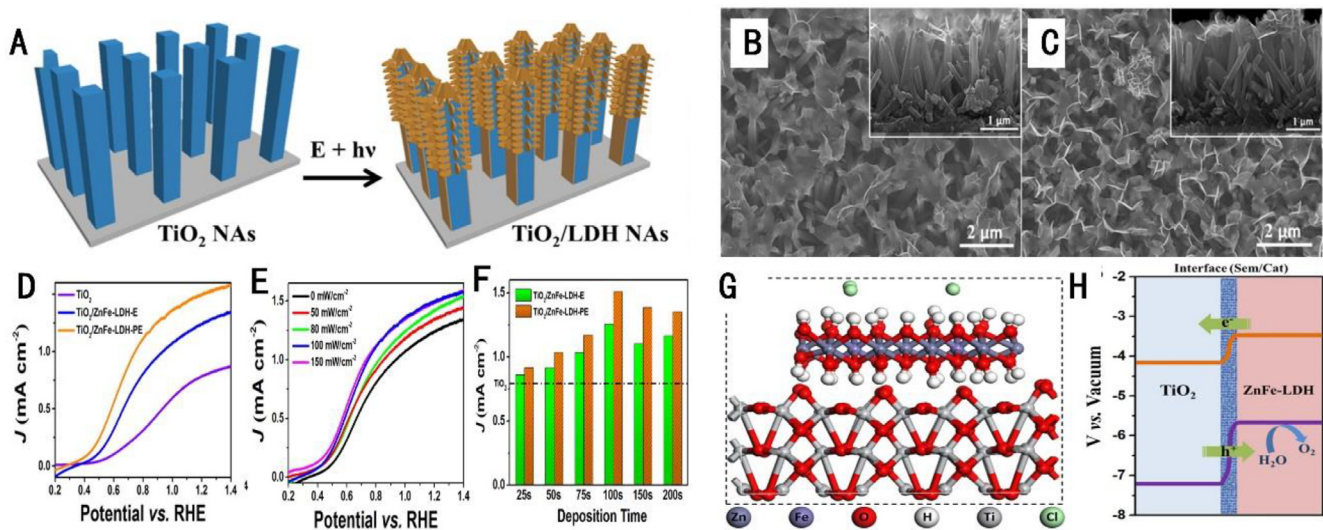


Fig. 13. (A) Schematic illustration for the fabrication of TiO₂/ZnFe-LDH-PE. (B) SEM image of TiO₂/ZnFe-LDH-E. (C) SEM image of TiO₂/ZnFe-LDH-PE. (D) J-V curves for TiO₂/ZnFe-LDH-PE, TiO₂, and TiO₂/ZnFe-LDH-E. (E) J-V curves for the five TiO₂/ZnFe-LDH-PE samples prepared with various illumination intensity. (F) Photocurrent density at 1.23 Vvs.RHE for the samples of TiO₂/ZnFe-LDH-E and TiO₂/ZnFe-LDH-PE with various deposition time. (G) Optimized geometry of TiO₂/ZnFe-LDH model. (H) A schematic illustration for the PEC water oxidation process over the TiO₂/ZnFe-LDH photoanode. (adapted with permission from Ref. [134] @Copyright 2017 Elsevier).

aiming to facilitate the superior charge separation. The PL intensity of these two peaks decreased sharply after the incorporation of Ni-Fe LDH or rGO, and further declined in the ternary TiO₂/rGO/NiFe-LDH system. For ternary TiO₂/rGO/LDH materials, rGO exhibited lower Fermi level than the CB of n-type TiO₂, suggesting an energetically favorable transfer of electrons from TiO₂ (CB) to rGO. With the rGO/LDH hybrid as co-catalyst, the LDH nanosheets receive holes and play as catalytic sites for O₂ evolution, of which the graphene sheet act as “highway” for electron transport. Benefiting from the synergistic effects, the enhanced photochemical performance of the overall TiO₂/rGO/LDH composition was obtained [115].

4.2.4. WO₃/Ldh

The effect of compositing LDH with WO₃ has also been recently examined and also showed desired PEC performance, resulted from the reasonably-matched band structure between WO₃ and Ni-Fe LDH [140]. The heterostructure WO_{3-x}/Ag/Zn-Cr LDH photocatalyst was constructed by photo deposition method and an in situ coprecipitation approach for photocatalytic Tetracycline degradation and H₂ evolution. The creation of defects resulted from surface oxygen vacancy in WO_{3-x} and the direct Z-scheme-based mode of charge transfer regulated the optical and photoelectronic properties of the WO_{3-x}/Ag/Zn-Cr LDH nanohybrids, resulting in the efficient spatial promotion of the generation, separation, and migration of photoinduced carriers. Eventually, the ternary heterostructure shows excellent visible light-driven H₂ evolution (29.375 mmol g⁻¹ h⁻¹) and Tetracycline removal (92% in 90 min) with high stability [174].

Further enhancements in terms of efficiency of water splitting devices have also been reported for a trinary integrating photoanode arrangement, with Fe₂O₃ “sandwiched” between WO₃ and Ni-Fe LDH. Compared to WO₃/Fe₂O₃, the optimized WO₃/Fe₂O₃/Ni-Fe LDH has a decreased band gap, which is beneficial for extending absorption of visible light. When α-Fe₂O₃ (as the primary light-absorber) and WO₃ (as an electron acceptor) came into contact, the n-n junction was formed at their interface. Upon irradiation, the band bending generated at the interface facilitated the carriers to spread in opposite direction until their Fermi levels arrive equivalence. The WO₃ conduction band accepted photogenerated electrons transferred from Fe₂O₃, whereas the holes flow to the

valence band of α-Fe₂O₃ from WO₃ for an efficient oxygen evolution reaction. After the cocatalyst LDH loading, the obtained α-Fe₂O₃/WO₃/LDH photoanode showed a photocurrent density of 3.0 mA·cm⁻², which is 5-times and 7-times higher than that of WO₃ and α-Fe₂O₃, respectively [141]. Most recently, aiming at exploring the critical role of WO₃ exposed facets in the enhanced PEC performance, Ag nanoparticles was firstly deposited on the edged electron rich {020} and {200} facets of WO₃ via a photoreduction manner, and then the Zn-Fe LDH nanosheets were preferentially dispersed onto hole-rich {002} facet via a electrochemical process [138]. The optimized geometries of {002}, {020}, and {200} facets of WO₃ were illustrated in Fig. 14a. Accordingly, the band gap energy of {002}, {020}, and {200} facet were calculated via DFT to be 2.344 eV, 1.119 eV, and 1.358 eV, respectively. Then valence band values were further calculated to be 1.895 eV, 1.098 eV, and 0.234 eV, respectively. Obviously, the {002} facet owned the more positive VB value relative to another two facets, indicating the photoinduced electrons on the CB of {002} facet will prefer to migrate to the VB of {200} and {020} facets (Fig. 14b). This migration model enabled the strongest oxidation capability for the photoinduced holes from {002} facet. Moreover, the charge carrier mobilities of electron and hole in faceted WO₃ along the lattice a-, b-, and c- directions were calculated and displayed in Fig. 14c. The largest mobility of electron along the a- direction and the highest mobility of hole along the c- direction endowed the faceted WO₃ with the successful photogenerated electron-hole separation. Under ultraviolet-visible irradiation, the photo-excited holes transferring along the c- direction will reach the {002} facet and then be captured by LDH. Meanwhile, electron generated on the VB of WO₃ travelled to the edged {200} and {020} facets and the hot plasmonic electrons of Ag derived by the local surface plasmonic resonance were quickly injected into the CB of WO₃. The extracted holes were ultimately used for the oxidation of Fe, which provides affordable active sites for water oxidation (Fig. 14d). It is worth noting that the salt chloride in seawater was beneficial for the photo-oxidation of H₂O to O₂. The enhanced PEC performance was ascribed to two facts. On the one hand, the redox process Cl⁻ to Cl₂ is a comparatively simple two-electron procedure, comparing with more complex four-electron redox process occurred in water oxidation. On the other hand, WO₃ clearly exhibited a smaller solution resistance as the salt

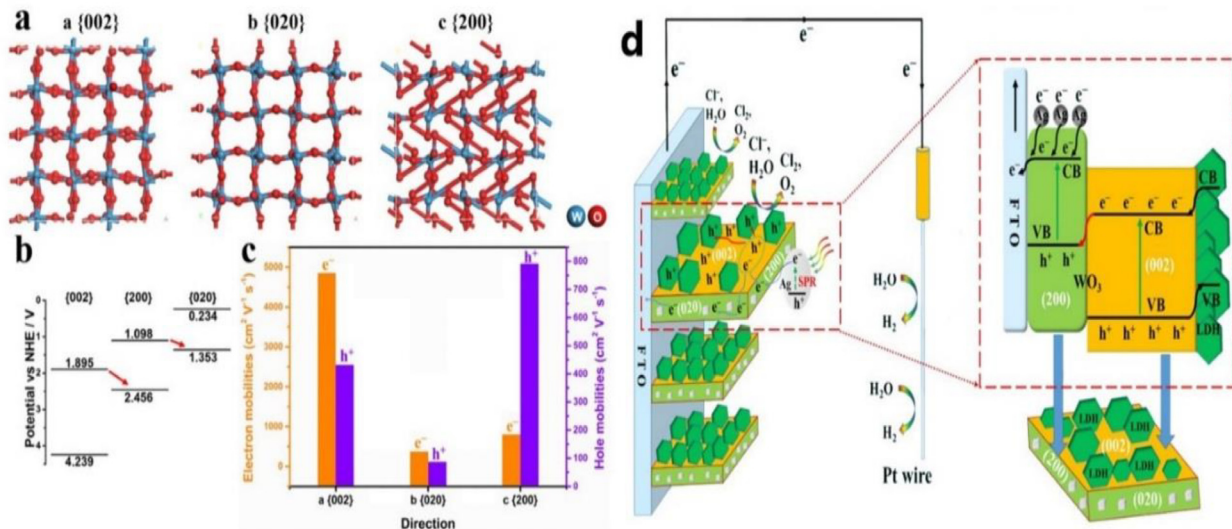


Fig. 14. (a) The optimized geometry of the {002}, {020}, and {200} facets for WO₃, the color of each element was labeled. (b) Band edge placements for the valence band maximum and conduction band minimum of {002}, {200}, and {020} facets for WO₃. (c) Mobilities for electron and hole in the lattice a-, b-, and c-directions. (d) Schematic diagram of a PEC device consisting of an Ag/WO₃/Zn-Fe LDH photoanode, and a Pt counter electrode; the square box shows the energy diagram of the Ag/WO₃/ZnFe-LDH photoanode and illustrates the basic operation mechanism for PEC natural seawater splitting (adapted with permission from Ref. [138] @Copyright 2020 Elsevier).

chlorides are stronger electrolytes compared to PBS, thus obtaining a faster interfacial charge transport in real seawater relative to that in PBS solution [138].

The research of WO₃/LDH is still in the early stages and there is no doubt that coupling faceted WO₃ films with LDH cocatalyst is a robust strategy to further boost PEC water splitting [175]. However, the controllable deposition of LDH cocatalyst onto monoclinic WO₃ facets, including {100} and other high-index facets, is still a challenge. In addition, the combination of certain thickness and morphology of WO₃ and LDH maybe another feasible way for achieving high PC/PEC performance. A deeper research of these effects of the selective facet exposure, morphologies, and WO₃ crystallinity on the light absorption is urgently required.

4.3. Metal sulfide/LDH

4.3.1. CdS/LDH

Recently, a great progress has been made on LDH decorated by Metal sulfide for achieving improved photocatalytic performance and these examples include ZnS/Zn-Al LDH [176], CdS/Mg-Al LDH [177] and CdS/Ni-V LDH [178]. To overcome the disadvantage of limited bonding sites for loading QDs, the 2D Ni-Fe LDH nanoplates can be further broken into FeNiS nanoparticles via a sulfurizing treatment. Although, FeNiS samples showed the rough surfaces relative to the smooth surfaces of the Ni-Fe-LDH. A large number of CdTe/CdS QDs with particle size of ~3 nm can be evenly deposited on the surface of FeNiS nanoparticles because of the presence of more sulfur species. The H₂ evolution rate of the FeNiS-CdTe/CdS QDs photocatalysts was an ~6 times enhancement (41.4 μmol/h), compared to that of FeNi-CdTe/CdS QDs (6.3 μmol/h). It was attributed to the more effective of FeNiS for hydrogen evolution and also the intimate combination between FeNiS and CdTe/CdS QDs for the rapid electrons transformation [108].

Compared to 0D-CdS, 1D-CdS exhibit not only controlled size and thickness, but also enable the carrier transportation in a unidirectional path. These properties are beneficial for reducing the carrier recombination rate and facilitating photocatalytic activity. Inspired by aforementioned advantages, Lee et al. prepared CdS/Ni-Fe LDH nanocomposites through ultrasonication method and demonstrated that 2D Ni-Fe LDH is anchored on the edges of CdS nanorods.

This strong interfacial contact equipped the obtained CdS/NiFe nanocomposites with an efficient pathway to prolong the lifetime of photoinduced electrons by regulating the electron transformation from CdS to Ni-Fe LDH, which ultimately reduced H⁺ for production of H₂. Consequently, CdS/Ni-Fe LDH exhibited a much enhanced evolution rate of hydrogen (72 mmol g⁻¹h⁻¹), compared to that of Ni-Fe LDH (0.09 mmol g⁻¹h⁻¹) and CdS (2.4 mmol g⁻¹h⁻¹) [107]. In specific, doping 2D CdS nanorods with P can not only reduce the resistance of pure CdS, but also elongate the lifetime of the charge carries. It was attributed to the mid-gap at the bottom of the CB of CdS. Subsequently, the highly dispersed Ni-Co LDH nanoplatelets on the surface of P-CdS nanorods could further improve the lifetime of electrons, due to the formation heterojunction between P-CdS and Ni-Co LDH. Thus, the visible-light catalytic H₂ production of P-CdS/LDH was about 45 times that of the pure CdS [109]. Pirkarami et al. constructed 3-D CdS@NiCo LDH core-shell photoelectrocatalyst supported on the Ni foam for overall water splitting [179]. The Ni-Co LDH were grown vertically on 3-D CdS nanowires, resulting in an increased surface area and active sites on photoelectrocatalyst. Under visible light radiation, the electrons generated from the CdS core can be effectively transferred to the Ni-Co LDH shell and the gaseous products can be rapidly released, which is resulted from the highly-conductive shell and particular layered structure of CdS@NiCo LDH. Therefore, this novel catalyst showed a current density values of 10 mA cm⁻² at a voltage of 132 mV for OER and 379 mV for HER respectively.

Admittedly, the great developments have been made for the constructing efficient CdS/semiconductors photocatalysts. However, Cadmium is a big concern to environment and human body. In addition, severe photo-corrosion of CdS caused by holes also hinder their use in PEC-related applications [180]. Hence, restricting the leach of Cd and photo-corrosion in PC/PEC process is a primary issue. Potential solutions can be focused on two aspects: (1) constructing Z-scheme structure to accelerate the consumption of VB-holes on CdS; and (2) the core shell structure can be constructed to stabilize the CdS core.

4.3.2. MoS_x/LDH

Recently, MoS_x materials including crystalline MoS₂, Mo-S molecular complexes, and amorphous MoS_x ($2 < x < 3$) have been

identified as promising alternatives to noble metals for HER due to its high activity and earth-abundance [181–183]. LDH can also be regarded as active substrate for the uniform dispersion of MoS₂ catalyst, which will not only enhance the catalyst distribution but also modify the electronic properties of the catalytic sites of deposited MoS₂ catalysts, resulting in targeted photocatalytic H₂ evolution performances. Parida et al. constructed an innovative type of 2D–2D direct Z-scheme heterojunction consisting of p-type MoS₂ and n-type Ni–Fe LDH via electrostatic self-assembled chemistry and in situ hydrothermal method. Under visible light excitation, the intensities PL peak of terephthalic acid solution for MoS₂/Ni–Fe LDH (MSLDH) heterojunction composites are obviously much higher than those in pure Ni–Fe LDH, which can be attributed to the construction of 2D and 2D heterojunction to improve ·OH production. Meanwhile, there were no intense peaks detected in MoS₂, demonstrating its inefficiency in producing ·OH radicals. If the typical heterojunction system showed in Fig. 15a is the photocatalytic reaction mechanism of MSLDH composites, the photogenerated holes are injected into the VB of MoS₂ with positive potential from the VB of Ni–Fe LDH with negative potential, the negative positive VB of MoS₂ in MSLDH than E(OH/OH⁻) = +1.99 eV vs NHE was not capable to generate ·OH. Alternatively, the Z-scheme heterostructure system could be demonstrated as the photocatalytic mechanism, and the electrons of Ni–Fe LDH conduction band can be transferred to the valence band of MoS₂. This kind of Z-scheme structure is conducive for photoinduced charge carriers to transfer to the higher potential energy band rather than accumulate on the lower energy band, leaving photogenerated electrons and holes with high redox abilities for participating in surface redox reactions [62]. As a result, the average H₂-evolution rate of Ni–Fe LDH alone was enhanced by 10.9 times, reaching up to 550.9 μmol/h by the decoration of MoS₂ [94]. Notably, when the Mg–Al LDH nanoplate was utilized as a support for amorphous MoS_x, neither Mg nor Al metal sites can initiate the chemical interaction with MoS_x, and hence only a few of stacked MoS_x nanoparticles were deposited on the edges of Mg–Al

LDH, resulting in an uneven dispersion of the MoS_x catalyst and then leading to low photocatalysis H₂ evolution activity. While with Co–Al LDH as a support, the photocatalytic H₂ evolution activity of the obtained Co–Al LDH/MoS_x catalyst was 13 times enhancement that is 450 μmol/h, than that of unsupported MoS_x. Moreover, Co–Al LDH was superior to Ni–Al LDH and Mg–Al LDH as a support for anchoring MoS_x catalysts for photocatalysis H₂ evolution. The reaction between unsaturated Co sites and [MoS₄]²⁻ enabled the firm anchoring of formed MoS_x on the one hand, and activated the unsaturated S atoms of MoS_x by forming additional highly active CoMoS sites on the other hand [110].

Notably, metal sulfide/LDHs have recently exhibited a high photocatalytic H₂ production activity. However, there are few examples of efficient metal sulfide core–shell nanostructured metal sulfide/LDHs photocatalytic system for hydrogen production so far. The interactions between the core and shell apparatuses can greatly enhance physical and chemical properties, provide active interfaces, and even produce new synergistic properties [184]. For example, other semiconductors with specific facets can further react with desirable {0001} facets of CdS nanoplates to generate core–shell nanohybrids through the self-assemble process, resulting in the reduction of large lattice mismatch at the interface [185].

4.4. Carbon materials/LDH

4.4.1. C₃N₄/LDH

Recent literatures also revealed that highly stable coupling of g-C₃N₄ with other layered structure semiconductor material resulted in a remarkable enhancement for photocatalytic performances [186–191]. An intimate contact and a strong electronic coupling between common layered structures of C₃N₄ and LDH greatly increases the system's photocatalytic activity [111,192]. Moreover, the long-term photostability and photocatalytic properties of LDH can be further improved via the support of highly stable g-C₃N₄ by the delocalized conjugated π structure, endow it with high charge

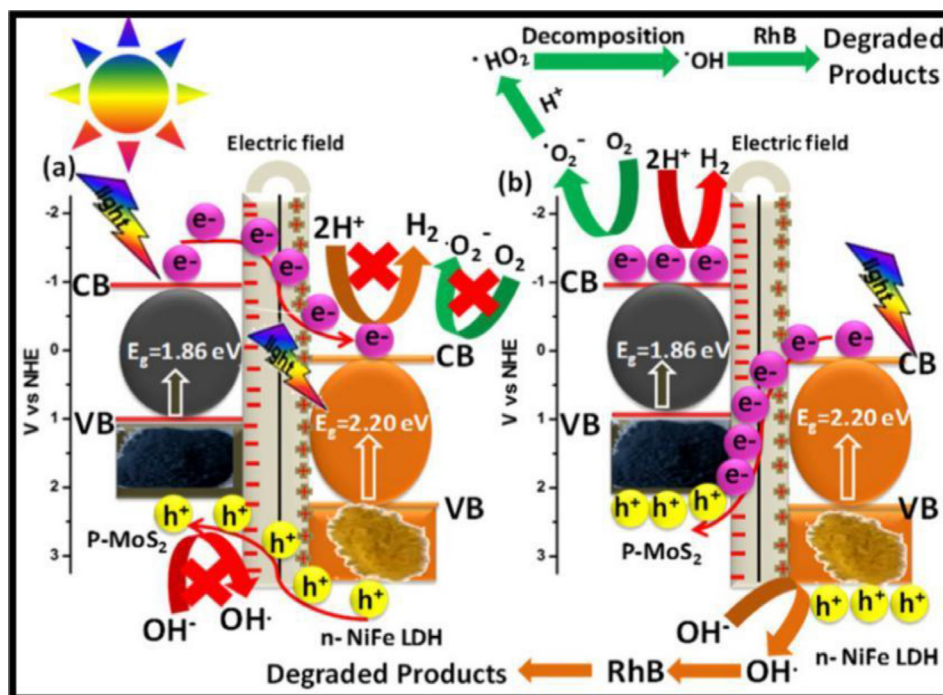


Fig. 15. Proposed Schematic Representation of the Charge-Transfer Mechanism over MSLDH under Exposure of Visible Light for (a) Double Charge and (b) p–n Heterojunctions with the Direct Z-Scheme Mechanism. (adapted with permission from Ref. [94] @Copyright 2019 American Chemical Society).

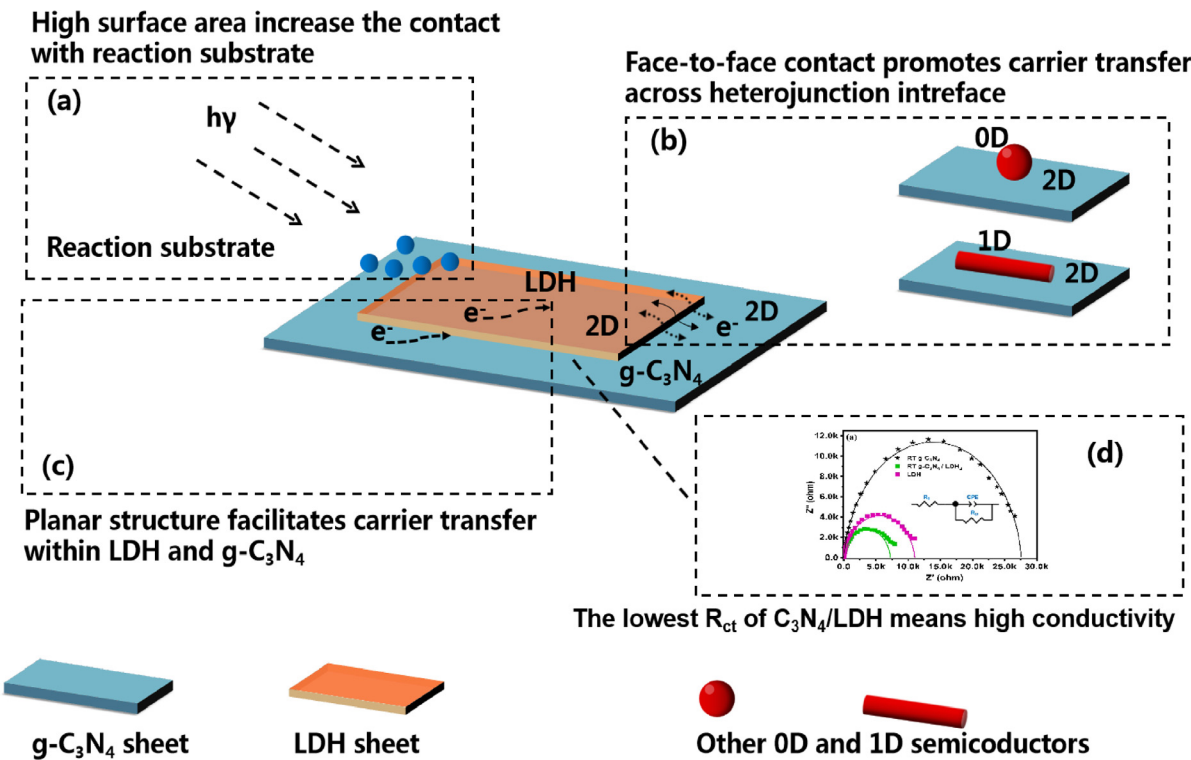


Fig. 16. Advantages of 2D/2D LDH/ $\text{g-C}_3\text{N}_4$ heterostructure in PC/PEC applications.

separation and transportation [193–197]. The notable synergistic effect between LDH nanosheets and C_3N_4 led to many advantages of the resulting inorganic/organic hybrid composites (Fig. 16), such as: (i) assembling two layered semiconductors to generate a hybrid semiconductor catalyst not only separates the photoinduced electron-hole pairs but also produces active sites for the H_2 and O_2 evolution, (ii) the layered structure is established capable of absorbing water and swelling up to some extent which maximizes the surface area, and (iii) the high conductivity of $\text{g-C}_3\text{N}_4/\text{LDH}$ nanostructures is beneficial for its superior charge transportation capability [193,198,199].

For illustration, the pristine Ni-Al LDH material exhibited visible light photocatalytic activity with an H_2 evolution rate of $3.17 \mu\text{mol g}^{-1}\text{h}^{-1}$ in the presence of triethanolamine (TEOA). In comparison, addition of a certain amount of C_3N_4 (30 wt% loading of C_3N_4 over LDH) onto the surfaces of the LDH resulted in a dramatical enhancement in photocatalytic H_2 evolution, yielding $3170 \mu\text{mol g}^{-1}\text{h}^{-1}$, which was 100 and 1000 times higher than pure $\text{g-C}_3\text{N}_4$ and pristine Ni-Al-LDH, respectively. Since the CB of C_3N_4 (-1.29 eV) was more negative than that of LDH (-0.94 eV), the photo-induced electrons at the CB of C_3N_4 could readily inject into the CB of LDH across its interfacial conjugation. Due to the more positive position of the VB edge potential of LDH ($+1.57 \text{ eV}$), as soon as the photo-induced holes are formed on the VB of LDH, they can directly travel to the VB of C_3N_4 and then can be captured for the oxidation of TEOA. Therefore, the mechanism for separation the photogenerated electron-hole pairs followed the conventional type-II heterojunction [200]. Notably, the nitrogen evolution was always accompanied with the oxygen evolution, as the valence holes can be also utilized for self-oxidization of C_3N_4 . Benefiting from the fast transformation of holes from C_3N_4 to Ni-Co LDHs surface, the selectivity for water oxidation for O_2 production of C_3N_4 increased from 52% to 91% in the presence of LDHs [111]. The introduction of Fe-Ni-LDH onto the $\text{g-C}_3\text{N}_4$ nanosheets surface also led to an increased hydrogen production activity from

$0.022 \text{ mmol g}^{-1}\text{h}^{-1}$ to $0.337 \text{ mmol g}^{-1}\text{h}^{-1}$. To further boost the performance of LDH/ $\text{g-C}_3\text{N}_4$, the Ni-Fe LDHs were sulfuretted to Fe-Ni-S nanoparticles and subsequently deposited on the $\text{g-C}_3\text{N}_4$ surface by a hydrothermal method. For comparation, the Fe-Ni-S/ $\text{g-C}_3\text{N}_4$ nanohybrids exhibited an increased hydrogen production activity to $1.152 \text{ mmol g}^{-1}\text{h}^{-1}$, which is about 25.6 and 4 times than that of Fe-Ni-LDH and Fe-Ni-LDH/ C_3N_4 , respectively. The enhanced photocatalytic capacity the of Fe-Ni-S/ $\text{g-C}_3\text{N}_4$ for H_2 production was attributed to the fact that the Fe-Ni-S transferred the photo-generated electron to the solution, and the S covalent binding with Fe-Ni alloy in the complexes served as the host lattice to inhibit the photo-corrosion [99]. The morphology of $\text{g-C}_3\text{N}_4$ could also improve its light absorption as well as charge separation, and thus optimize the photocatalytic activity. The in-situ growth of carbonate-intercalated Zn-Cr LDH over ruptured tubular structured graphite-like carbon nitride has been first constructed by Aboubakr et al. [39] through co-precipitation method. The higher amount of LDH in the Zn-Cr LDH/ C_3N_4 resulted in lower band gap, lower charge transfer resistance, and higher electron-hole pairs separation ability. Exactly, the ability for separation of electron-hole pairs of the resulting Zn-Cr LDH/ C_3N_4 was 5- and 2-folds higher relative to bulk $\text{g-C}_3\text{N}_4$ and ruptured tubular $\text{g-C}_3\text{N}_4$ [39].

The amount of CN loading in $\text{C}_3\text{N}_4/\text{LDH}$ played a pivotal role for semiconductor photocatalysts, as the high contents of $\text{g-C}_3\text{N}_4$ may hindered the photocatalytic activities of the $\text{C}_3\text{N}_4/\text{LDH}$ composites. The reasons have been reported in several aspects, including (i) an increase in the opacity of the catalyst, (ii) the larger size and thickness of layered structure, (iii) the weakened the bond between LDH and $\text{g-C}_3\text{N}_4$ leading to the damage of the heterojunction, (iv) the active sites that hindered the transportation of photo generated charges were diminished [193,198]. Additionally, morphology tuning of C_3N_4 can be used as a strategy to reduce the bandgap and enhance charge separation, thus improving photocatalysis performance of $\text{g-C}_3\text{N}_4$ [201,202]. Recent research studies on $\text{C}_3\text{N}_4/\text{LDH}$

have been mainly focused on 2D/2D configuration (seen from table 2). Herein, we tentatively suggest a further investigation of 3D C_3N_4 (hollow spheres), 1D C_3N_4 (nanofibres), and 0D C_3N_4 (quantum dots) hybridization with LDH. There has been considerable research about photocatalytic hydrogen evolution, carbon dioxide reduction via $\text{C}_3\text{N}_4/\text{LDH}$ materials [203]. But the research of photocatalytic hydrogen peroxide production and nitrogen fixation over $\text{C}_3\text{N}_4/\text{LDH}$ photocatalysts is quite limited, thus more studies in both fields are encouraged.

4.4.2. GO/Ldh

GO/LDHs nanocomposites have wide applications ranging from supercapacitors [204], adsorbents for wastewater [205], CO_2 reduction [206,207]. With particular attention, assembling RGO with Co-Al LDH can facilitate the separation rates of the photo-generated electrons and then extend the longevity of charge carriers. Under visible-light irradiation, the as-prepared CoAl-LDHs/RGO showed an enhanced H_2 production of $1571.84 \mu\text{mol h}^{-1} \text{g}^{-1}$, which is 3.5-fold higher relative to pure CoAl-LDHs [208]. Parida et al. firstly prepared GO/ C_3N_4 and then annealed at 550°C under flow of N_2 , attaining a perfect N-doped graphene matrix. The ternary N-GO/ $\text{C}_3\text{N}_4/\text{Ni-Fe}$ LDH heterojunction was formed by an electrostatic self-assembly of Ni-Fe LDH nanosheets on the surface of GO/ C_3N_4 . The ternary heterojunction possessed the lower PL intensity, reduced arc of the Nyquist plot and higher photocurrent density than those of $\text{C}_3\text{N}_4/\text{LDH}$, demonstrating the importance of N-rGO solid state mediator in charge transportation of two semiconductors. In particular, both DMPO- O_2^- and DMPO-OH high-intensity signals were observed by N-rGO/ $\text{C}_3\text{N}_4/\text{Ni-Fe}$ LDH. While the electrons on the CB of Ni-Fe LDH was not negative enough to produce O_2^- and HO_2 radicals. Hence, superoxide radicals were generated on the CB of C_3N_4 , due to the more negative CB edge potential of C_3N_4 (-0.54 V vs. NHE). These findings demonstrated the electrons in the CB of Ni-Fe LDH can be recombined with holes generated by the VB of C_3N_4 over N-rGO surface. Hence, the N-rGO/ $\text{C}_3\text{N}_4/\text{Ni-Fe}$ LDH operated via the Z-scheme carrier transfer mechanism between Ni-Fe LDH and C_3N_4 , which is different from the type-II mechanistic path exhibited by other $\text{C}_3\text{N}_4/\text{Ni-Fe}$ LDH photocatalysts [99,193]. Accordingly, the N-rGO/ $\text{C}_3\text{N}_4/\text{Ni-Fe}$ LDH exhibited superior O_2 production rate of $640 \mu\text{mol g}^{-1}\text{h}^{-1}$ and H_2 production rate of $1254 \mu\text{mol g}^{-1}\text{h}^{-1}$, which are 1.44 times and 1.7 times higher than C_3N_4 -LDH, respectively [113]. By assembling 2D graphdiyne (GYD) with 2D planar $\text{g-C}_3\text{N}_4$ and Ni-Fe LDH OER catalyst together, a new strongly attached ternary photoelectrode $\text{g-C}_3\text{N}_4/\text{GYD}/\text{Ni-Fe}$ LDH can be fabricated by a facile hydrothermal method. Due to the face-to-face contact between GYD and $\text{g-C}_3\text{N}_4$, a built-in electric field generated with a direction from $\text{g-C}_3\text{N}_4$ to GYD in equilibrium state. The photogenerated holes transferred easily from $\text{g-C}_3\text{N}_4$ to Ni-Fe LDH owing to the GYD behaving as a conductive electron transport "highway", and ultimately oxidized the water to generate oxygen. As expected, a high photocurrent density of $178.66 \mu\text{A cm}^{-2}$ (at 1.4 V vs RHE), as well as a maximum IPCE of 3.59% at wavelength of 350 nm were obtained for this elaborately designed photoelectrode. Furthermore, the coupling interaction between 3d transition metal atoms and the carbon–carbon triple bonds and carboxyl bonds in GYD prevented its photo-corrosion, retaining about 95% of its photocurrent for 3600 s of stability testing [209]. In comparison with 2D graphene, 3D graphene aerogels matrix exhibits more efficiency for electron migration and charge separation. This remarkable advantage of 3D graphene aerogels was predominantly attributed to its unique hierarchically porous structure, which is beneficial for mass transfer, and reducing the transport limitation of electrolytes, together with other advantageous attributes such as multidimensional electron transport pathways, and outstanding electrical conductivity. Hou et al.

constructed a 3D macroscopic hierarchical structure comprised of nitrogen deficient porous $\text{g-C}_3\text{N}_4$ (DPCN), employing 3D N-doped reduced graphene oxide (N-rGO) as an electron mediator and Ni-Fe LDH as OEC. The surface area of the 3D DPCN/NRGO/NiFe-LDH hybrid sample was calculated and the amount was $85 \text{ m}^2 \text{ g}^{-1}$, which was significantly higher than those of PCN ($31 \text{ m}^2 \text{ g}^{-1}$), DPCN ($43 \text{ m}^2 \text{ g}^{-1}$), and DPCN/NRGO ($69 \text{ m}^2 \text{ g}^{-1}$). Such type of layered aerogel feature and flexible structure not only induce more reaction sites and provide the transport pathways for efficient charge transfer but also decrease distance for the charge transportation, thus facilitating the charge separation efficiency. Furthermore, the nitrogen vacancies in C_3N_4 could extend the light absorption range via tuning the band position of C_3N_4 effectively. Benefiting from these advantageous features, a high photocurrent of $162.3 \mu\text{A cm}^{-2}$ at 1.4 V and a maximum incident photon-to-current efficiency of 2.5% at 350 nm under AM 1.5G irradiation was achieved [142].

5. Summary and outlook

Designing and preparing highly active and stable photocatalysts are crucial to enhance the efficiency of OER and HER. Recently, Layered double hydroxide derived materials have shown prospective potential to be the candidate for photoanode/photocatalyst, which is resulted from their changeable 2D lamellar structure, various component of electrochemical active transition metal ions, visible light response, and tunable intrinsic electronic structure. The recent reports of the synthetic methods and application of LDH based materials in PC and PEC water splitting have been well summarized in Table 1, Table 2 and Table 3, respectively. This article has systematically summarized recent achievements in the engineering and fabrication of LDH-based nano-catalysts as well as highlighting structure–activity and chemical composition–performance relationships in PC/PEC water splitting reactions. We censoriously focused on the current progress and development of the most frequently used LDH based materials (Bin/ternary LDH, $\text{C}_3\text{N}_4/\text{LDH}$, TiO_2/LDH , WO_3/LDH , BiVO_4/LDH , $\alpha\text{-Fe}_2\text{O}_3/\text{LDH}$, Metal sulfide/LDH, and WO_3/LDH) for photocatalytic and PEC water splitting. In spite of the significant achievements described above, opportunities and invigorating perspectives in the design, synthesis, and future research of nanostructured LDH-based photocatalysts, which is outlined in Fig. 17.

- (i) Due to the outstanding adsorption capacity and high photocatalytic activity of LDHs toward to pollutants, it is trustworthy for LDHs catalysts that photocatalytic water splitting for H_2 production when organic pollutants acted as the sacrificial agent to consume photogenic holes. However, we have found the studies on this topic were limited [210–212]. That is quite meaningful to apply LDH based photocatalyst for PC/PEC hydrogen generation and environmental remediation applications (degradation of emerging pollutants or the disinfection) simultaneously and more attempts in the field of are encouraged.
- (ii) There is a large space for us to fabricate “adaptive-interface” in the heterostructure of photoanodes. More effective integrating treatments for the interface optimization between the semiconductors and LDHs, which would greatly inhibit the charge carrier recombination and transfer across the intimate interfaces, will be potentially applied to realize integrated PEC systems. Feasible methods include fabricating defects or vacancies, nanostructuring, rational selection of conductive supports, photo-assisted electrodeposition technique, interfacial modulation, controlling particle structure and size, etc.

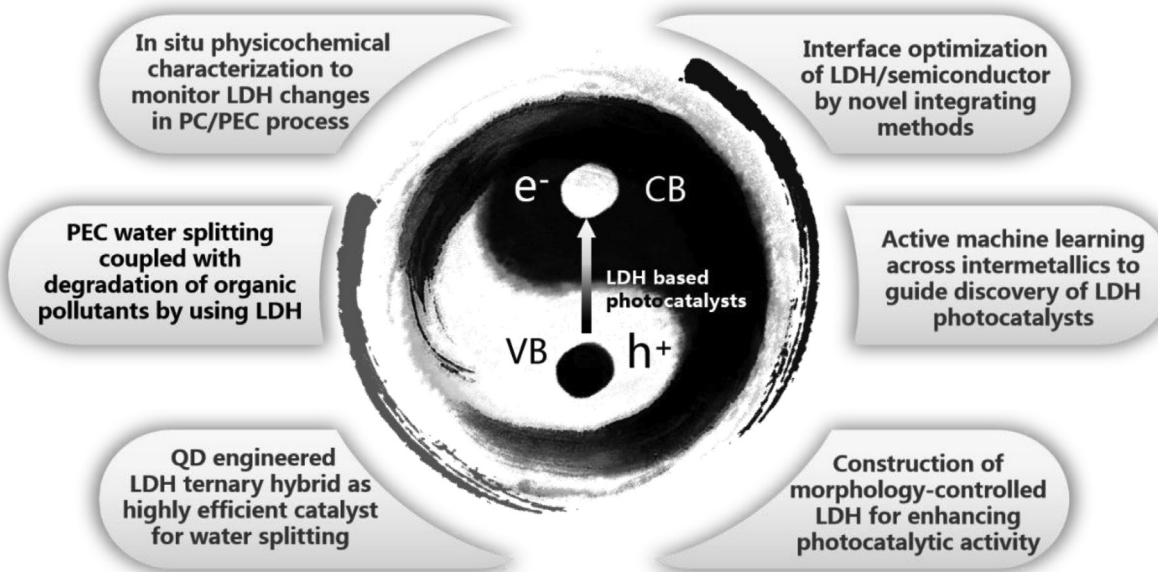


Fig. 17. Future challenges and research directions for LDH photocatalysis water splitting.

- (iii) Beyond the regular bulk hexagonal morphology of LDHs, 3D hierarchical morphology, can achieve reduction of diffusion length of electron-hole pairs, a high light-harvesting capabilities [213], the exposure of active sites, less agglomeration [214], and a rich aperture for gas transformation [215]. Therefore, the synthesis of LDH-based photocatalysts by the kinds of morphology engineering is worthwhile. As for a core-shell structure, the LDHs can act as either shell component or core materials. The wide selection of skeletons made 3D LDH (core@shell, yolk@shell) materials with some unique physicochemical properties, such as excellent hydrophilicity for adsorption of water molecules and the release of oxygen molecules [216].
- (iv) The combination of nanosheet LDHs with other semiconductor generated binary hybrids, offering a reliable way for further improving the photocatalytic efficiency. Beyond binary hybrid materials, multi-hybrid LDH based nanostructures may provide outstanding properties. We can see from **Table 2** and **Table 3**, the current research studies have been focused on the binary systems. Note that Graphene Quantum Dots, which has become one of the hottest topics for material science, are capable of decomposing water for H_2/O_2 evolution under visible light illumination [217,218], the elaboration of single-layer LDHs/Graphene Quantum Dots based ternary materials is expected to be able to provide more opportunities for enhanced PC/PEC performance.
- (v) At present, the transformations of chemical states of metal ions in LDHs during the PEC water splitting process are the main route to clarify the OER mechanism. However, the evolution of the surface structure of LDHs, the component variations within bin/ternary hybrid systems, as well as the formation of intermediates have not been fully addressed. In this context, *in situ* structural and electrical characterization techniques are urgently needed for deeper insight into the underlying mechanisms as well as reaction processes of the PEC-HER and PEC-OER at the molecular/atomic level. It is highly desirable to address the above issues in order to better realize the control of the types and quantities of active sites.

(vi) DFT method enable the full examination of structure–property relationships of LDHs catalysts [219–221] and Xu et al have already realized the effective theoretical and experimental combined method to screen possible LDH photocatalysts for oxygen generation in PC cell [85,222]. In a more recent study, Sun and co-workers offered an intelligent method that comprised of a integration of machine learning and optimization to guide DFT, offered an intelligent method that comprised of a integration of machine learning and optimization to guide DFT, and the optimized DFT was applied to screen the covalency competition in spinel oxides, with a mean absolute error of 0.05 eV [223]. Bear these encouraging findings in mind, active machine learning across intermetallics is definitely of significant potential to fabricate and screen LDH catalysts for PC/PEC water splitting.

Declaration of Competing Interest

The authors declare that they have no known competing financial interests or personal relationships that could have appeared to influence the work reported in this paper.

Acknowledgements

We thank the National Natural Science Foundation of China (51179068, 51679086, 51521006, 51879102, and 51809089). Research and Development Projects in Key Areas of Hunan Province, China (2019NK2062). The authors also thank Cao sisi for her help in the English writing.

References

- [1] S.J.A. Moniz, S.A. Shevlin, D.J. Martin, Z.-X. Guo, J. Tang, Visible-light driven heterojunction photocatalysts for water splitting – a critical review, *Energy Environ. Sci.* 8 (2015) 731–759, <https://doi.org/10.1039/C4EE03271C>.
- [2] K. Li, B. Peng, T. Peng, Recent advances in heterogeneous photocatalytic CO_2 conversion to solar fuels, *ACS Catal.* 6 (2016) 7485–7527, <https://doi.org/10.1021/acscatal.6b02089>.

- [3] X. Gao, H. Liu, D. Wang, J. Zhang, Graphdiyne: synthesis, properties, and applications, *Chem. Soc. Rev.* 48 (2019) 908–936, <https://doi.org/10.1039/C8CS00773J>.
- [4] J. Li, X. Zhang, Y. Sun, L. Liang, B. Pan, W. Zhang, X. Guan, Advances in sulfidation of zerovalent iron for water decontamination, *Environ. Sci. Technol.* 51 (2017) 13533–13544, <https://doi.org/10.1021/acs.est.7b02695>.
- [5] C.R. Lhermitte, K. Sivula, Alternative oxidation reactions for solar-driven fuel production, *ACS Catal.* 9 (2019) 2007–2017, <https://doi.org/10.1021/acscatal.8b04565>.
- [6] Y. Liu, D. Huang, M. Cheng, Z. Liu, C. Lai, C. Zhang, C. Zhou, W. Xiong, L. Qin, B. Shao, Q. Liang, Metal sulfide/MOF-based composites as visible-light-driven photocatalysts for enhanced hydrogen production from water splitting, *Coord. Chem. Rev.* 409 (2020), <https://doi.org/10.1016/j.ccr.2020.213220>.
- [7] Y. Liu, M. Cheng, Z. Liu, G. Zeng, H. Zhong, M. Chen, C. Zhou, W. Xiong, B. Shao, B. Song, Heterogeneous Fenton-like catalyst for treatment of rhamnolipid-solubilized hexadecane wastewater, *Chemosphere* 236 (2019), <https://doi.org/10.1016/j.chemosphere.2019.124387> 124387.
- [8] Y. Liu, G. Zeng, H. Zhong, Z. Wang, Z. Liu, M. Cheng, G. Liu, X. Yang, S. Liu, Effect of rhamnolipid solubilization on hexadecane bioavailability: enhancement or reduction?, *J. Hazard. Mater.* 322 (2017) 394–401, <https://doi.org/10.1016/j.jhazmat.2016.10.025>.
- [9] Z. Wang, Z. Zeng, H. Wang, G. Zeng, P. Xu, R. Xiao, D. Huang, S. Chen, Y. He, C. Zhou, M. Cheng, H. Qin, Bismuth-based metal-organic frameworks and their derivatives: opportunities and challenges, *Coord. Chem. Rev.* 439 (2021), <https://doi.org/10.1016/j.ccr.2021.213902> 213902.
- [10] L. Du, W. Xu, S. Liu, X. Li, D. Huang, X. Tan, Y. Liu, Activation of persulfate by graphitized biochar for sulfamethoxazole removal: the roles of graphitic carbon structure and carbonyl group, *J. Colloid Interface Sci.* 577 (2020) 419–430, <https://doi.org/10.1016/j.jcis.2020.05.096>.
- [11] F. Qin, Y. Peng, G. Song, Q. Fang, R. Wang, C. Zhang, G. Zeng, D. Huang, C. Lai, Y. Zhou, X. Tan, M. Cheng, S. Liu, Degradation of sulfamethazine by biochar-supported bimetallic oxide/persulfate system in natural water: performance and reaction mechanism, *J. Hazard. Mater.* 398 (2020), <https://doi.org/10.1016/j.jhazmat.2020.122816> 122816.
- [12] H. Zhang, L. Tang, J. Wang, J. Yu, H. Feng, Y. Lu, Y. Chen, Y. Liu, J. Wang, Q. Xie, Enhanced surface activation process of persulfate by modified bagasse biochar for degradation of phenol in water and soil: active sites and electron transfer mechanism, *Colloids Surf., A* 599 (2020), <https://doi.org/10.1016/j.colsurfa.2020.124904> 124904.
- [13] J.M. Gonçalves, M. Ireno da Silva, L. Angnes, K. Araki, Vanadium-containing electro and photocatalysts for the oxygen evolution reaction: a review, *J. Mater. Chem. A* 8 (2020) 2171–2206, <https://doi.org/10.1039/C9TA10857B>.
- [14] M. Tayebi, B.-K. Lee, Recent advances in BiVO₄ semiconductor materials for hydrogen production using photoelectrochemical water splitting, *Renew. Sustain. Energy Rev.* 111 (2019) 332–343, <https://doi.org/10.1016/j.rser.2019.05.030>.
- [15] Y. Park, K.J. McDonald, K.-S. Choi, Progress in bismuth vanadate photoanodes for use in solar water oxidation, *Chem. Soc. Rev.* 42 (2013) 2321–2337, <https://doi.org/10.1039/C2CS35260E>.
- [16] H.L. Tan, R. Amal, Y.H. Ng, Alternative strategies in improving the photocatalytic and photoelectrochemical activities of visible light-driven BiVO₄: a review, *J. Mater. Chem. A* 5 (2017) 16498–16521, <https://doi.org/10.1039/C7TA04441K>.
- [17] K. Takanabe, Photocatalytic water splitting: quantitative approaches toward photocatalyst by design, *ACS Catal.* 7 (2017) 8006–8022, <https://doi.org/10.1021/acscatal.7b02662>.
- [18] C. Ding, J. Shi, Z. Wang, C. Li, Photoelectrocatalytic water splitting: significance of cocatalysts, electrolyte, and interfaces, *ACS Catal.* 7 (2017) 675–688, <https://doi.org/10.1021/acscatal.6b03107>.
- [19] Q. Wang, K. Domen, Particulate photocatalysts for light-driven water splitting: mechanisms, challenges, and design strategies, *Chem. Rev.* 120 (2020) 919–985, <https://doi.org/10.1021/acs.chemrev.9b00201>.
- [20] J. Kosco, M. Bidwell, H. Cha, T. Martin, C.T. Howells, M. Sachs, D.H. Anjum, S. Gonzalez Lopez, L. Zou, A. Wadsworth, W. Zhang, L. Zhang, J. Tellam, R. Sougrat, F. Laquai, D.M. DeLongchamp, J.R. Durrant, I. McCulloch, Enhanced photocatalytic hydrogen evolution from organic semiconductor heterojunction nanoparticles, *Nat. Mater.* 19 (2020) 559–565, <https://doi.org/10.1038/s41563-019-0591-1>.
- [21] M.T. Mayer, Y. Lin, G. Yuan, D. Wang, Forming heterojunctions at the nanoscale for improved photoelectrochemical water splitting by semiconductor materials: case studies on hematite, *Acc. Chem. Res.* 46 (2013) 1558–1566, <https://doi.org/10.1021/ar300302z>.
- [22] L. Wang, L. Xie, W. Zhao, S. Liu, Q. Zhao, Oxygen-facilitated dynamic active-site generation on strained MoS₂ during photo-catalytic hydrogen evolution, *Chem. Eng. J.* 405 (2021), <https://doi.org/10.1016/j.cej.2020.127028> 127028.
- [23] Y. Liu, H. Cheng, M. Cheng, Z. Liu, D. Huang, G. Zhang, B. Shao, Q. Liang, S. Luo, T. Wu, S. Xiao, The application of Zeolitic imidazolate frameworks (ZIFs) and their derivatives based materials for photocatalytic hydrogen evolution and pollutants treatment, *Chem. Eng. J.* 417 (2021), <https://doi.org/10.1016/j.cej.2020.127914> 127914.
- [24] L. Jing, W. Zhou, G. Tian, H. Fu, Surface tuning for oxide-based nanomaterials as efficient photocatalysts, *Chem. Soc. Rev.* 42 (2013) 9509, <https://doi.org/10.1039/c3cs60176e>.
- [25] C. Liang, H.-Y. Niu, H. Guo, C.-G. Niu, Y.-Y. Yang, H.-Y. Liu, W.-W. Tang, H.-P. Feng, Efficient photocatalytic nitrogen fixation to ammonia over bismuth monoxide quantum dots-modified defective ultrathin graphitic carbon nitride, *Chem. Eng. J.* 406 (2021), <https://doi.org/10.1016/j.cej.2020.126868> 126868.
- [26] S. Chandrasekaran, L. Yao, L. Deng, C. Bowen, Y. Zhang, S. Chen, Z. Lin, F. Peng, P. Zhang, Recent advances in metal sulfides: from controlled fabrication to electrocatalytic, photocatalytic and photoelectrochemical water splitting and beyond, *Chem. Soc. Rev.* 48 (2019) 4178–4280, <https://doi.org/10.1039/C8CS00664D>.
- [27] H.-Y. Liu, C.-G. Niu, H. Guo, C. Liang, D.-W. Huang, L. Zhang, Y.-Y. Yang, L. Li, In situ constructing 2D/1D MgIn₂S₄/CdS heterojunction system with enhanced photocatalytic activity towards treatment of wastewater and H₂ production, *J. Colloid Interface Sci.* 576 (2020) 264–279, <https://doi.org/10.1016/j.jcis.2020.05.025>.
- [28] Y. Wu, P. Lazic, G. Hautier, K. Persson, G. Ceder, First principles high throughput screening of oxynitrides for water-splitting photocatalysts, *Energy Environ. Sci.* 6 (2013) 157–168, <https://doi.org/10.1039/C2EE23482C>.
- [29] C. Chen, L. Tao, S. Du, W. Chen, Y. Wang, Y. Zou, S. Wang, Advanced exfoliation strategies for layered double hydroxides and applications in energy conversion and storage, *Adv. Funct. Mater.* 30 (2020) 1909832, <https://doi.org/10.1002/adfm.201909832>.
- [30] Y. Hu, L. Mao, X. Guan, K.A. Tucker, H. Xie, X. Wu, J. Shi, Layered perovskite oxides and their derivative nanosheets adopting different modification strategies towards better photocatalytic performance of water splitting, *Renew. Sustain. Energy Rev.* 119 (2020), <https://doi.org/10.1016/j.rser.2019.109527> 109527.
- [31] Z. Li, X. Zhang, H. Cheng, J. Liu, M. Shao, M. Wei, D.G. Evans, H. Zhang, X. Duan, Confined synthesis of 2D nanostructured materials toward electrocatalysis, *Adv. Energy Mater.* 10 (2020) 1900486, <https://doi.org/10.1002/aenm.201900486>.
- [32] W. Xie, Z. Li, M. Shao, M. Wei, Layered double hydroxide-based core-shell nanoarrays for efficient electrochemical water splitting, *Front. Chem. Sci. Eng.* 12 (2018) 537–554, <https://doi.org/10.1007/s11705-018-1719-6>.
- [33] R. Gao, X. Mei, D. Yan, R. Liang, M. Wei, Nano-photosensitizer based on layered double hydroxide and isophthalic acid for singlet oxygenation and photodynamic therapy, *Nat. Commun.* 9 (2018) 2798, <https://doi.org/10.1038/s41467-018-05223-3>.
- [34] Z. Li, H. Duan, M. Shao, J. Li, D. O'Hare, M. Wei, Z.L. Wang, Ordered-vacancy-induced cation intercalation into layered double hydroxides: a general approach for high-performance supercapacitors, *Chem* 4 (2018) 2168–2179, <https://doi.org/10.1016/j.chempr.2018.06.007>.
- [35] Y. Lee, J.H. Choi, H.J. Jeon, K.M. Choi, J.W. Lee, J.K. Kang, Titanium-embedded layered double hydroxides as highly efficient water oxidation photocatalysts under visible light, *Energy Environ. Sci.* 4 (2011) 914, <https://doi.org/10.1039/c0ee00285b>.
- [36] L. Mohapatra, K. Parida, A review on the recent progress, challenges and perspective of layered double hydroxides as promising photocatalysts, *J. Mater. Chem. A* 4 (2016) 10744–10766, <https://doi.org/10.1039/C6TA01668E>.
- [37] M. Xu, M. Wei, Layered double hydroxide-based catalysts: recent advances in preparation, structure, and applications, *Adv. Funct. Mater.* 28 (2018) 1802943, <https://doi.org/10.1002/adfm.201802943>.
- [38] B. Song, Z. Zeng, G. Zeng, J. Gong, R. Xiao, S. Ye, M. Chen, C. Lai, P. Xu, X. Tang, Powerful combination of g-C₃N₄ and LDHs for enhanced photocatalytic performance: a review of strategy, synthesis, and applications, *Adv. Colloid Interface Sci.* 272 (2019), <https://doi.org/10.1016/j.cis.2019.101999> 101999.
- [39] A.E.A. Aboubakr, W.M.A. El Rouby, M.D. Khan, A.A. Farghalni, N. Revaprasadu, ZnCr₂O₄ LDH/ruptured tubular g-C₃N₄ composite with increased specific surface area for enhanced photoelectrochemical water splitting, *Appl. Surf. Sci.* 508 (2020), <https://doi.org/10.1016/j.apsusc.2019.145100> 145100.
- [40] S. Xia, M. Qian, X. Zhou, Y. Meng, J. Xue, Z. Ni, Theoretical and experimental investigation into the photocatalytic degradation of hexachlorobenzene by ZnCr layered double hydroxides with different anions, *Mol. Catal.* 435 (2017) 118–127, <https://doi.org/10.1016/j.mcat.2017.03.024>.
- [41] T.-T. Kong, J. Huang, X.-G. Jia, W.-Z. Wang, Y. Zhou, Synthesis and optimization of Ti/Li/Al ternary layered double hydroxides for efficient photocatalytic reduction of CO₂ to CH₄, *Sci. Rep.* 9 (2019) 5659, <https://doi.org/10.1038/s41598-019-41979-4>.
- [42] X.-T. Xu, L. Pan, X. Zhang, L. Wang, J.-J. Zou, Rational design and construction of cocatalysts for semiconductor-based photo-electrochemical oxygen evolution: a comprehensive review, *Adv. Sci.* 6 (2019) 1801505, <https://doi.org/10.1002/advs.201801505>.
- [43] B. Shao, Z. Liu, G. Zeng, Y. Liu, Q. Liang, Q. He, T. Wu, Y. Pan, J. Huang, Z. Peng, S. Luo, C. Liang, X. Liu, S. Tong, J. Liang, Synthesis of 2D/2D CoAl-LDHs/Ti3C₂T_x Schottky-junction with enhanced interfacial charge transfer and visible-light photocatalytic performance, *Appl. Catal. B* 286 (2021), <https://doi.org/10.1016/j.apcatb.2020.119867> 119867.
- [44] D.K. Lee, D. Lee, M.A. Lumley, K.-S. Choi, Progress on ternary oxide-based photoanodes for use in photoelectrochemical cells for solar water splitting, *Chem. Soc. Rev.* 48 (2019) 2126–2157, <https://doi.org/10.1039/C8CS00761F>.
- [45] J. Li, S. Jiang, M. Shao, M. Wei, Host-guest engineering of layered double hydroxides towards efficient oxygen evolution reaction: recent advances and perspectives, *Catalysts* 8 (2018) 214, <https://doi.org/10.3390/catal8050214>.
- [46] Z. Cai, X. Bu, P. Wang, J.C. Ho, J. Yang, X. Wang, Recent advances in layered double hydroxide electrocatalysts for the oxygen evolution reaction, *J. Mater. Chem. A* 7 (2019) 5069–5089, <https://doi.org/10.1039/C8TA11273H>.
- [47] H. Zhong, C. Campos-Roldán, Y. Zhao, S. Zhang, Y. Feng, N. Alonso-Vante, Recent advances of cobalt-based electrocatalysts for oxygen electrode

- reactions and hydrogen evolution reaction, *Catalysts* 8 (2018) 559, <https://doi.org/10.3390/catal8110559>.
- [48] L. Lv, Z. Yang, K. Chen, C. Wang, Y. Xiong, 2D layered double hydroxides for oxygen evolution reaction: from fundamental design to application, *Adv. Energy Mater.* 9 (2019) 1803358, <https://doi.org/10.1002/aenm.201803358>.
- [49] X. Lu, H. Xue, H. Gong, M. Bai, D. Tang, R. Ma, T. Sasaki, 2D layered double hydroxide nanosheets and their derivatives toward efficient oxygen evolution reaction, *Nano-Micro Lett.* 12 (2020) 86, <https://doi.org/10.1007/s40820-020-00421-5>.
- [50] L. Zhou, M. Shao, M. Wei, X. Duan, Advances in efficient electrocatalysts based on layered double hydroxides and their derivatives, *J. Energy Chem.* 26 (2017) 1094–1106, <https://doi.org/10.1016/j.jechem.2017.09.015>.
- [51] Y. Chen, K. Rui, J. Zhu, S.X. Dou, W. Sun, Recent progress on nickel-based oxide/(oxy)hydroxide electrocatalysts for the oxygen evolution reaction, *Chem. Eur. J.* 25 (2019) 703–713, <https://doi.org/10.1002/chem.201802068>.
- [52] S. Ananthraj, K. Karthick, S. Kundu, Evolution of layered double hydroxides (LDH) as high performance water oxidation electrocatalysts: a review with insights on structure, activity and mechanism, *Mater. Today Energy* 6 (2017) 1–26, <https://doi.org/10.1016/j.mtener.2017.07.016>.
- [53] J. Mohammed-Ibrahim, A review on NiFe-based electrocatalysts for efficient alkaline oxygen evolution reaction, *J. Power Sources* 448 (2020), <https://doi.org/10.1016/j.jpowsour.2019.227375>.
- [54] P.M. Bodhankar, P.B. Sarawade, G. Singh, A. Vinu, D.S. Dhawale, Recent advances in highly active nanostructured NiFe LDH catalyst for electrochemical water splitting, *J. Mater. Chem. A.* 9 (2021) 3180–3208, <https://doi.org/10.1039/DOTA10712C>.
- [55] R. Sahoo, A. Pal, T. Pal, 2D materials for renewable energy storage devices: outlook and challenges, *Chem. Commun.* 52 (2016) 13528–13542, <https://doi.org/10.1039/C6CC05357B>.
- [56] Y. Zhao, X. Jia, G.I.N. Waterhouse, L.-Z. Wu, C.-H. Tung, D. O'Hare, T. Zhang, Layered double hydroxide nanostructured photocatalysts for renewable energy production, *Adv. Energy Mater.* 6 (2016) 1501974, <https://doi.org/10.1002/aenm.201501974>.
- [57] G. Zhao, J. Zou, X. Chen, J. Yu, F. Jiao, Layered double hydroxides materials for photo(electro-) catalytic applications, *Chem. Eng. J.* 397 (2020), <https://doi.org/10.1016/j.cej.2020.125407> 125407.
- [58] M. Ge, Q. Li, C. Cao, J. Huang, S. Li, S. Zhang, Z. Chen, K. Zhang, S.S. Al-Deyab, Y. Lai, One-dimensional TiO₂ nanotube photocatalysts for solar water splitting, *Adv. Sci.* 4 (2017) 1600152, <https://doi.org/10.1002/advs.201600152>.
- [59] C. Prasad, H. Tang, Q.Q. Liu, S. Zulfiqar, S. Shah, I. Bahadur, An overview of semiconductors/layered double hydroxides composites: properties, synthesis, photocatalytic and photoelectrochemical applications, *J. Mol. Liq.* 289 (2019), <https://doi.org/10.1016/j.molliq.2019.111114> 111114.
- [60] M. Hadnadjev-Kostic, T. Vulic, R. Marinkovic-Neducin, D. Lončarević, J. Dostanić, S. Markov, D. Jovanović, Photo-induced properties of photocatalysts: a study on the modified structural, optical and textural properties of TiO₂ –ZnAl layered double hydroxide based materials, *J. Cleaner Prod.* 164 (2017) 1–18, <https://doi.org/10.1016/j.jclepro.2017.06.091>.
- [61] E. Boccalon, G. Gorrasí, M. Nocchetti, Layered double hydroxides are still out in the bloom: syntheses, applications and advantages of three-dimensional flower-like structures, *Adv. Colloid Interface Sci.* 285 (2020), <https://doi.org/10.1016/j.jcis.2020.102284> 102284.
- [62] Z. Yang, C. Zhang, G. Zeng, X. Tan, H. Wang, D. Huang, K. Yang, J. Wei, C. Ma, K. Nie, Design and engineering of layered double hydroxide based catalysts for water depollution by advanced oxidation processes: a review, *J. Mater. Chem. A.* 8 (2020) 4141–4173, <https://doi.org/10.1039/C9TA13522G>.
- [63] Y. Pan, X. Liu, W. Zhang, Z. Liu, G. Zeng, B. Shao, Q. Liang, Q. He, X. Yuan, D. Huang, M. Chen, Advances in photocatalysis based on fullerene C60 and its derivatives: properties, mechanism, synthesis, and applications, *Appl. Catal. B* 265 (2020), <https://doi.org/10.1016/j.apcatb.2019.118579> 118579.
- [64] J. Prince, A. Montoya, G. Ferrat, J.S. Valente, Proposed general sol–gel method to prepare multimetallic layered double hydroxides: synthesis, characterization, and envisaged application, *Chem. Mater.* 21 (2009) 5826–5835, <https://doi.org/10.1021/cm902741c>.
- [65] G.M. Tomboc, J. Kim, Y. Wang, Y. Son, J. Li, J.Y. Kim, K. Lee, Hybrid layered double hydroxides as multifunctional nanomaterials for overall water splitting and supercapacitor applications, *J. Mater. Chem. A.* (2021) 10.1039/DOTA11606H. DOI: 10.1039/DOTA11606H.
- [66] A.M.P. Sakita, R.D. Noce, E. Vallés, A.V. Benedetti, Pulse electrodeposition of CoFe thin films covered with layered double hydroxides as a fast route to prepare enhanced catalysts for oxygen evolution reaction, *Appl. Surf. Sci.* 434 (2018) 1153–1160, <https://doi.org/10.1016/j.apusc.2017.11.042>.
- [67] H. Wu, K. Yin, W. Qi, X. Zhou, J. He, J. Li, Y. Liu, J. He, S. Gong, Y. Li, Rapid fabrication of Ni/NiO@CoFe layered double hydroxide hierarchical nanostructures by femtosecond laser ablation and electrodeposition for efficient overall water splitting, *ChemSusChem* 12 (2019) 2773–2779, <https://doi.org/10.1002/cssc.201900479>.
- [68] R. Patel, J.T. Park, M. Patel, J.K. Dash, E.B. Gowd, R. Karpoormath, A. Mishra, J. Kwak, J.H. Kim, Transition-metal-based layered double hydroxides tailored for energy conversion and storage, *J. Mater. Chem. A.* 6 (2018) 12–29, <https://doi.org/10.1039/C7TA09370E>.
- [69] M. Shao, R. Zhang, Z. Li, M. Wei, D.G. Evans, X. Duan, Layered double hydroxides toward electrochemical energy storage and conversion: design, synthesis and applications, *Chem. Commun.* 51 (2015) 15880–15893, <https://doi.org/10.1039/C5CC07296D>.
- [70] S. Han, S. Liu, S. Yin, L. Chen, Z. He, Electrodeposited co-doped Fe3O4 thin films as efficient catalysts for the oxygen evolution reaction, *Electrochim. Acta* 210 (2016) 942–949, <https://doi.org/10.1016/j.electacta.2016.05.194>.
- [71] Y. Wang, Z. Yin, G. Yan, Z. Wang, X. Li, H. Guo, J. Wang, New insight into the electrodeposition of NiCo layered double hydroxide and its capacitive evaluation, *Electrochim. Acta* 336 (2020), <https://doi.org/10.1016/j.electacta.2020.135734> 135734.
- [72] R. Li, Y. Li, P. Yang, D. Wang, H. Xu, B. Wang, F. Meng, J. Zhang, M. An, Electrodeposition: synthesis of advanced transition metal-based catalyst for hydrogen production via electrolysis of water, *J. Energy Chem.* 57 (2021) 547–566, <https://doi.org/10.1016/j.jechem.2020.08.040>.
- [73] H. She, P. Yue, X. Ma, J. Huang, L. Wang, Q. Wang, Fabrication of BiVO₄ photoanode cocatalyzed with NiCo-layered double hydroxide for enhanced photoactivity of water oxidation, *Appl. Catal. B* 263 (2020), <https://doi.org/10.1016/j.apcatb.2019.118280> 118280.
- [74] X. Fan, T. Wang, B. Gao, X. Xie, S. Zhang, X. Meng, H. Gong, Y. Guo, X. Huang, J. He, Layered double hydroxides decorated graphic carbon nitride film as efficient photoanodes for photoelectrochemical water splitting, *Catal. Today* 335 (2019) 423–428, <https://doi.org/10.1016/j.cattod.2019.01.034>.
- [75] Y.B. Park, J.H. Kim, Y.J. Jang, J.H. Lee, M.H. Lee, B.J. Lee, D.H. Youn, J.S. Lee, Exfoliated NiFe layered double hydroxide cocatalyst for enhanced photoelectrochemical water oxidation with hematite photoanode, *ChemCatChem* 11 (2019) 443–448, <https://doi.org/10.1002/cctc.201801490>.
- [76] X. Yu, J. Liu, W. Yin, T. Wang, L. Quan, Y. Ran, J. Cui, L. Wang, Y. Zhang, Ultrathin NiMn-layered double hydroxide nanosheets coupled with α -Fe2O3 nanorod arrays for photoelectrochemical water splitting, *Appl. Surf. Sci.* 492 (2019) 264–271, <https://doi.org/10.1016/j.apsusc.2019.06.162>.
- [77] T.S. Sinclair, H.B. Gray, A.M. Müller, Photoelectrochemical performance of BiVO₄ photoanodes integrated with [NiFe]-layered double hydroxide nanocatalysts: photoelectrochemical performance of BiVO₄ photoanodes integrated with [NiFe]-layered double hydroxide nanocatalysts, *Eur. J. Inorg. Chem.* 2018 (2018) 1060–1067, <https://doi.org/10.1002/ejic.201701231>.
- [78] H. Li, X. Hao, Y. Liu, Y. Li, Z. Jin, ZnxCd1-xS nanoparticles dispersed on CoAl-layered double hydroxide in 2D heterostructure for enhanced photocatalytic hydrogen evolution, *J. Colloid Interface Sci.* 572 (2020) 62–73, <https://doi.org/10.1016/j.jcis.2020.03.052>.
- [79] D. Kandi, D.P. Sahoo, S. Martha, K. Parida, Rational design of a coupled confronting Z-scheme system toward photocatalytic refractory pollutant degradation and water splitting reaction, *Adv. Mater. Interfaces*. 6 (2019) 1900370, <https://doi.org/10.1002/admi.201900370>.
- [80] L. Jafari Foruzin, Z. Rezvani, Ultrasonication construction of the nano-petal NiCoFe-layered double hydroxide: An excellent water oxidation electrocatalyst, *Ultrason. Sonochem.* 64 (2020), <https://doi.org/10.1016/j.ultrsonch.2019.104919> 104919.
- [81] G. Liu, Y. Sheng, J.W. Ager, M. Kraft, R. Xu, Research advances towards large-scale solar hydrogen production from water, *EnergyChem.* 1 (2019), <https://doi.org/10.1016/j.enchem.2019.100014> 100014.
- [82] N. Fajrina, M. Tahir, A critical review in strategies to improve photocatalytic water splitting towards hydrogen production, *Int. J. Hydrogen Energy* 44 (2019) 540–577, <https://doi.org/10.1016/j.ijhydene.2018.10.200>.
- [83] K. Afroz, M. Moniruddin, N. Bakravon, S. Kudaibergenov, N. Nuraje, A heterojunction strategy to improve the visible light sensitive water splitting performance of photocatalytic materials, *J. Mater. Chem. A.* 6 (2018) 21696–21718, <https://doi.org/10.1039/C8TA04165B>.
- [84] S. Zhang, H. Ye, J. Hua, H. Tian, Recent advances in dye-sensitized photoelectrochemical cells for water splitting, *EnergyChem.* 1 (2019), <https://doi.org/10.1016/j.enchem.2019.100015> 100015.
- [85] S.-M. Xu, H. Yan, M. Wei, Band structure engineering of transition-metal-based layered double hydroxides toward photocatalytic oxygen evolution from water: a theoretical-experimental combination study, *J. Phys. Chem. C* 121 (2017) 2683–2695, <https://doi.org/10.1021/acs.jpcc.6b10159>.
- [86] S. Xie, Q. Zhang, G. Liu, Y. Wang, Photocatalytic and photoelectrocatalytic reduction of CO₂ using heterogeneous catalysts with controlled nanostructures, *Chem. Commun.* 52 (2016) 35–59, <https://doi.org/10.1039/C5CC07613G>.
- [87] A. Fujishima, K. Honda, Electrochemical photolysis of water at a semiconductor electrode, *Nature* 238 (1972) 37–38, <https://doi.org/10.1038/238037a0>.
- [88] Y. Zhao, N. Hoivik, K. Wang, Recent advance on engineering titanium dioxide nanotubes for photochemical and photoelectrochemical water splitting, *Nano Energy* 30 (2016) 728–744, <https://doi.org/10.1016/j.nanoen.2016.09.027>.
- [89] P. Sharma, J. Jang, J.S. Lee, Key strategies to advance the photoelectrochemical water splitting performance of α -Fe₂O₃ photoanode, *ChemCatChem* 11 (2019) 157–179, <https://doi.org/10.1002/cctc.201801187>.
- [90] G. Zheng, J. Wang, H. Liu, V. Murugadoss, G. Zu, H. Che, C. Lai, H. Li, T. Ding, Q. Gao, Z. Guo, Tungsten oxide nanostructures and nanocomposites for photoelectrochemical water splitting, *Nanoscale*. 11 (2019) 18968–18994, <https://doi.org/10.1039/C9NR03474A>.
- [91] J.H. Kim, J.S. Lee, Elaborately modified BiVO₄ photoanodes for solar water splitting, *Adv. Mater.* 31 (2019) 1806938, <https://doi.org/10.1002/adma.201806938>.
- [92] R. Gao, D. Yan, Recent development of Ni/Fe-based micro/nanostructures toward photo/electrochemical water oxidation, *Adv. Energy Mater.* 10 (2020) 1900954, <https://doi.org/10.1002/aenm.201900954>.

- [93] J. Ran, J. Zhang, J. Yu, M. Jaroniec, S.Z. Qiao, Earth-abundant cocatalysts for semiconductor-based photocatalytic water splitting, *Chem. Soc. Rev.* 43 (2014) 7787–7812, <https://doi.org/10.1039/C3CS60425J>.
- [94] S. Nayak, G. Swain, K. Parida, Enhanced photocatalytic activities of RhB degradation and H₂ evolution from in situ formation of the electrostatic heterostructure MoS₂/NiFe LDH nanocomposite through the Z-Scheme mechanism via p-n heterojunctions, *ACS Appl. Mater. Interfaces* 11 (2019) 20923–20942, <https://doi.org/10.1021/acsami.9b06511>.
- [95] M. Gong, Y. Li, H. Wang, Y. Liang, J.Z. Wu, J. Zhou, J. Wang, T. Regier, F. Wei, H. Dai, An advanced Ni-Fe layered double hydroxide electrocatalyst for water oxidation, *J. Am. Chem. Soc.* 135 (2013) 8452–8455, <https://doi.org/10.1021/ja4027715>.
- [96] C.G. Morales-Guio, M.T. Mayer, A. Yella, S.D. Tilley, M. Grätzel, X. Hu, An optically transparent iron nickel oxide catalyst for solar water splitting, *J. Am. Chem. Soc.* 137 (2015) 9927–9936, <https://doi.org/10.1021/jacs.5b05544>.
- [97] S. Kment, F. Riboni, S. Pausova, L. Wang, L. Wang, H. Han, Z. Hubicka, J. Krysa, P. Schmuki, R. Zboril, Photoanodes based on TiO₂ and α -Fe₂O₃ for solar water splitting – superior role of 1D nanoarchitectures and of combined heterostructures, *Chem. Soc. Rev.* 46 (2017) 3716–3769, <https://doi.org/10.1039/C6CS00015K>.
- [98] J. Chen, C. Wang, Y. Zhang, Z. Guo, Y. Luo, C.-J. Mao, Engineering ultrafine NiS cocatalysts as active sites to boost photocatalytic hydrogen production of MgAl layered double hydroxide, *Appl. Surf. Sci.* 506 (2020), <https://doi.org/10.1016/j.apsusc.2019.144999> 144999.
- [99] B. Wang, J. Pan, Z. Jiang, Z. Dong, C. Zhao, J. Wang, C. Song, Y. Zheng, C. Li, The bimetallic iron–nickel sulfide modified g-C3N4 nano-heterojunction and its photocatalytic hydrogen production enhancement, *J. Alloy. Compd.* 766 (2018) 421–428, <https://doi.org/10.1016/j.jallcom.2018.06.377>.
- [100] Y. Zhao, B. Li, Q. Wang, W. Gao, C.J. Wang, M. Wei, D.G. Evans, X. Duan, D. O'Hare, NiTi-layered double hydroxides nanosheets as efficient photocatalysts for oxygen evolution from water using visible light, *Chem. Sci.* 5 (2014) 951–958, <https://doi.org/10.1039/C3SC52546E>.
- [101] N. Hirata, K. Tadanaga, M. Tatsumisago, Photocatalytic O₂ evolution from water over Zn–Cr layered double hydroxides intercalated with inorganic anions, *Mater. Res. Bull.* 62 (2015) 1–4, <https://doi.org/10.1016/j.materresbull.2014.11.013>.
- [102] Y. Fu, F. Ning, S. Xu, H. An, M. Shao, M. Wei, Terbium doped ZnCr-layered double hydroxides with largely enhanced visible light photocatalytic performance, *J. Mater. Chem. A* 4 (2016) 3907–3913, <https://doi.org/10.1039/C5TA10093C>.
- [103] A.R. Amani-Ghadim, ZnS quantum dot intercalated layered double hydroxide semiconductors for solar water splitting and organic pollutant degradation, *J. Mater. Chem. A* (2019) 15.
- [104] L. Jafari Foruzin, Z. Rezvani, K. Nejati, Z. Hou, H. Dai, K. Asadpour-Zeynali, High quantum efficiency of photocatalytic water oxidation over the TiO₂/MMO nanocomposite under visible-light irradiation, *J. Mol. Liq.* 288 (2019), <https://doi.org/10.1016/j.molliq.2019.111035> 111035.
- [105] Y. Dou, S. Zhang, T. Pan, S. Xu, A. Zhou, M. Pu, H. Yan, J. Han, M. Wei, D.G. Evans, X. Duan, TiO₂@layered double hydroxide core-shell nanospheres with largely enhanced photocatalytic activity toward O₂ generation, *Adv. Funct. Mater.* 25 (2015) 2243–2249, <https://doi.org/10.1002/adfm.201404496>.
- [106] H. Zhou, Y. Song, Y. Liu, H. Li, W. Li, Z. Chang, Fabrication of CdS/Ni Fe LDH heterostructure for improved photocatalytic hydrogen evolution from aqueous methanol solution, *Int. J. Hydrogen Energy* 43 (2018) 14328–14336, <https://doi.org/10.1016/j.ijhydene.2018.05.172>.
- [107] H. Lee, D.A. Reddy, Y. Kim, S.Y. Chun, R. Ma, D.P. Kumar, J.K. Song, T.K. Kim, Drastic improvement of 1D-CdS solar-driven photocatalytic hydrogen evolution rate by integrating with NiFe layered double hydroxide nanosheets synthesized by liquid-phase pulsed-laser ablation, *ACS Sustainable Chem. Eng.* 6 (2018) 16734–16743, <https://doi.org/10.1021/acssuschemeng.8b04000>.
- [108] D. Yue, X. Qian, M. Kan, M. Ren, Y. Zhu, L. Jiang, Y. Zhao, Sulfurated [NiFe]-based layered double hydroxides nanoparticles as efficient co-catalysts for photocatalytic hydrogen evolution using CdTe/CdS quantum dots, *Appl. Catal. B* 209 (2017) 155–160, <https://doi.org/10.1016/j.apcatb.2017.02.075>.
- [109] S. Li, L. Wang, Y. Li, L. Zhang, A. Wang, N. Xiao, Y. Gao, N. Li, W. Song, L. Ge, J. Liu, Novel photocatalyst incorporating Ni-Co layered double hydroxides with P-doped CdS for enhancing photocatalytic activity towards hydrogen evolution, *Appl. Catal. B* 254 (2019) 145–155, <https://doi.org/10.1016/j.apcatb.2019.05.001>.
- [110] S. Min, J. Hou, Y. Lei, X. Liu, Y. Li, Y. Xue, E. Cui, W. Yan, W. Hai, F. Wang, CoAl-layered double hydroxide nanosheets as an active matrix to anchor an amorphous MoS_x catalyst for efficient visible light hydrogen evolution, *Chem. Commun.* 54 (2018) 3243–3246, <https://doi.org/10.1039/C8CC00059J>.
- [111] M. Zhang, Z. Luo, M. Zhou, G. Zhang, K.A. Alamry, L.A. Taib, A.M. Asiri, X. Wang, Ni-Co layered double hydroxides cocatalyst for sustainable oxygen photosynthesis, *Appl. Catal. B* 210 (2017) 454–461, <https://doi.org/10.1016/j.apcatb.2017.03.080>.
- [112] J. Shi, S. Li, F. Wang, L. Gao, Y. Li, X. Zhang, J. Lu, 2D/2D g-C3N4/MgFe MMO nanosheet heterojunctions with enhanced visible-light photocatalytic H₂ production, *J. Alloy. Compd.* 769 (2018) 611–619, <https://doi.org/10.1016/j.jallcom.2018.08.028>.
- [113] S. Nayak, K.M. Parida, Deciphering Z-scheme charge transfer dynamics in heterostructure NiFe-LDH/N-rGO/g-C3N4 nanocomposite for photocatalytic pollutant removal and water splitting reactions, *Sci. Rep.* 9 (2019) 2458, <https://doi.org/10.1038/s41598-019-39009-4>.
- [114] K.-H. Kim, J.W. Choi, H. Lee, B.C. Moon, D.G. Park, W.H. Choi, J.K. Kang, Plasma-mediated fabrication of ultrathin NiAl nanosheets having rich oxygen vacancies and doped nitrogen sites and their utilization for high activity and robust stability in photoelectrochemical water oxidation, *J. Mater. Chem. A* 6 (2018) 23283–23288, <https://doi.org/10.1039/C8TA08334G>.
- [115] R.A. Sayed, S.E. Abd El Hafiz, N. Gamal, Y. GadelHak, W.M.A. El Rouby, Co-Fe layered double hydroxide decorated titanate nanowires for overall photoelectrochemical water splitting, *J. Alloy. Compd.* 728 (2017) 1171–1179, <https://doi.org/10.1016/j.jallcom.2017.09.083>.
- [116] S. Zheng, J. Lu, D. Yan, Y. Qin, H. Li, D.G. Evans, X. Duan, An inexpensive co-intercalated layered double hydroxide composite with electron donor-acceptor character for photoelectrochemical water splitting, *Sci. Rep.* 5 (2015) 12170, <https://doi.org/10.1038/srep12170>.
- [117] H.-J. Ahn, A. Goswami, F. Riboni, S. Kment, A. Naldoni, S. Mohajernia, R. Zboril, P. Schmuki, Hematite photoanode with complex nanoarchitecture providing tunable gradient doping and low onset potential for photoelectrochemical water splitting, *ChemSusChem* 11 (2018) 1873–1879, <https://doi.org/10.1002/cssc.201800256>.
- [118] Y. Zhu, X. Zhao, J. Li, H. Zhang, S. Chen, W. Han, D. Yang, Surface modification of hematite photoanode by NiFe layered double hydroxide for boosting photoelectrocatalytic water oxidation, *J. Alloy. Compd.* 764 (2018) 341–346, <https://doi.org/10.1016/j.jallcom.2018.06.064>.
- [119] R. Chong, B. Wang, C. Su, D. Li, L. Mao, Z. Chang, L. Zhang, Dual-functional CoAl layered double hydroxide decorated α -Fe₂O₃ as an efficient and stable photoanode for photoelectrochemical water oxidation in neutral electrolyte, *J. Mater. Chem. A* 5 (2017) 8583–8590, <https://doi.org/10.1039/C7TA01586K>.
- [120] R. Chong, G. Wang, Y. Du, Y. Jia, X. Wang, C. Li, Z. Chang, L. Zhang, Anion engineering of exfoliated CoAl layered double hydroxides on hematite photoanode toward highly efficient photoelectrochemical water splitting, *Chem. Eng. J.* 366 (2019) 523–530, <https://doi.org/10.1016/j.cej.2019.02.127>.
- [121] C. Wang, X. Long, S. Wei, T. Wang, F. Li, L. Gao, Y. Hu, S. Li, J. Jin, Conformally coupling CoAl-layered double hydroxides on fluorine-doped hematite: surface and bulk co-modification for enhanced photoelectrochemical water oxidation, *ACS Appl. Mater. Interfaces* 11 (2019) 29799–29806, <https://doi.org/10.1021/acsami.9b07417>.
- [122] G. Wang, B. Wang, C. Su, D. Li, L. Zhang, R. Chong, Z. Chang, Enhancing and stabilizing α -Fe₂O₃ photoanode towards neutral water oxidation: introducing a dual-functional NiCoAl layered double hydroxide overlayer, *J. Catal.* 359 (2018) 287–295, <https://doi.org/10.1016/j.jcat.2018.01.011>.
- [123] D. Xu, Y. Rui, Y. Li, Q. Zhang, H. Wang, Zn-Co layered double hydroxide modified hematite photoanode for enhanced photoelectrochemical water splitting, *Appl. Surf. Sci.* 358 (2015) 436–442, <https://doi.org/10.1016/j.apsusc.2015.08.160>.
- [124] J. Huang, G. Hu, Y. Ding, M. Pang, B. Ma, Mn-doping and NiFe layered double hydroxide coating: effective approaches to enhancing the performance of α -Fe₂O₃ in photoelectrochemical water oxidation, *J. Catal.* 340 (2016) 261–269, <https://doi.org/10.1016/j.jcat.2016.05.007>.
- [125] Y. Tang, R. Wang, Y. Yang, D. Yan, X. Xiang, Highly enhanced photoelectrochemical water oxidation efficiency based on triadic quantum dot/layered double hydroxide/BiVO₄ photoanodes, *ACS Appl. Mater. Interfaces* 8 (2016) 19446–19455, <https://doi.org/10.1021/acsami.6b04937>.
- [126] X. Zhang, R. Wang, F. Li, Z. An, M. Pu, X. Xiang, Enhancing photoelectrochemical water oxidation efficiency of BiVO₄ photoanodes by a hybrid structure of layered double hydroxide and graphene, *Ind. Eng. Chem. Res.* 56 (2017) 10711–10719, <https://doi.org/10.1021/acs.iecr.7b02960>.
- [127] X. Lv, X. Xiao, M. Cao, Y. Bu, C. Wang, M. Wang, Y. Shen, Efficient carbon dots/NiFe-layered double hydroxide/BiVO₄ photoanodes for photoelectrochemical water splitting, *Appl. Surf. Sci.* 439 (2018) 1065–1071, <https://doi.org/10.1016/j.apsusc.2017.12.182>.
- [128] R. Wang, L. Luo, X. Zhu, Y. Yan, B. Zhang, X. Xiang, J. He, Plasmon-enhanced layered double hydroxide composite BiVO₄ photoanodes: layering-dependent modulation of the water-oxidation reaction, *ACS Appl. Energy Mater.* 1 (2018) 3577–3586, <https://doi.org/10.1021/acsae.8b00831>.
- [129] J. Guo, X. Yang, S. Bai, X. Xiang, R. Luo, J. He, A. Chen, Effect of Mo doping and NiFe-LDH cocatalyst on PEC water oxidation efficiency, *J. Colloid Interface Sci.* 540 (2019) 9–19, <https://doi.org/10.1016/j.jcis.2018.12.069>.
- [130] L. Sun, J. Sun, X. Yang, S. Bai, Y. Feng, R. Luo, D. Li, A. Chen, An integrating photoanode consisting of BiVO₄, rGO and LDH for photoelectrochemical water splitting, *Dalton Trans.* 48 (2019) 16091–16098, <https://doi.org/10.1039/C9DT01819K>.
- [131] W. Liu, H. Liu, L. Dang, H. Zhang, X. Wu, B. Yang, Z. Li, X. Zhang, L. Lei, S. Jin, Amorphous cobalt-iron hydroxide nanosheet electrocatalyst for efficient electrochemical and photo-electrochemical oxygen evolution, *Adv. Funct. Mater.* 27 (2017) 1603904, <https://doi.org/10.1002/adfm.201603904>.
- [132] W. Chen, T. Wang, J. Xue, S. Li, Z. Wang, S. Sun, Cobalt-nickel layered double hydroxides modified on TiO₂ nanotube arrays for highly efficient and stable PEC water splitting, *Small* 13 (2017) 1602420, <https://doi.org/10.1002/smll.201602420>.
- [133] J. Guo, C. Mao, R. Zhang, M. Shao, M. Wei, P. Feng, Reduced titania@layered double hydroxide hybrid photoanodes for enhanced photoelectrochemical water oxidation, *J. Mater. Chem. A* 5 (2017) 11016–11025, <https://doi.org/10.1039/C7TA00770A>.
- [134] R. Zhang, M. Shao, S. Xu, F. Ning, L. Zhou, M. Wei, Photo-assisted synthesis of zinc-iron layered double hydroxides/TiO₂ nanoarrays toward highly-efficient photoelectrochemical water splitting, *Nano Energy* 33 (2017) 21–28, <https://doi.org/10.1016/j.nanoen.2017.01.020>.

- [135] F. Ning, M. Shao, S. Xu, Y. Fu, R. Zhang, M. Wei, D.G. Evans, X. Duan, TiO_2 / graphene/NiFe-layered double hydroxide nanorod array photoanodes for efficient photoelectrochemical water splitting, *Energy Environ. Sci.* 9 (2016) 2633–2643, <https://doi.org/10.1039/C6EE01092j>.
- [136] L. Ran, L. Yin, Ternary Hierarchical $\text{Cu}_{7.5}\text{Fe}_{2.5}\text{O}_{10}$ /CoCr-LDH heterostructured nanorod arrays with multiphase reaction interfaces for more efficient photoelectrochemical water splitting, *Adv. Mater. Interfaces*. 6 (2019) 1800970, <https://doi.org/10.1002/admi.201800970>.
- [137] C. Hao, R. Zhang, W. Wang, Y. Liang, J. Fu, B. Zou, H. Shi, Efficient charge transfer and separation of TiO_2 @NiCo-LDH core-shell nanowire arrays for enhanced photoelectrochemical water-splitting, *J Solid State Electrochem.* 23 (2019) 2343–2353, <https://doi.org/10.1007/s10008-019-04304-7>.
- [138] J. Liu, S.-M. Xu, Y. Li, R. Zhang, M. Shao, Facet engineering of WO_3 arrays toward highly efficient and stable photoelectrochemical hydrogen generation from natural seawater, *Appl. Catal. B* 264 (2020), <https://doi.org/10.1016/j.apcatb.2019.118540>.
- [139] X. Cao, C. Xu, J. Ma, Y. Dong, C. Dong, M. Yue, Y. Ding, Enhanced photoelectrochemical performance of WO_3 -based composite photoanode coupled with carbon quantum dots and NiFe layered double hydroxide, *ChemSusChem* 12 (2019) 4685–4692, <https://doi.org/10.1002/cssc.2019101803>.
- [140] X. Fan, B. Gao, T. Wang, X. Huang, H. Gong, H. Xue, H. Guo, L. Song, W. Xia, J. He, Layered double hydroxide modified WO_3 nanorod arrays for enhanced photoelectrochemical water splitting, *Appl. Catal. A* 528 (2016) 52–58, <https://doi.org/10.1016/j.apcata.2016.09.014>.
- [141] S. Bai, X. Yang, C. Liu, X. Xiang, R. Luo, J. He, A. Chen, An integrating photoanode of WO_3 / Fe_{2}O_3 heterojunction decorated with NiFe-LDH to improve PEC water splitting efficiency, *ACS Sustainable Chem. Eng.* 6 (2018) 12906–12913, <https://doi.org/10.1021/acssuschemeng.8b02267>.
- [142] Y. Hou, Z. Wen, S. Cui, X. Feng, J. Chen, Strongly coupled ternary hybrid aerogels of N-deficient porous graphitic-C₃N₄ nanosheets/N-doped graphene/NiFe-layered double hydroxide for solar-driven photoelectrochemical water oxidation, *Nano Lett.* 16 (2016) 2268–2277, <https://doi.org/10.1021/acs.nanolett.5b04496>.
- [143] M. Arif, G. Yasin, M. Shakeel, X. Fang, R. Gao, S. Ji, D. Yan, Coupling of bifunctional CoMn-layered double hydroxide@graphitic-C₃N₄ nanohybrids towards efficient photoelectrochemical overall water splitting, *Chem. Asian J.* 13 (2018) 1045–1052, <https://doi.org/10.1002/asia.201800016>.
- [144] M. Arif, G. Yasin, M. Shakeel, M.A. Mushtaq, W. Ye, X. Fang, S. Ji, D. Yan, Hierarchical CoFe-layered double hydroxide and g-C₃N₄ heterostructures with enhanced bifunctional photo/electrocatalytic activity towards overall water splitting, *Mater. Chem. Front.* 3 (2019) 520–531, <https://doi.org/10.1039/C8QM00677F>.
- [145] M.S. Mostafa, C. Lan, M.A. Betiha, R. Zhang, Y. Gaoa, G. Ge, Enhanced infrared-induced water oxidation by one-pot synthesized CoTi-nanorods as highly infrared responsive photocatalyst, *J. Power Sources* 464 (2020), <https://doi.org/10.1016/j.jpowsour.2020.228176>.
- [146] M. Suárez-Quezada, G. Romero-Ortiz, J.E. Samaniego-Benítez, V. Suárez, A. Mantilla, H₂ production by the water splitting reaction using photocatalysts derived from calcined ZnAl LDH, *Fuel* 240 (2019) 262–269, <https://doi.org/10.1016/j.fuel.2018.11.155>.
- [147] D. Yan, J. Lu, M. Wei, J. Han, J. Ma, F. Li, D.G. Evans, X. Duan, Ordered poly-layered double hydroxide ultrathin films with blue luminescence by layer-by-layer assembly, *Angew. Chem. Int. Ed.* 48 (2009) 3073–3076, <https://doi.org/10.1002/anie.2009000178>.
- [148] L. Lei, D. Huang, C. Zhou, S. Chen, X. Yan, Z. Li, W. Wang, Demystifying the active roles of NiFe-based oxides/(oxy)hydroxides for electrochemical water splitting under alkaline conditions, *Coord. Chem. Rev.* 408 (2020), <https://doi.org/10.1016/j.ccr.2019.213177>.
- [149] X. Tao, C. Yang, L. Huang, S. Shang, Novel plasma assisted preparation of ZnCuFeCr layered double hydroxides with improved photocatalytic performance of methyl orange degradation, *Appl. Surf. Sci.* 507 (2020), <https://doi.org/10.1016/j.apsusc.2019.145053>.
- [150] Y. Zhao, G. Chen, T. Bian, C. Zhou, G.I.N. Waterhouse, L.-Z. Wu, C.-H. Tung, L.J. Smith, D. O'Hare, T. Zhang, Defect-rich ultrathin ZnAl-layered double hydroxide nanosheets for efficient photoreduction of CO₂ to CO with water, *Adv. Mater.* 27 (2015) 7824–7831, <https://doi.org/10.1002/adma.201503730>.
- [151] Y.-C. Zhang, Z. Li, L. Zhang, L. Pan, X. Zhang, L. Wang, J.-J. Fazal-e-Aleem, Role of oxygen vacancies in photocatalytic water oxidation on ceria oxide: experiment and DFT studies, *Appl. Catal. B* 224 (2018) 101–108, <https://doi.org/10.1016/j.apcatb.2017.10.049>.
- [152] Z. Mo, H. Xu, Z. Chen, X. She, Y. Song, J. Lian, X. Zhu, P. Yan, Y. Lei, S. Yuan, H. Li, Construction of MnO₂/Monolayer g-C₃N₄ with Mn vacancies for Z-scheme overall water splitting, *Appl. Catal. B* 241 (2019) 452–460, <https://doi.org/10.1016/j.apcatb.2018.08.073>.
- [153] D. Chen, M. Qiao, Y.-R. Lu, L. Hao, D. Liu, C.-L. Dong, Y. Li, S. Wang, Preferential cation vacancies in perovskite hydroxide for the oxygen evolution reaction, *Angew. Chem.* 130 (2018) 8827–8832, <https://doi.org/10.1002/ange.201805520>.
- [154] D.P. Sahoo, S. Nayak, K.H. Reddy, S. Martha, K. Parida, Fabrication of a Co(OH)₂/ZnCr LDH “p–n” heterojunction photocatalyst with enhanced separation of charge carriers for efficient visible-light-driven H₂ and O₂ evolution, *Inorg. Chem.* 57 (2018) 3840–3854, <https://doi.org/10.1021/acs.inorgchem.7b03213>.
- [155] L. Xi, P.S. Bassi, S.Y. Chiam, W.F. Mak, P.D. Tran, J. Barber, J.S. Chye Loo, L.H. Wong, Surface treatment of hematite photoanodes with zinc acetate for water oxidation, *Nanoscale*. 4 (2012) 4430, <https://doi.org/10.1039/c2nr30862b>.
- [156] C.C.L. McCrory, S. Jung, J.C. Peters, T.F. Jaramillo, Benchmarking heterogeneous electrocatalysts for the oxygen evolution reaction, *J. Am. Chem. Soc.* 135 (2013) 16977–16987, <https://doi.org/10.1021/ja407115p>.
- [157] D. Chen, Z. Liu, S. Zhang, Enhanced PEC performance of hematite photoanode coupled with bimetallic oxyhydroxide NiFeOOH through a simple electroless method, *Appl. Catal. B* 265 (2020), <https://doi.org/10.1016/j.apcatb.2019.118580>.
- [158] Y. Fu, C.-L. Dong, W. Zhou, Y.-R. Lu, Y.-C. Huang, Y. Liu, P. Guo, L. Zhao, W.-C. Chou, S. Shen, A ternary nanostructured α -Fe₂O₃/Au/TiO₂ photoanode with reconstructed interfaces for efficient photoelectrocatalytic water splitting, *Appl. Catal. B* 260 (2020), <https://doi.org/10.1016/j.apcatb.2019.118206>.
- [159] A.G. Tamirat, J. Rick, A.A. Dubale, W.-N. Su, B.-J. Hwang, Using hematite for photoelectrochemical water splitting: a review of current progress and challenges, *Nanoscale Horiz.* 1 (2016) 243–267, <https://doi.org/10.1039/C5NH00098J>.
- [160] J. Zhang, M. Si, L. Jiang, X. Yuan, H. Yu, Z. Wu, Y. Li, J. Guo, Core-shell Ag@nitrogen-doped carbon quantum dots modified BiVO₄ nanosheets with enhanced photocatalytic performance under Vis-NIR light: synergism of molecular oxygen activation and surface plasmon resonance, *Chem. Eng. J.* 410 (2021), <https://doi.org/10.1016/j.cej.2020.128336>.
- [161] M. Yu, C. Shang, G. Ma, Q. Meng, Z. Chen, M. Jin, L. Shui, Y. Zhang, Z. Zhang, M. Yuan, X. Wang, G. Zhou, Synthesis and characterization of mesoporous BiVO₄ nanofibers with enhanced photocatalytic water oxidation performance, *Appl. Surf. Sci.* 481 (2019) 255–261, <https://doi.org/10.1016/j.apsusc.2019.03.056>.
- [162] D. He, R.-T. Gao, S. Liu, M. Sun, X. Liu, K. Hu, Y. Su, L. Wang, Yttrium-induced regulation of electron density in NiFe layered double hydroxides yields stable solar water splitting, *ACS Catal.* 10 (2020) 10570–10576, <https://doi.org/10.1021/acscatal.0c03272>.
- [163] L. Luo, Z. Wang, X. Xiang, D. Yan, J. Ye, Selective activation of benzyl alcohol coupled with photoelectrochemical water oxidation via a radical relay strategy, *ACS Catal.* 10 (2020) 4906–4913, <https://doi.org/10.1021/acscatal.0c00660>.
- [164] R. Gao, D. He, L. Wu, K. Hu, X. Liu, Y. Su, L. Wang, Towards long-term photostability of nickel hydroxide/BiVO₄ photoanodes for oxygen evolution catalysts via *in situ* catalyst tuning, *Angew. Chem. Int. Ed.* 59 (2020) 6213–6218, <https://doi.org/10.1002/anie.201915671>.
- [165] I. Abdellaoui, M.M. Islam, M. Remeika, Y. Higuchi, T. Kawaguchi, T. Harada, C. Budich, T. Maeda, T. Wada, S. Ikeda, T. Sakurai, Photocarrier recombination dynamics in BiVO₄ for visible light-driven water oxidation, *J. Phys. Chem. C* 124 (2020) 3962–3972, <https://doi.org/10.1021/acs.jpcc.9b10621>.
- [166] W. Wang, P.J. Strohbeen, D. Lee, C. Zhou, J.K. Kawasaki, K.-S. Choi, M. Liu, G. Galli, The role of surface oxygen vacancies in BiVO₄, *Chem. Mater.* 32 (2020) 2899–2909, <https://doi.org/10.1021/acs.chemmater.9b05047>.
- [167] S. Ju, H.-J. Seok, J. Jun, D. Huh, S. Son, K. Kim, W. Kim, S. Baek, H.-K. Kim, H. Lee, Fully blossomed WO_3 /BiVO₄ structure obtained via active facet engineering of patterned FTO for highly efficient Water splitting, *Appl. Catal. B* 263 (2020), <https://doi.org/10.1016/j.apcatb.2019.118362>.
- [168] Y. Li, D. Liao, T. Li, W. Zhong, X. Wang, X. Hong, H. Yu, Plasmonic Z-scheme Pt-Au/BiVO₄ photocatalyst: synergistic effect of crystal-facet engineering and selective loading of Pt-Au cocatalyst for improved photocatalytic performance, *J. Colloid Interface Sci.* 570 (2020) 232–241, <https://doi.org/10.1016/j.jcis.2020.02.093>.
- [169] T. Liu, R. Liu, Q. Li, J. Yang, Theoretical insight into the role of defects and facets in the selectivity of products in water oxidation over bismuth vanadate (BiVO₄), *ACS Sustainable Chem. Eng.* 8 (2020) 1980–1988, <https://doi.org/10.1021/acssuschemeng.9b06404>.
- [170] W.-K. Jo, S. Moru, S. Tonda, A green approach to the fabrication of a TiO₂ / NiAl-LDH core–shell hybrid photocatalyst for efficient and selective solar-powered reduction of CO₂ into value-added fuels, *J. Mater. Chem. A* 8 (2020) 8020–8032, <https://doi.org/10.1039/DOTA00104J>.
- [171] Z. Yang, J. Wei, G. Zeng, H. Zhang, X. Tan, C. Ma, X. Li, Z. Li, C. Zhang, A review on strategies to LDH-based materials to improve adsorption capacity and photoreduction efficiency for CO₂, *Coord. Chem. Rev.* 386 (2019) 154–182, <https://doi.org/10.1016/j.ccr.2019.01.018>.
- [172] S. Kreft, D. Wei, H. Junge, M. Beller, Recent advances on TiO₂-based photocatalytic CO₂ reduction, *EnergyChem.* 2 (2020), <https://doi.org/10.1016/j.enchem.2020.100044>.
- [173] W. Cui, H. Bai, J. Shang, F. Wang, D. Xu, J. Ding, W. Fan, W. Shi, Organic-inorganic hybrid-photoanode built from NiFe-MOF and TiO₂ for efficient PEC water splitting, *Electrochim. Acta* 349 (2020), <https://doi.org/10.1016/j.electacta.2020.136383>.
- [174] D.P. Sahoo, S. Patnaik, K. Parida, Construction of a Z-scheme dictated WO_{3-x} / Ag/ZnCr LDH synergistically visible light-induced photocatalyst towards tetracycline degradation and H₂ evolution, *ACS Omega* 4 (2019) 14721–14741, <https://doi.org/10.1021/acsomega.9b01146>.
- [175] S. Wang, G. Liu, L. Wang, Crystal facet engineering of photoelectrodes for photoelectrochemical water splitting, *Chem. Rev.* 119 (2019) 5192–5247, <https://doi.org/10.1021/acs.chemrev.8b00584>.
- [176] J.J. Gil, O. Aguilar-Martínez, Y. Piña-Pérez, R. Pérez-Hernández, C.E. Santolalla-Vargas, R. Gómez, F. Tzompantzi, Efficient ZnS-ZnO/ZnAl-LDH composite for

- H₂ production by photocatalysis, *Renewable Energy* 145 (2020) 124–132, <https://doi.org/10.1016/j.renene.2019.06.001>.
- [177] Z. Li, M. Chen, Z. Ai, L. Wu, Q. Zhang, Mechanochemical synthesis of CdS/MgAl LDH-precursor as improved visible-light driven photocatalyst for organic dye, *Appl. Clay Sci.* 163 (2018) 265–272, <https://doi.org/10.1016/j.clay.2018.07.037>.
- [178] M. Yang, K. Wang, Y. Li, K. Yang, Z. Jin, Pristine hexagonal CdS assembled with NiV LDH nanosheet formed p-n heterojunction for efficient photocatalytic hydrogen evolution, *Appl. Surf. Sci.* 548 (2021), <https://doi.org/10.1016/j.apsusc.2021.149212> 149212.
- [179] A. Pirkarami, S. Rasouli, E. Ghasemi, 3-D CdS@NiCo layered double hydroxide core-shell photoelectrocatalyst used for efficient overall water splitting, *Appl. Catal. B* 241 (2019) 28–40, <https://doi.org/10.1016/j.apcatb.2018.09.021>.
- [180] L. Zheng, F. Teng, X. Ye, H. Zheng, X. Fang, Photo/Electrochemical Applications of Metal Sulfide/TiO₂ Heterostructures, *Adv. Energy Mater.* 10 (2020) 1902355, <https://doi.org/10.1002/aenm.201902355>.
- [181] Z. Jin, X. Yan, X. Hao, Rational design of a novel p-n heterojunction based on 3D layered nanoflower MoS_x supported CoWO₄ nanoparticles for superior photocatalytic hydrogen generation, *J. Colloid Interface Sci.* 569 (2020) 34–49, <https://doi.org/10.1016/j.jcis.2020.02.052>.
- [182] J. Xu, Y. Li, S. Peng, Photocatalytic hydrogen evolution over Erythrosin B-sensitized graphitic carbon nitride with in situ grown molybdenum sulfide cocatalyst, *Int. J. Hydrogen Energy* 40 (2015) 353–362, <https://doi.org/10.1016/j.ijhydene.2014.10.150>.
- [183] K. Chang, Z. Mei, T. Wang, Q. Kang, S. Ouyang, J. Ye, MoS₂/graphene cocatalyst for efficient photocatalytic H₂ evolution under visible light irradiation, *ACS Nano* 8 (2014) 7078–7087, <https://doi.org/10.1021/nn5019945>.
- [184] X. Zhang, H. Liang, H. Li, Y. Xia, X. Zhu, L. Peng, W. Zhang, L. Liu, T. Zhao, C. Wang, Z. Zhao, C. Hung, M.M. Zagho, A.A. Elzatahry, W. Li, D. Zhao, Sequential chemistry toward core-shell structured metal sulfides as stable and highly efficient visible-light photocatalysts, *Angew. Chem. Int. Ed.* 59 (2020) 3287–3293, <https://doi.org/10.1002/anie.201913600>.
- [185] J. Zhang, X. Yuan, M. Si, L. Jiang, H. Yu, Core-shell structured cadmium sulfide nanocomposites for solar energy utilization, *Adv. Colloid Interface Sci.* 282 (2020), <https://doi.org/10.1016/j.cis.2020.102209> 102209.
- [186] J. Su, G. Li, X. Li, J. Chen, 2D/2D heterojunctions for catalysis, *Adv. Sci.* 6 (2019) 1801702, <https://doi.org/10.1002/advs.201801702>.
- [187] X. Zhang, X. Yuan, L. Jiang, J. Zhang, H. Yu, H. Wang, G. Zeng, Powerful combination of 2D g-C₃N₄ and 2D nanomaterials for photocatalysis: recent advances, *Chem. Eng. J.* 390 (2020), <https://doi.org/10.1016/j.cej.2020.124475> 124475.
- [188] H. Guo, C.-G. Niu, Y.-Y. Yang, C. Liang, H.-Y. Niu, H.-Y. Liu, L. Li, N. Tang, Interfacial Co-N bond bridged CoB/g-C₃N₄ Schottky junction with modulated charge transfer dynamics for highly efficient photocatalytic *Staphylococcus aureus* inactivation, *Chem. Eng. J.* 422 (2021), <https://doi.org/10.1016/j.cej.2021.130029> 130029.
- [189] H. Guo, C.-G. Niu, C. Liang, H.-Y. Niu, Y.-Y. Yang, H.-Y. Liu, N. Tang, H.-X. Fang, Highly crystalline porous carbon nitride with electron accumulation capacity: promoting exciton dissociation and charge carrier generation for photocatalytic molecular oxygen activation, *Chem. Eng. J.* 409 (2021), <https://doi.org/10.1016/j.cej.2020.128030> 128030.
- [190] J. Wang, H. Chen, L. Tang, G. Zeng, Y. Liu, M. Yan, Y. Deng, H. Feng, J. Yu, L. Wang, Antibiotic removal from water: a highly efficient silver phosphobased Z-scheme photocatalytic system under natural solar light, *Sci. Total Environ.* 639 (2018) 1462–1470, <https://doi.org/10.1016/j.scitotenv.2018.05.258>.
- [191] L. Jiang, J. Yang, S. Zhou, H. Yu, J. Liang, W. Chu, H. Li, H. Wang, Z. Wu, X. Yuan, Strategies to extend near-infrared light harvest of polymer carbon nitride photocatalysts, *Coord. Chem. Rev.* 439 (2021), <https://doi.org/10.1016/j.ccr.2021.213947> 213947.
- [192] D. Huang, Z. Li, G. Zeng, C. Zhou, W. Xue, X. Gong, X. Yan, S. Chen, W. Wang, M. Cheng, Megamerger in photocatalytic field: 2D g-C₃N₄ nanosheets serve as support of 0D nanomaterials for improving photocatalytic performance, *Appl. Catal. B* 240 (2019) 153–173, <https://doi.org/10.1016/j.apcatb.2018.08.071>.
- [193] S. Nayak, L. Mohapatra, K. Parida, Visible light-driven novel g-C₃N₄/NiFe-LDH composite photocatalyst with enhanced photocatalytic activity towards water oxidation and reduction reaction, *J. Mater. Chem. A* 3 (2015) 18622–18635, <https://doi.org/10.1039/C5TA00502B>.
- [194] Y. Yang, X. Li, C. Zhou, W. Xiong, G. Zeng, D. Huang, C. Zhang, W. Wang, B. Song, X. Tang, X. Li, H. Guo, Recent advances in application of graphitic carbon nitride-based catalysts for degrading organic contaminants in water through advanced oxidation processes beyond photocatalysis: a critical review, *Water Res.* 184 (2020), <https://doi.org/10.1016/j.watres.2020.116200> 116200.
- [195] Y. Yang, G. Zeng, D. Huang, C. Zhang, D. He, C. Zhou, W. Wang, W. Xiong, B. Song, H. Yi, S. Ye, X. Ren, In situ grown single-atom cobalt on polymeric carbon nitride with bidentate ligand for efficient photocatalytic degradation of refractory antibiotics, *Small* 16 (2020) 2001634, <https://doi.org/10.1002/smll.202001634>.
- [196] Z. Wang, H. Wang, Z. Zeng, G. Zeng, P. Xu, R. Xiao, D. Huang, X. Chen, L. He, C. Zhou, Y. Yang, Z. Wang, W. Wang, W. Xiong, Metal-organic frameworks derived Bi₂O₂CO₃/porous carbon nitride: a nanosized Z-scheme systems with enhanced photocatalytic activity, *Appl. Catal. B* 267 (2020), <https://doi.org/10.1016/j.apcatb.2020.118700> 118700.
- [197] H. Chen, X. Zhang, L. Jiang, X. Yuan, J. Liang, J. Zhang, H. Yu, W. Chu, Z. Wu, H. Li, Y. Li, Strategic combination of nitrogen-doped carbon quantum dots and g-C₃N₄: efficient photocatalytic peroxydisulfate for the degradation of tetracycline hydrochloride and mechanism insight, *Sep. Purif. Technol.* 272 (2021), <https://doi.org/10.1016/j.seppur.2021.118947> 118947.
- [198] M. Shakeel, M. Arif, G. Yasin, B. Li, H.D. Khan, Layered by layered Ni-Mn-LDH/g-C₃N₄ nanohybrid for multi-purpose photo/electrocatalysis: morphology controlled strategy for effective charge carriers separation, *Appl. Catal. B* 242 (2019) 485–498, <https://doi.org/10.1016/j.apcatb.2018.10.005>.
- [199] Y. Wu, H. Wang, Y. Sun, T. Xiao, W. Tu, X. Yuan, G. Zeng, S. Li, J.W. Chew, Photogenerated charge transfer via interfacial internal electric field for significantly improved photocatalysis in direct Z-scheme oxygen-doped carbon nitrogen/CoAl-layered double hydroxide heterojunction, *Appl. Catal. B* 227 (2018) 530–540, <https://doi.org/10.1016/j.apcatb.2018.01.069>.
- [200] S. Megala, M. Sathish, S. Harish, M. Navaneethan, S. Sohila, B. Liang, R. Ramesh, Enhancement of photocatalytic H₂ evolution from water splitting by construction of two dimensional gC₃N₄/NiAl layered double hydroxides, *Appl. Surf. Sci.* 509 (2020), <https://doi.org/10.1016/j.apsusc.2019.144656> 144656.
- [201] Q. Liang, Z. Li, X. Yu, Z.-H. Huang, F. Kang, Q.-H. Yang, Macroscopic 3D porous graphitic carbon nitride monolith for enhanced photocatalytic hydrogen evolution, *Adv. Mater.* 27 (2015) 4634–4639, <https://doi.org/10.1002/adma.201502057>.
- [202] A. Naseri, M. Samadi, A. Pourjavadi, A.Z. Moshfegh, S. Ramakrishna, Graphitic carbon nitride (g-C₃N₄)-based photocatalysts for solar hydrogen generation: recent advances and future development directions, *J. Mater. Chem. A* 5 (2017) 23406–23433, <https://doi.org/10.1039/C7TA05131>.
- [203] C. Bie, B. Cheng, J. Fan, W. Ho, J. Yu, Enhanced solar-to-chemical energy conversion of graphitic carbon nitride by two-dimensional cocatalysts, *EnergyChem* 3 (2021), <https://doi.org/10.1016/j.enchem.2021.100051> 100051.
- [204] X. Wang, X. Li, C. Huang, C. Hao, C. Ge, Y. Guo, Fabrication of NiCoAl-layered double hydroxide/N-GO for high energy all-solid-state asymmetric supercapacitors, *Appl. Surf. Sci.* 527 (2020), <https://doi.org/10.1016/j.apcatb.2020.146891> 146891.
- [205] W. Yao, J. Wang, P. Wang, X. Wang, S. Yu, Y. Zou, J. Hou, T. Hayat, A. Alsaedi, X. Wang, Synergistic coagulation of GO and secondary adsorption of heavy metal ions on Ca/Al layered double hydroxides, *Environ. Pollut.* 229 (2017) 827–836, <https://doi.org/10.1016/j.envpol.2017.06.084>.
- [206] K. Wang, C. Miao, Y. Liu, L. Cai, W. Jones, J. Fan, D. Li, J. Feng, Vacancy enriched ultrathin TiMgAl-layered double hydroxide/graphene oxides composites as highly efficient visible-light catalysts for CO₂ reduction, *Appl. Catal. B* 270 (2020), <https://doi.org/10.1016/j.apcatb.2020.118878> 118878.
- [207] D. Qin, Y. Zhou, W. Wang, C. Zhang, G. Zeng, D. Huang, L. Wang, H. Wang, Y. Yang, L. Lei, S. Chen, D. He, Recent advances in two-dimensional nanomaterials for photocatalytic reduction of CO₂: insights into performance, theories and perspective, *J. Mater. Chem. A* 8 (2020) 19156–19195, <https://doi.org/10.1039/C9TA07460H>.
- [208] A. Kumaresan, S. Yang, K. Zhao, N. Ahmad, J. Zhou, Z. Zheng, Y. Zhang, Y. Gao, H. Zhou, Z. Tang, Facile development of CoAl-LDHs/RGO nanocomposites as photocatalysts for efficient hydrogen generation from water splitting under visible-light irradiation, *Inorg. Chem. Front.* 6 (2019) 1753–1760, <https://doi.org/10.1039/C9QJ00307J>.
- [209] D. Sun, D. Chi, Z. Yang, Z. Xing, J. Yin, Z. Li, Q. Zhu, W. Zhou, Mesoporous g-C₃N₄/Zn-Ti LDH laminated van der Waals heterojunction nanosheets as remarkable visible-light-driven photocatalysts, *Int. J. Hydrogen Energy* 44 (2019) 16348–16358, <https://doi.org/10.1016/j.ijhydene.2019.04.275>.
- [210] R. Zhu, F. Tian, R. Yang, J. He, J. Zhong, B. Chen, Z scheme system ZnIn₂S₄/RGO/BiVO₄ for hydrogen generation from water splitting and simultaneous degradation of organic pollutants under visible light, *Renewable Energy* 139 (2019) 22–27, <https://doi.org/10.1016/j.renene.2019.02.049>.
- [211] J. Liu, J. Li, Y. Li, J. Guo, S.-M. Xu, R. Zhang, M. Shao, Photoelectrochemical water splitting coupled with degradation of organic pollutants enhanced by surface and interface engineering of BiVO₄ photoanode, *Appl. Catal. B* 278 (2020), <https://doi.org/10.1016/j.apcatb.2020.119268> 119268.
- [212] R.A. Rather, I.M.C. Lo, Photoelectrochemical sewage treatment by a multifunctional g-C₃N₄/Ag/AgCl/BiVO₄ photoanode for the simultaneous degradation of emerging pollutants and hydrogen production, and the disinfection of *E. coli*, *Water Res.* 168 (2020), <https://doi.org/10.1016/j.watres.2019.115166> 115166.
- [213] E. Samuel, B. Joshi, M.-W. Kim, M.T. Swihart, S.S. Yoon, Morphology engineering of photoelectrodes for efficient photoelectrochemical water splitting, *Nano Energy* 72 (2020), <https://doi.org/10.1016/j.nanoen.2020.104648>.
- [214] L. Hou, Q. Du, L. Su, S. Di, Z. Ma, L. Chen, G. Shao, Ni-Co layered double hydroxide with self-assembled urchin like morphology for asymmetric supercapacitors, *Mater. Lett.* 237 (2019) 262–265, <https://doi.org/10.1016/j.jmatlet.2018.11.123>.
- [215] Y. Yuan, H. Xu, W. Liu, L. Chen, Z. Quan, P. Liu, Z. Qu, N. Yan, Morphology-controlled synthesis and sulfur modification of 3D hierarchical layered double hydroxides for gaseous elemental mercury removal, *J. Colloid Interface Sci.* 536 (2019) 431–439, <https://doi.org/10.1016/j.jcis.2018.10.062>.
- [216] C. Zhang, M. Shao, L. Zhou, Z. Li, K. Xiao, M. Wei, Hierarchical NiFe layered double hydroxide hollow microspheres with highly-efficient behavior toward oxygen evolution reaction, *ACS Appl. Mater. Interfaces* 8 (2016) 33697–33703, <https://doi.org/10.1021/acsami.6b12100>.
- [217] T.-F. Yeh, C.-Y. Teng, S.-J. Chen, H. Teng, Nitrogen-doped graphene oxide quantum dots as photocatalysts for overall water-splitting under visible light

- illumination, *Adv. Mater.* 26 (2014) 3297–3303, <https://doi.org/10.1002/adma.201305299>.
- [218] W. Liu, M. Li, G. Jiang, G. Li, J. Zhu, M. Xiao, Y. Zhu, R. Gao, A. Yu, M. Feng, Z. Chen, Graphene quantum dots-based advanced electrode materials: design, synthesis and their applications in electrochemical energy storage and electrocatalysis, *Adv. Energy Mater.* (2020) 2001275, <https://doi.org/10.1002/aenm.202001275>.
- [219] Y. Zhao, S. Zhang, R. Shi, G.I.N. Waterhouse, J. Tang, T. Zhang, Two-dimensional photocatalyst design: a critical review of recent experimental and computational advances, *Mater. Today* 34 (2020) 78–91, <https://doi.org/10.1016/j.mattod.2019.10.022>.
- [220] X. Xiong, Y. Zhao, R. Shi, W. Yin, Y. Zhao, G.I.N. Waterhouse, T. Zhang, Selective photocatalytic CO₂ reduction over Zn-based layered double hydroxides containing tri or tetravalent metals, *Sci. Bull.* 65 (2020) 987–994, <https://doi.org/10.1016/j.scib.2020.03.032>.
- [221] Y. Zhao, G.I.N. Waterhouse, G. Chen, X. Xiong, L.-Z. Wu, C.-H. Tung, T. Zhang, Two-dimensional-related catalytic materials for solar-driven conversion of CO_x into valuable chemical feedstocks, *Chem. Soc. Rev.* 48 (2019) 1972–2010, <https://doi.org/10.1039/C8CS00607E>.
- [222] S.-M. Xu, T. Pan, Y.-B. Dou, H. Yan, S.-T. Zhang, F.-Y. Ning, W.-Y. Shi, M. Wei, Theoretical and experimental study on M^{II}M^III-layered double hydroxides as efficient photocatalysts toward oxygen evolution from water, *J. Phys. Chem. C* 119 (2015) 18823–18834, <https://doi.org/10.1021/acs.jpc.5b01819>.
- [223] Y. Sun, H. Liao, J. Wang, B. Chen, S. Sun, S.J.H. Ong, S. Xi, C. Diao, Y. Du, J.-O. Wang, M.B.H. Breese, S. Li, H. Zhang, Z.J. Xu, Covalency competition dominates the water oxidation structure-activity relationship on spinel oxides, *Nat Catal.* (2020), <https://doi.org/10.1038/s41929-020-0465-6>.